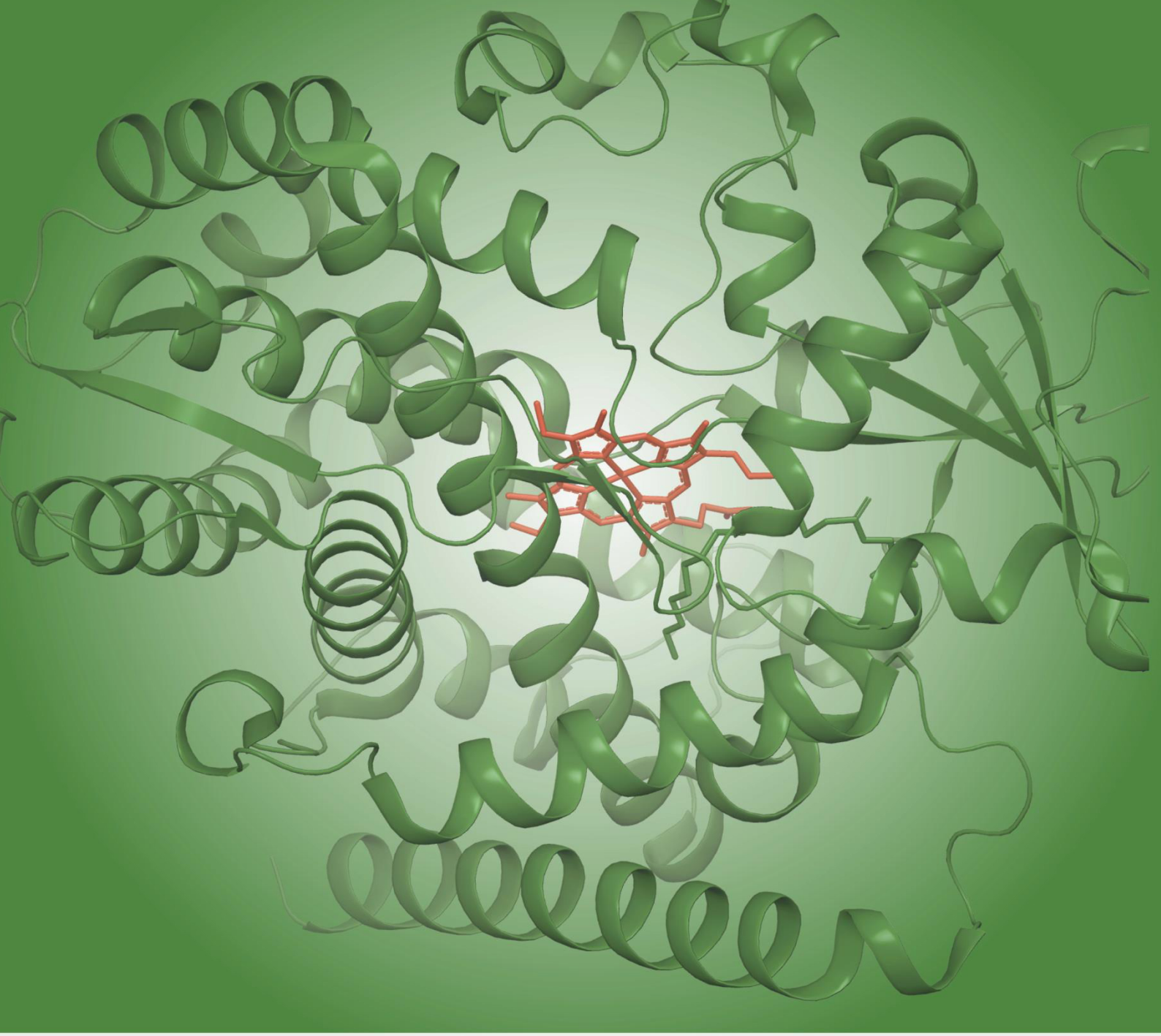

Cornelia Ritter

Towards Bioorthogonal Enzymatic Uncaging Reactions

Dissertation

Philipps Universität Marburg

Towards Bioorthogonal Enzymatic Uncaging Reactions

Dissertation

presented to
the Department of Chemistry
of the Philipps-Universität Marburg
in partial fulfilment
for the degree of

Doctor of Science
(Dr. rer. nat.)

by

Cornelia Ritter, M.Sc.
from München

Marburg/Lahn 2015

Die vorliegende Dissertation entstand in der Zeit von Oktober 2012 bis Dezember 2015 am Fachbereich Chemie der Philipps-Universität Marburg in der Arbeitsgruppe und unter der Betreuung von Herrn Prof. Dr. Eric Meggers.
Vom Fachbereich Chemie der Philipps-Universität Marburg (Hochschulkennziffer: 1180) als Dissertation am 11.01.2016 angenommen.

Erstgutachter: Prof. Dr. Eric Meggers
Zweitgutachter: Prof. Dr. Manfred T. Reetz

Tag der mündlichen Prüfung: 05.02.2016

“The more you learn,
the more you know that you know nothing.”

— Ayn Rand

Acknowledgements

Danken möchte ich zuallererst Herrn Professor MEGGERS, der mich in seiner Gruppe aufgenommen hat, ohne mich vorher zu kennen, und mir ein neues, interdisziplinäres Projekt anvertraut hat. Bis zum Erfolg war es nicht immer leicht, aber es gab auf allen Ebenen unglaublich viel zu lernen und darauf werde ich noch lange aufbauen können.
Herrn Professor REETZ danke ich für die gute Zusammenarbeit, die Übernahme der Zweitkorrektur, aber ganz besonders auch für die aufmunternden Worte nach Rückschlägen – manchmal machen kleine Dinge einen großen Unterschied.
Danke auch an Herrn Professor TALLAREK, der bereitwillig der Prüfungskommission beitrat.

To my collaborators: ¡*Muchas gracias* CARLOS!, who taught me a lot about protein expression in general, P450$_{BM3}$ in particular, and some insight into life as a scientist on top. *Спасибо*, MISCHA! Together we learned a lot about delivery, microscopes and the peculiarities of my enzymes – never forgetting to have a laugh, no matter how many defeats we suffered. Für all die Ratschläge, Denkanstöße und Hintergrundinfos möchte ich SABRINA danken, die sich immer Zeit dafür genommen hat, und besonders auch für all die Energie, die sie aufgebracht hat, um das generelle Arbeitsklima zu verbessern. INA, LILU, ANDREA, und vor allem unsere „ehemalige“ gute Seele KATJA, die jeden Tag das Labor und die Gruppe am Laufen gehalten haben.

Allen Mitgliedern der Service-Abteilungen am Fachbereich, die hinter den Kulissen für die nötigen Voraussetzungen sorgen, und auch bei kleinen und größeren Sonderfällen stets behilflich sind.

A big *Thank You* goes out to all current and former group members, who welcomed me in a new group, new department and new city and made the group what it is. Besonders zu erwähnen sind dabei NETTI, SABINE, MANU, JENS, MELANIE, RAJI, ADRIANA, RICHARD und natürlich meine „Labor-Ehefrau" LISSI – die nicht nur im Labor sondern auch in der Freizeit, sei es an gemütlichen Abenden oder beim Skifahren, Zelten oder auf Festivals, die Zeit versüßt haben und am Institut bei unzähligen Kaffeepausen und Grillabenden, sowie mit Aufmunterung und Unterstützung auch an schlechten Tagen die Motivation gesichert haben. Ich möchte euch nie missen müssen!

Meinen Studenten in Praktika, meinem Vertiefer ROBERT und ganz besonders der Süddeutschen Fraktion, CHRISTIAN und LISA, die sich nicht nur wissenschaftlich sondern auch kulinarisch eingebracht und die Tage bereichert haben.

Special thanks to ADRIANA, CARLOS, LISSI, MISCHA, NETTI, OLALLA, SABINE, TIBOR and WIGO for all the efforts of spell-checking, corrections and improvements on this thesis.

DAN, weil ich ohne ihn all diese Erfahrungen nicht gemacht hätte. TIBOR, für grandiose Zeiten in Dekadenz, Abenteuer, all die Unterstützung und auch für jede Herausforderung! OLALLA, que ilumina Marburg. Donde otros se dan por vencidos, comienza su energía – y es contagiosa!

Meinen Freunden in München und dem Rest der Welt, zu denen die Verbindung trotz aller Hektik nie ganz abreißt und es sich auch nach Monaten oder Jahren anfühlt wie immer, wenn man sich endlich wieder sieht.
No matter how far away they might be, my friends are always in my heart!

Und abschließend gebührt der größte Dank meiner Familie.
CLAUDI, weil ich ohne sie nicht ich wäre. MEINEN GROßELTERN, und am Allermeisten MEINEN ELTERN, weil sie immer hinter mir und meinen Entscheidungen standen (auch wenn sie sie nicht immer nachvollziehen konnten), mich unterstützt haben wo immer es ging, unendliche Geduld in all den stressigen Zeiten des Studiums hatten, und es immer noch und immer wieder schaffen, mir ein Gefühl von Zuhause zu geben.

Publications

Parts of this work have been published in peer-reviewed scientific journals or have been presented at conferences:

Peer-reviewed Articles

C. Ritter, N. Nett, C. G. Acevedo-Rocha, R. Lonsdale, K. Kräling, F. Dempwolff, S. Hoebenreich, P. L. Graumann, M. T. Reetz, E. Meggers,
Angew. Chemie (Int. Ed.) ***2015***, *54, 13440–3.*
Bioorthogonal Enzymatic Activation of Caged Compounds
Angew. Chemie **2015**, 127, 13640–4.
Bioorthogonale enzymatische Aktivierung maskierter Verbindungen

Contributions at Conferences

Poster Presentation
C. Ritter, N. Nett, C. G. Acevedo-Rocha, M. T. Reetz, E. Meggers,
FEBS J. **2015**, *282*, S1, 241; doi: 10.1111/febs.13339
P15-010 –
Bioorthogonal enzymatic cleavage of protection groups for prodrug activation

Oral Presentations
C. Ritter, at *YSF (FEBS)* **2015**, Berlin
Bioorthogonal enzymatic cleavage of protection groups for prodrug activation.

C. Ritter, M. Zyuzin, at *SynChemBio (Loewe)* **2015**, Marburg
B2 – Bioorthogonal Enzymatic Activation of Caged Compounds

Abstract

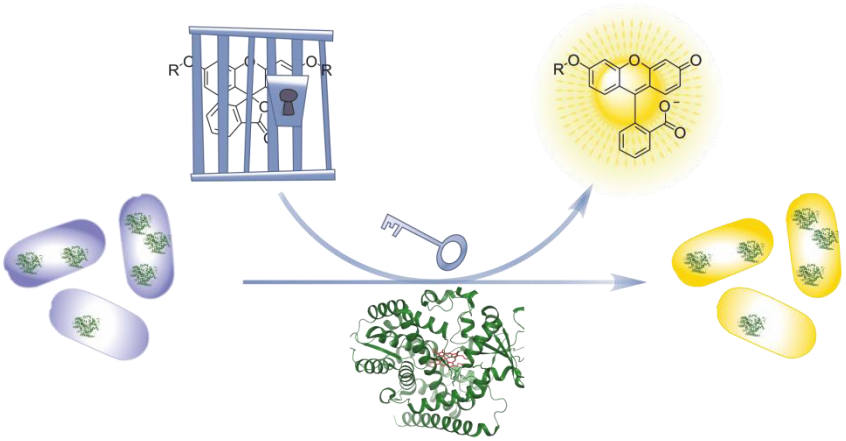

How to escape from jail:
Engineered cytochrome P450 monooxygenases are used for the deprotection of different ethers, thereby releasing uncaged alcohols, which in this case display fluorescence properties. Bioorthogonal enzyme / protection group pairs provide possible solutions for the selective release of imaging agents as well as the catalytic activation of prodrugs at their site of action. Figure reproduced with permission from JOHN WILEY & SONS LTD.[1]

In this thesis, engineered cytochrome P450 monooxygenase mutants are reported as highly active and selective catalysts for the bioorthogonal uncaging of different ether protected substrates, including the successful transfer of the uncaging reaction into living bacteria. This proof-of-principle study points towards the utility of bioorthogonal enzyme/protecting group pairs for applications in the life sciences.

In the first part of this thesis, enzyme-substrate pairs were identified and characterized: First, various ether-protected fluorescein derivatives were synthesized via WILLIAMSON ether synthesis. Existing protocols for the evaluation of $P450_{BM3}$ variants were then modified for their applicability towards these fluorescent substrates, and enzyme libraries available from the REETZ group with a total of over 1000 mutants were screened for their activity. Motivated

by promising initial results, two different coumarin scaffolds were modified with the same ether protection groups and the libraries screened again for their activity towards these new substrates. Active ("hit") mutants were isolated, sequenced, and expressed at larger scales for purification. Purified mutants were then characterized with regard to their kinetic performance, while theoretical investigations using induced-fit docking and molecular dynamics simulations supported the rationalization of site influences.

The second part of the study concentrates on the transfer of the uncaging system into a biological environment. Experiments using mammalian cells were conducted in collaboration with the PARAK lab. Either the purified protein or the corresponding mRNA was transfected using commercially available delivery agents, with only modest success. At the same time, microcapsules were investigated for suitability towards this system, and extensive enzyme stability tests were performed in the process. Ultimately, a successful transfer of the system to living *E. coli* is reported, proving the general feasibility of the deprotection system for *in vivo* applications.

Abstract (Deutsch)

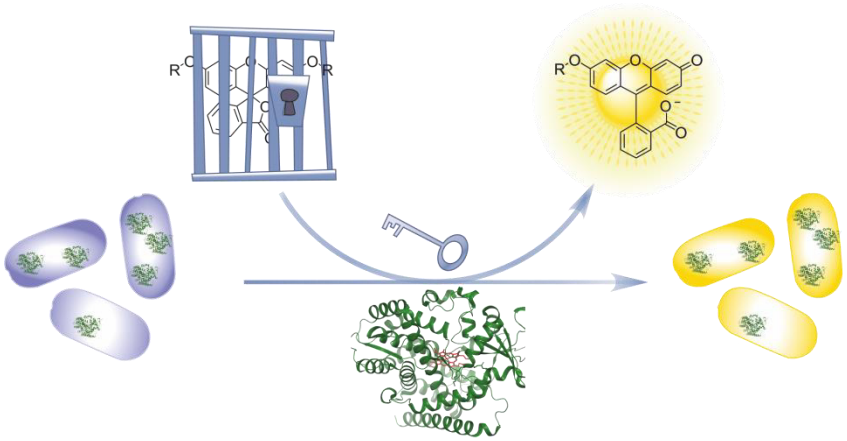

Wie man entkommt:
Evolvierte Cytochrom-P450-Monooxygenasen werden genutzt, um verschiedene ether-maskierte Verbindungen *in vitro* und in lebenden *E. coli* zu entschützen, und dabei Alkohole freizusetzen, die in diesem Fall fluoreszenzaktiv sind. Solche bioorthogonalen Paare aus Enzym und Schutzgruppe ermöglichen die selektive Freisetzung bildgebender Verbindungen oder die katalytische Aktivierung von Wirkstoffvorläufern an deren Zielort. Grafik reproduziert mit Erlaubnis von JOHN WILEY & SONS LTD.[2]

In der vorliegenden Arbeit wird die Verwendung evolvierter Mutanten von Cytochrom-P450-Monooxygenasen als hochaktive und hochselektive Katalysatoren für die bioorthogonale Aktivierung ethermaskierter Substrate berichtet, einschließlich der erfolgreichen Entschützung in lebenden Bakterien. Der mögliche Nutzen von bioorthogonalen Paaren aus Enzym und Schutzgruppe für Anwendungen in den Lebenswissenschaften wird veranschaulicht.

Der Fokus des ersten Teils der Arbeit liegt auf der Identifikation und Charakterisierung von Paaren aus Schutzgruppe und Enzym: zunächst wurden verschiedene ethermaskierte Fluoreszein-Derivate nach einer WILLIAMSON-Ethersynthese dargestellt. Literaturbekannte Protokolle zur Untersuchung von $P450_{BM3}$-Mutanten wurden modifiziert, um sie an die

Verwendung mit fluoreszenzaktiven Substraten anzupassen. Daraufhin wurden Enzymbibliotheken aus der REETZ-Gruppe mit insgesamt über 1000 Varianten auf ihre Aktivität hin untersucht. Aufbauend auf den ersten positiven Ergebnissen, wurden zwei verschiedene Cumaringerüste mit analogen Ether-Schutzgruppen versehen, und die Bibliotheken wiederum auf aktive Mutanten („Hits“) durchsucht. Gefundene Hit-Mutanten wurden sequenziert und zur Aufreinigung im größeren Maßstab exprimiert. Aufgereinigte Enzyme wurden in Hinsicht auf ihre kinetischen Parameter untersucht, wobei theoretische Betrachtungen mittels *induced fit docking* und molekulardynamischen Simulationen genutzt wurden, um die Einflüsse einzelner veränderter Positionen abzuschätzen.

Der zweite Teil der Studie beschäftigt sich mit dem Transfer des Demaskierungs-Systems in ein biologisches Umfeld. Experimente mit Säugerzellen wurden in Kollaboration mit der PARAK-Gruppe durchgeführt. Entweder das aufgereinigte Protein oder die korrespondierende mRNA wurde mittels kommerziell erhältlicher Agenzien transfiziert, allerdings mit mäßigem Erfolg. Gleichzeitig wurden Micro-Kapseln auf ihre Eignung für das vorliegende $P450_{BM3}$-System hin untersucht, und das Enzym wurde dafür ausgiebigen Stabilitätstests unterzogen. Schlussendlich gelang der Transfer des Demaskierungs-Systems in lebende *E. coli*, und damit der Beweis für die generelle Eignung des Systems für *in vivo* Anwendungen.

Table of Contents

1 Introduction

1.1 Chemical Biology

The curiosity about our surroundings is the driving force behind all science. People have always tried to understand and manipulate their environment for their own advantage, creating the technologically advanced society we now live in. With our growing knowledge about the intricate interplay of different aspects, our tools have to become ever more sophisticated to match our increasingly complex questions. This is especially true on the frontier of life, where inanimate matter comes together in an elaborate symphony to create nature's diversity.

Studies in biochemistry have made great leaps in understanding the involved processes, showing us just how complex life is. Countless scientists are working in this field, and the fact that multiple Nobel prizes have been awarded emphasizes their importance: It was BÜCHNER who, in the early 20th century, achieved a breakthrough in this area, when he performed cell-free fermentation experiments. Thereafter, studies covered pigments, cofactors, vitamins, nucleobases, and their derivatives, before they continued to the isolation, crystallization, sequencing, and structural investigation of proteins. Later, manipulation techniques like PCR and mutagenesis were devised, allowing researchers to investigate entire pathways, involving for example the molecular backgrounds of transcription, protein degradation, or the immune system.[3,4]

Nowadays, the comparably new field of chemical biology takes up the challenge of creating chemical tools and probes for the investigation of biological systems. It connects various different fields and draws from their expertise, including, but not limited to, chemistry, synthetic biology, genetics, structural biology, and the range of newer –omics studies (*cf.* Figure 1-1). This interdisciplinary approach with its combined methods not only allows

sampling vast amounts of data, but also making sense of them and putting them in a larger context of interactions between various classes of (bio)molecules.

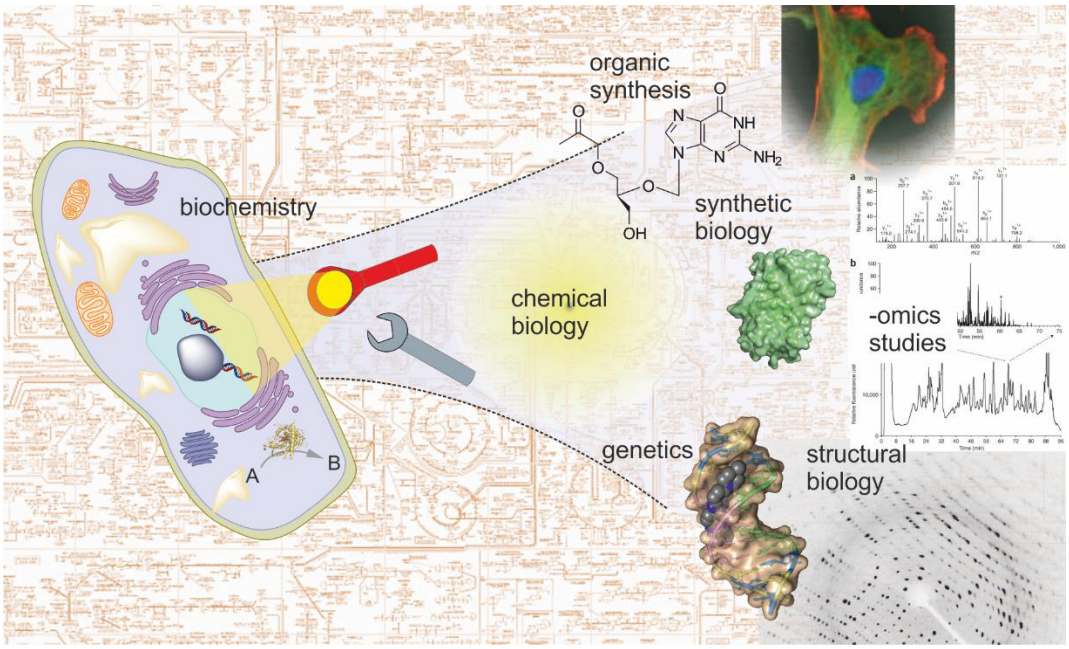

Figure 1-1. Chemical biology provides the tools needed to influence and study cellular processes, connecting biochemistry with many other branches of the life sciences.

1.1.1 Bioorthogonality

It is advantageous to study and control chemical reactions inside living cells without interfering with their native biochemistry, *i.e.* using bioorthogonal approaches. The term "bioorthogonality" was coined around the turn of the century in BERTOZZI'S lab, and was first mentioned in literature in 2003, kickstarting a new field of research.[5] The development of autonomous, reliable reactions that can take place inside living cells soon led to a multitude of options allowing the temporally or spatially controlled activation, modification, or tracking of molecules.[6,7] Applications can be found not only in biochemistry and chemical biology, but also in cellular biology (e.g. labelling of proteins,[8] lipids,[9] sugars,[10] and nucleic acids[11]) and medicinal chemistry (e.g. activation of inactivated compounds).[12,13] A versatile and probably the most widely used approach for detection, quantification, and imaging of the targeted compounds or structures is the chemical reporter strategy, which relies on a two-step mechanism (*cf.* Figure 1-2). A cellular target (dark green rectangle) can be tagged using a modified substrate derivative (light green rectangle), that carries a chemical reporter moiety (blue circle). In the second step, the reporter is selectively connected to a probe (blue arc) carrying a marker (orange star) that can be detected, for example using fluorescence. Both steps have to selectively react with the intended partners and avoid side reactions with

the plethora of biomolecules (gray shapes). The range of feasible targets is constantly being extended, and methods are continually refined and specialized, optimizing selectivity and reliability. The ongoing relevance of the concept is expressed in the recent endeavor initiated by a large group of researchers from academia and industry around EDWARD to create the *Chemical Probes Portal*, an open database listing and annotating chemical probes and their respective targets.[14,15]

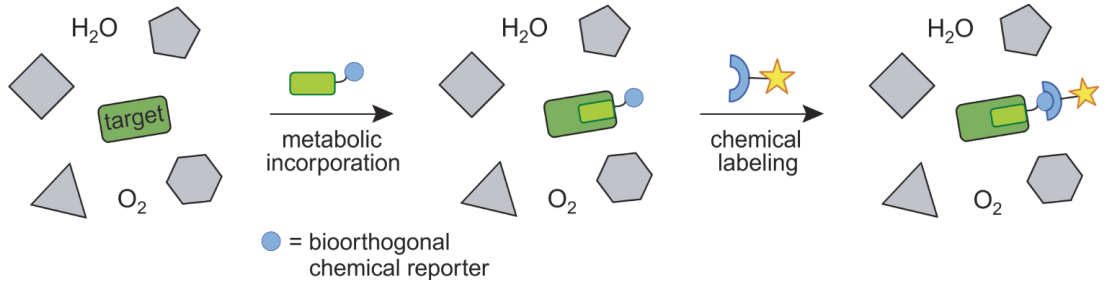

Figure 1-2. Schematic representation of a chemical reporter strategy used in chemical biology: after the target (dark green) is tagged using a reporter (blue), detection occurs by fusing the reporter to a signaling probe (orange). Adapted from PRESCHER et al. with permission from MACMILLAN PUBLISHERS LTD.[6]

Recent research in the area of bioorthogonal reactions generally has mostly concentrated on bond formation rather than cleavage,[16] often utilizing metal-induced or metal-catalyzed transformations,[17,18] or click chemistry. The latter term has come to describe a family of reactions with very specific properties, mostly resulting in the formation of carbon-heteroatom bonds. These reactions have to be reliable, versatile, efficient and create no or only inconspicuous byproducts.[19] Due to these favorable features, some of them have been adapted for applications in biological surroundings.[20–23] The first approaches used azide groups as biostable handles to introduce functionality, either by STAUDINGER ligation[24] or via a modified version of classical copper(I)-catalyzed HUISGEN cycloadditions.[25,26] A copper-free version utilizing ring-strain in cyclic alkynes to drive the reaction was developed later on.[27] Great progress has been made since, mastering the art of selectively and rapidly coupling compounds with various functionalities, for example allowing the covalent tagging of biomolecules *in vivo*.[28,29] These strategies peak in the development of mutually orthogonal, bioorthogonal reactions allowing the use of multiple tags, probes, or sensors in the same system.[30]

1.1.2 Caging

However, not every problem in chemical biology can be solved by tagging and bond formation reactions, so that in some cases bond cleavage can be a better option - for example for compound activation. Caging is one of the most versatile routes for the controlled release

of active species, with methods available for various classes of compounds (e.g. peptides,[31] nucleic acids,[32] or small molecules like drugs or dyes[33]). The term describes the modification of a bioactive or fluorogenic compound with a protection group, resulting in a temporary loss of function. This allows the caged, *i.e.* inactivated, compound to reach its intended site of action, minimizing unintended interference on the way. Upon arrival at the target site, some form of controlled activation mechanism is then required. Classical protection groups used in synthetic chemistry often rely on ester or amide bonds, which are easily cleaved in biological systems[34] and therefore have limited feasibility for this type of biological applications. Consequently it is a more promising approach for the caging of desired molecules for *in vivo* applications to use more inert connection motifs, such as aza or ether groups. The caged compound can subsequently be released, with multiple options available as a trigger (*cf.* Figure 1-3).

The most widely used approach works by applying light (photo-uncaging, path A).[12,35] Examples and details of commonly used photocages and their respective advantages have been reviewed repeatedly.[36,37] The combination of this method with a fluorescent signal allows the application for example as probes in chemical biology[38] or as a diagnostic cancer marker,[39] and is extensively used for bioimaging on a par with reversible photoswitches.[40] However, photo-cleavage often relies on tissue-damaging UV-light and requires the operation of a light source, necessarily confining the method to tissue close to the irradiation source.[37]

Chemically induced cleaving reactions (path B) on the other hand rely on stoichiometric amounts of additional reagents to release the caged group. Unfortunately, they are often not reactive or specific enough and can be toxic. Some major improvements in this regard are the recently popular approaches to modify established bioorthogonal reversed DIELS-ALDER reactions to trigger the release of a leaving group.[13,41] Probably the smallest caging group described in the literature is an azide moiety, which in a case presented by PAWLAK *et al.* is repurposed from the common click reactions and instead introduced as a cage on cell surface proteins to modulate an immune response, activatable by biocompatible reduction.[42] A new technique for intracellular deprotection presented by KIM and BERTOZZI utilizes small molecule boron reagents, which undergo a specific reaction with *N*-oxides.[43] Derivatives of the latter do occur naturally in some microbial species, but are absent in most higher organisms, rendering them inherently bioorthogonal.

The third option is shown in path C, activation via catalysis, which relies on the turnover of multiple molecules and thus basically constitutes a signal amplification mechanism. A challenge, especially for conventional metal catalysts, is their often limited efficiency due to deactivation of catalysts in physiological environments, although some progress has been made in this area.[44,45] A more detailed discussion of the general concept of catalysis *in vivo* is given in the next chapter.

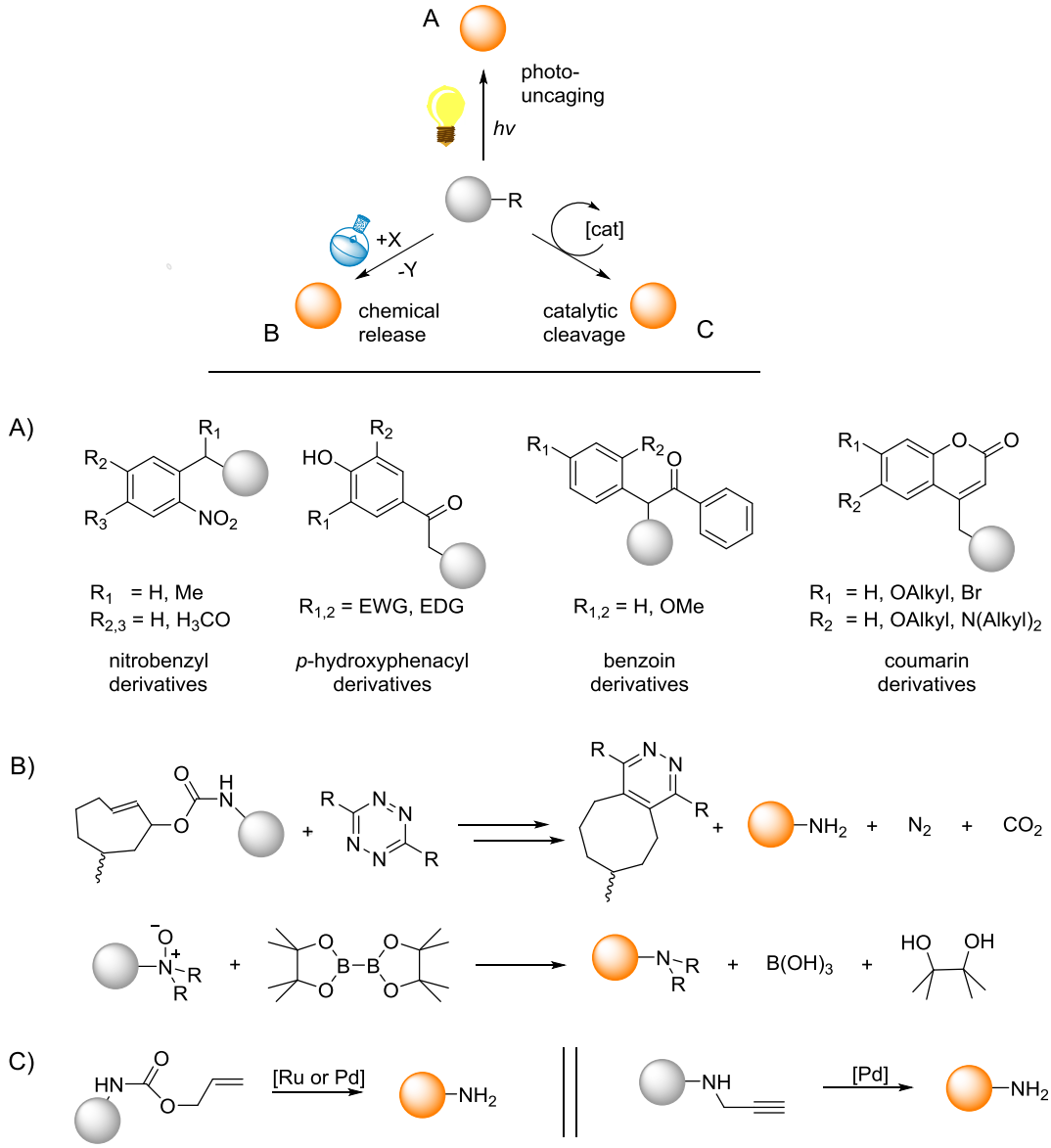

Figure 1-3. Typical uncaging approaches. Cleavage of the protection group can either be light-triggered (A), chemically induced (B), or facilitated by a catalyst (C). The gray spheres represent the site of attachment for the caged molecule, while R residues show variable positions for derivatization. Examples for each approach are shown below: A) Commonly used scaffolds for photo-uncaging reactions, as reviewed by CASEY *et al.*[36] B) Chemically induced activation by a click-to-release approach[13,41] (top) and N-oxide/boron release system (bottom).[43] C) Metal-mediated uncaging reactions reported in biological environments.[45]

The ultimate showcase application of caged compounds is again the successful implementation of not only one, but multiple independently controlled release systems in the same environment. Reports about this type of orthogonal reactions have been published, utilizing photo-uncaging with different wavelengths for the selective activation of two antibiotics or fluorophores.[33,46]

1.1.3 Catalysis in Living Systems

The use of catalyzed reactions has undebatable advantages over their slower counterpart in terms of reaction rate. Applied as a drug, dosages could be cut drastically, thus helping to eliminate side effects or toxicity.[47,48] Additionally, catalysts can increase the selectivity of a transformation to convey stereo-information and reduce undesired side products. However, the application of metal-based catalysts most often used in conventional organic synthesis is impeded in biological systems by the plethora of biomolecules that can interfere with the reaction, either by attacking the reactants or by poisoning the catalyst itself.[49] Nevertheless, this formidable challenge has been addressed in a variety of studies over the last 15 years, achieving some progress in the area, and different methods are illustrated in Figure 1-4: One approach omits metal-catalysts, and instead relies on cellular DNA or RNA oligonucleotides to act as a template and thus facilitate the reaction by placing the reactants in close proximity (panel A).[50] The template can undergo multiple turnovers, thus acting as a signal amplifier.[51] Reported reactions cover a wide range, from organocatalytic transformations[52] to coupling-driven uncaging reactions, similar to panel B in Figure 1-3.[53] Especially redox reactions are being investigated for their anti-tumor activity, since cancerous cells show an inherently different reaction to oxidative and reductive stress and are less able to counteract these interferences.[54,55] Although some cases of reductive strategies are reported,[56,57] the main approach is to increase levels of reactive oxygen species (ROS), inducing cell death (panel E). In combination with photo-activation, this method has long been used in medicine for the treatment of accessible tumors, with the roots dating back to the early 20th century,[58] and is now termed photo-dynamic therapy (PDT).[59] The catalyst, in this special case serving as a photo-sensitizer, can be based on purely organic scaffolds like porphyrins, or transition metal complexes.[60]

In fact, due to the familiarity with their design and their broad applicability, most efforts for the use of catalyzed reactions in physiological environments are based on metal-derived compounds, despite their downsides. Some of them have already been mentioned above, with the most common being the bioorthogonal copper(I)-catalyzed HUISGEN cycloaddition, [25,26] but other bond forming reactions as well, which are especially useful for tagging biomolecules (panel C).[18] The large majority of metal-based catalytic transformations in cells is not developed for bioorthogonality, but for the use as catalytic metallodrugs.[47,61] Their profound ability for the catalysis of hydrolysis reactions can be harnessed by attaching selective probes for proteins or RNA sequences, allowing the targeted lysis of intracellular compounds (panel B).[62,63] This technique is being investigated to be used against amyloid diseases,[64] as well as for its antimicrobial activity, opening a gate to the solution of the rising bacterial resistance problem.[65] However, not only deactivation can be achieved by hydrolysis, but it is equally feasible to restore functionality upon the removal of a caging group (panel D): proteins[66] or small molecules, used for example for DNA binding[67] or as

drugs,[17,68] can be activated in this manner, and the activity can even be controlled with light.[69] Multiple general or metal specific reviews on the topic are available,[18,45,70] and recently a general method for the evaluation of metal catalysis in living systems was reported.[71]

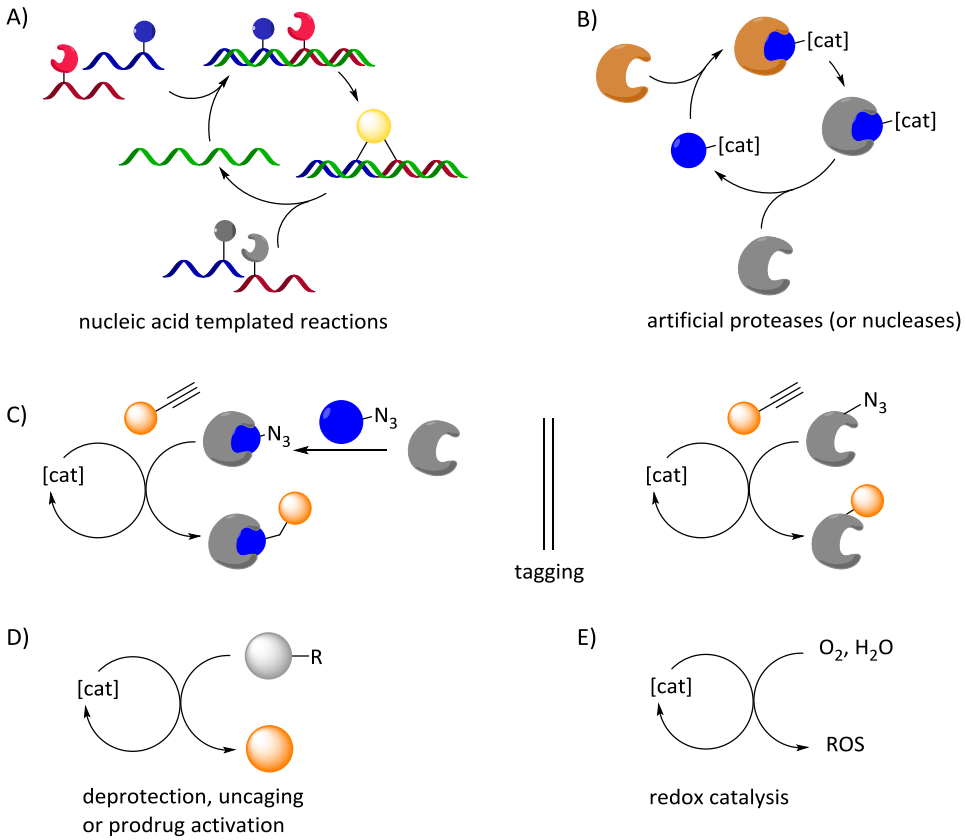

Figure 1-4. Catalysis *in vivo* – examples for different approaches. A) Nucleic acid templated reactions use naturally occurring oligomers to facilitate reactions, either for detection or prodrug release; B) artificial proteases and nucleases are equipped with a specific ligand, directing them to their target, which can then be deactivated by hydrolysis; C) tagging of biomolecules for their detection can be achieved either by using a specific ligand with a click-handle (left) or by directly introducing the handle via non-natural amino acids (right); D) a variety of methods are used for the activation of different compounds, and applications range from sensing to prodrug activation; E) interfering with the redox state of cells can be beneficial in anti-cancer treatments, with the generation of reactive oxygen species (ROS) as main approach.

An alternative strategy to metal-based catalysts would be the use of a biomolecule, which has multiple advantages, especially when working in aqueous media or biosystems. Nature's biocatalysts – enzymes in most cases, but also catalytically active oligonucleotides – are speeding up and controlling almost every reaction in living organisms. Without them, life as we know it would not be possible. They are highly selective towards substrates and reaction types, and have evolved to be extremely efficient in physiological environments[72] that often prove detrimental to conventional metal-based catalysts, which are particularly vulnerable

towards the thiols ubiquitously present inside cells. Moreover, the use of biopolymers consisting of natural building blocks could reduce the risk of the formation of toxic degradation products, while addressing performance issues present in metal-dependent bioorthogonal uncaging reactions. At the same time, they can avoid the detrimental mutagenic effects in cells and tissues when employing classical deprotection methods based on irradiation using UV-light. And in fact, oligonucleotides with catalytic activity (RNA/DNAzymes) are easily adjusted for their specific properties, and already widely investigated as selective metal ion sensors or for the recognition of other cofactors.[73] An even wider scope is offered by enzymes, nature's all-purpose workhorses, either in their natural form or adapted for specific applications. Apart from our own work,[2,1] only one bioorthogonal approach has been published so far where an engineered enzyme was used for mRNA modification, priming them for a subsequent click reaction.[74]

1.2 Enzymes in Medicine and Industry

Due to the advantages described above, the use of enzymes in biocatalysis,[75–77] and for medical applications is rapidly increasing.[78] However, it is by no means a new concept to use enzymes for our needs: Historically probably best known, and still appreciated by many today, is rennet, an enzymatic extract from the stomach of ruminants used to make cheese. The nature of these powerful tools was not understood for a long time, until PAYEN and PERSOZ successfully isolated diastase from malt solution in 1833, which is able to break down starch during the brewing process.[79] It took almost another century until SUMNER was able to prove in 1929 on the case of urease that enzymes are (usually) proteins.[80,81] Since then, scientists have been tirelessly working on improving the available methods for isolation, purification, and characterization. Structure determination, both by sequencing and crystallography, is well established today, so that thousands of enzymes are known.

Often without us knowing, they are part of our daily life: breaking down stains as part of laundry detergents,[82] softening our bread,[83] protecting our skin in cosmetics,[84] whitening our paper,[85] or cleaning our waste water.[86] Chemical and pharmaceutical industry have accepted their superior selectivity over conventional catalysts and use them for particularly challenging synthesis steps or sequences in the production of fine chemicals.[75,76,87] An overview of uses in industry is given by AEHLE.[88]

In medicine, freshly prepared ointments from plant and animal matter were used in early civilizations, some of which undoubtedly had enzymatic activity. But probably the earliest intentional example of an enzyme as a drug is the protecting activity of a parenterally administered enzyme against *Pneumococcus* infections by breaking down their protective polysaccharide capsules.[89] Following achievements include the treatment of fibrin clots by proteolysis with plasmin,[90] the anti-tumor activity of *L*-asparaginase,[91] and of course various replacement therapies for patients with enzyme deficiency conditions,[92] the latter of which are now so widely applied that most reviews can only cover specific diseases.[93–95] A general overview over the role of enzymes in medical therapy is covered in multiple review articles.[78,96–98] Examples include the topical application of proteolytic enzymes to burned skin, which can be used to facilitate the breakdown of denatured enzymes and thus replace traditional mechanical debridement methods.[99,100] Anti-cancer efforts focus either on depleting the blood stream of nutrients essential for cancer cells,[101,102] or removing metabolic products of chemotherapy to alleviate side effects.[103] Generally, treatment with polyethylene-glycol (PEGylation) has proven beneficial to the pharmacological properties of enzymes, prolonging their plasma lifetime and preventing premature lysis by proteases and kidney filtration.[104,105]

1.2.1 Protein Engineering

Unfortunately, natural enzymes do not always display the necessary traits required for selectively catalyzing reactions of non-native substrates, such as enhanced activity, stereo- and regioselectivity, and/or thermal or chemical stability, which are desirable for specific applications. But proteins are known to be highly evolvable,[106] a trait that is harnessed by protein engineers to enhance stability towards temperature[107] or organic solvents,[108] or to control enantio-, stereo- and regioselectivity, as has been shown in lipases, esterases, epoxide hydrolases, aldolases, nitrilases, aminotransferases, and oxidases including BAYER-VILLIGER and cytochrome P450 monooxygenases (CYPs).[109,110]

As a tool to address these shortcomings, directed evolution (*cf.* Figure 1-5) has emerged as one of the most promising methods in protein engineering.[109,111,112] It consists of repeated cycles of diversity generation by random or focused mutagenesis, which is always followed either by screening or selection of the properties to be improved. After the screening, (usually) the best mutant is isolated, and can be used as a starting point for the next iterative round.

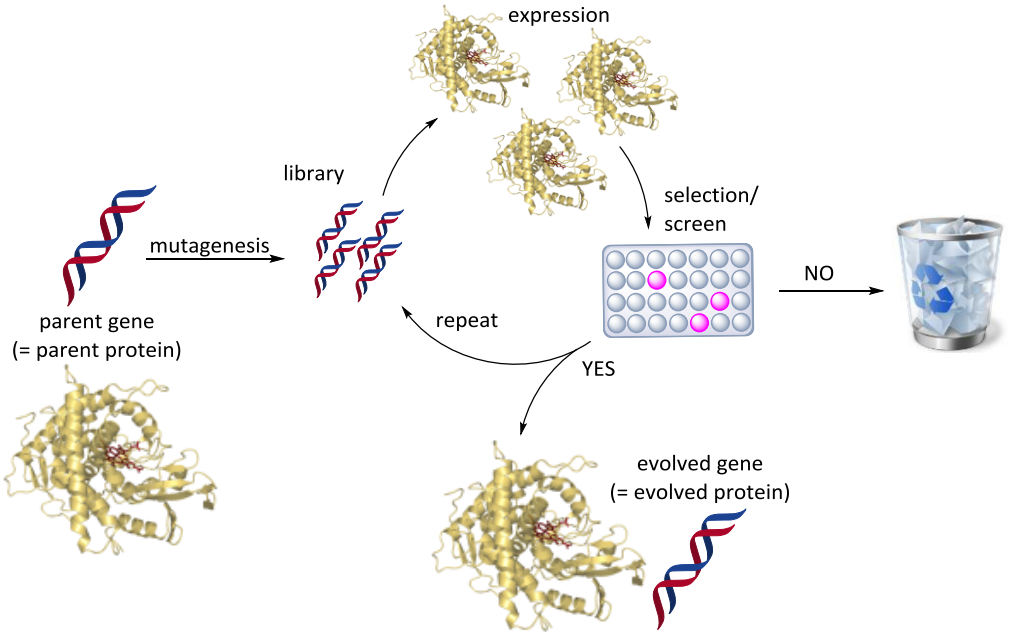

Figure 1-5. Iterative cycle of directed evolution. Starting from a parent gene usually found in nature, diversity is generated by mutagenesis. The resulting gene library is then transfected into a host species for expression, in order to select or screen for the desired trait. The identified improved variants can then be used as starting point for another iteration, until the desired performance is reached by the evolved protein.

Both a random and a targeted approach provide valuable solutions for different problems: While directed mutagenesis allows more efficient screening with smaller libraries, the introduction of random mutations (for example using error-prone PCR) is able to identify

new sites with an influence on performance.[113] Recent reviews for the advances of directed evolution are regularly reported, for example by LANE and SEELIG,[112] or DENARD *et al*.[111] An increasingly popular approach is the use of uncanonical, or non-natural amino acids, to expand nature's 23 building blocks to even more functionalities.[114,115] Computational methods can support the experimental efforts by either rationalizing the effects observed in hit mutants or finding new promising residues. For example, docking studies followed by molecular dynamics simulations can find the optimal position of a given substrate inside an enzyme pocket, visualizing interactions with the surrounding side chains and the backbone.[116–118] A different approach uses the transition state of the conversion instead of substrates as a starting point for redesigning enzymes.[119] With these methods combined, the resulting variants with their new properties have been changing industry and medicine,[109,120–122] for example allowing selective conversions on a large scale, or modifying drug properties: since 2013, more than half of the insulin doses prescribed in Germany are modified, either for longer half-life or quicker response.[123]

1.2.2 Cytochromes P450

Among the best studied enzymes is the large family of cytochrome P450 enzymes (CYPs), which get their name from the characteristic absorption band at 450 nm that stems from the CO-complex of their reduced prosthetic heme-*b* group. They are not only involved in the biosynthesis of steroids, terpenes, alkaloids, flavonoids and vitamins, but also responsible for the biggest part of drug metabolism in humans and the breakdown of environmental pollutants.[124] Of particular interest to synthetic organic chemistry is their ability to catalyze a variety of reactions, including epoxidation of C=C double bonds, *N*-oxidation, deamination, dehalogenation, and *N*-, *O*- and *S*-dealkylation.[125] Recently, a P450 enzyme was found to be able to catalyze bimolecular phenol coupling reactions.[126] The most common CYP-catalyzed reactions, however, are C-H activations of sp^2 and sp^3 hybridized carbon atoms, leading to epoxidation or hydroxylation. They have many applications in the chemical, pharmaceutical and environmental sectors,[125] biotechnology,[127–130] and more recently in medicine, *e.g.* for the development of MRI probes (magnetic resonance imaging).[131,132] Across species, they show a surprising degree of structural similarity, especially in the cofactor and substrate binding regions, even though overall sequence conservation in outlying regions is low.[133,134] CYPs used to be categorized into two classes; while class I depends on an NAD(P)H ferredoxin reductase as an electron source, class II CYPs partner up with an FAD- and FMN-containing NADPH-dependent cytochrome P450 reductase (CPR). However, the continuous discovery of different redox mechanisms in CYPs showed that these categories are by no means sufficient, leading to further differentiation. HANNEMANN *et al.* kept differences in domain topology of the electron shuttling mechanism as a criterion, but refined the system to

determine ten P450 classes I-X.[135] They differ in the reducing cofactor (NADH, NADPH or none at all), in the number of subunits involved (up to three) and whether some or all of the domains are present as a distinct enzyme or fused together. Another factor which is not part of this classification scheme is their solubility: while bacterial P450s are mostly present in the cytosol, their eukaryotic counterparts are usually membrane-bound.

To better harness the wide reaction space of P450s, a range of test reactions and activity assays have been published. The depletion of the cofactor NADPH can be directly followed photometrically,[136] allowing a good basis for kinetic estimations. For activity screens however, this slow progress is not sufficient, and TSOTSOU *et al.* modified the assay for higher throughput in microtiter plates (MTPs).[137] Increased sensitivity can be achieved with an assay based on the dealkylation of *p*-nitrophenoxycarboxylic acid derivatives (pNCAs), under formation of *p*-nitrophenolate, which can be detected by absorption at 410 nm.[138] This was also adapted for whole cells, rendering lysis steps obsolete.[139] For the investigation of reactions similar to the ones catalyzed by human P450s, indole oxidation with indigo formation has proven to be a good estimate, allowing a colorimetric read-out of colonies.[140] IC_{50} values for P450s or inhibitor strength can be investigated using coumarin-based fluorescence assays.[141,142] Fluorescence assays based on the dealkylation of allyloxyresorufin allow activity and affinity screenings in MTPs or via continuous-flow, but no direct analysis of other substrates.[143] To determine exact values for turnover or product specificity, mostly chromatographic methods like gas chromatography (GC) or high performance liquid chromatography (HPLC) are being used.

The case of CYP102A1 ($P450_{BM3}$)

The first described P450 enzyme with fused redox subunits is the flavocytochrome $P450_{BM3}$ (CYP102A1), a self-sufficient and soluble fatty acid hydroxylase from *Bacillus megaterium*.[144] This particularly interesting class VIII fusion system carries its own FMN/FAD reductase domain,[145] and thus only depends on the presence of its cofactors, NADPH and oxygen.

Because of its solubility and self-sufficiency, $P450_{BM3}$ has been intensely studied, and recombinant expression was achieved by WEN and FULCO in 1987.[146] Various efforts over the course of almost three decades have shown that it is an immensely valuable and versatile candidate for enzyme engineering and directed evolution, yielding highly active and selective mutants for different applications.[147] Its similarity to human P450s also make it a valuable tool for medicinal chemists.[148] General overviews can be found by WHITEHOUSE,[149] GUENGERICH,[150] RENAULT,[151] and MCINTOSH.[152]

Figure 1-6 shows a structural model. In its active form, $P450_{BM3}$ is present as a dimer (P450 subdomain only, panel A).[153] Since there is no published full structure of all subunits, panel B) shows a potential model of the monomer, which was created by aligning $P450_{BM3}$ and its FMN domain with a homologue. Together with its oxidase and FMN/FAD subdomains the

monomer amounts to a size of 119 kDa. The narrow connection between FMN and FAD acts as a hinge region, allowing the enzyme to change between an open and closed conformation, thus enabling electron transfer.[154]

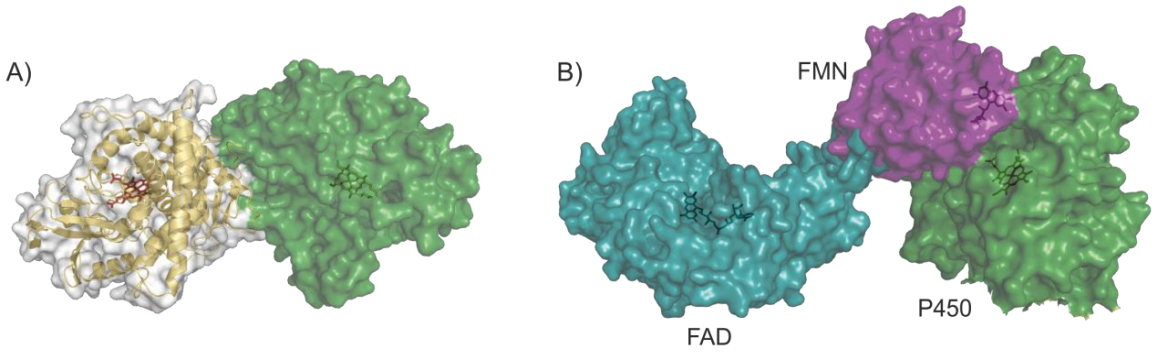

Figure 1-6. Model of $P450_{BM3}$, a class VIII oxidoreductase. A) Dimerization is necessary for oxygenase activity (PDB-ID 1BVY[155]); B) Potential model of the three subdomains. The P450 and FMN subunit of BM3 (green and purple, respectively; PDB-ID 1BVY) were aligned with the FAD subdomain of a yeast–human NADPH cytochrome P450 reductase (blue, PDB-ID 3FJO[156]) along their FMN domain. Reproduced in analogy to AIGRAIN *et al.*[154]

Tackling the persisting challenge[157] of efficiently controlling selectivity in CYPs, the REETZ lab recently reported the regio- and stereoselective hydroxylation of many diverse substrates, including small-functionalized molecules,[158] tetralones,[159] acyloins,[160] and steroids,[161,162] while other groups expanded the reaction range to terpenes.[163,164] Since the natively used cofactor NADPH decomposes quickly in aqueous solution and is rather expensive, there are efforts towards the development of alternative electron sources: Changing the recognition site towards better acceptance of NADH,[165] or replacing the reductase domain by photoactive metal complexes,[129,166] an organic photosensitizer,[167] or electrochemical reduction,[168,169] are only a few examples.

Mechanism

Despite the wide range of transformations they catalyze, the model reaction of P450 oxygenases still is the formal insertion of one oxygen atom into a CH-bond. The overall mechanism is shown in Figure 1-7. The oxidation process in CYPs occurs at a cysteine-bound prosthetic heme group, whose active iron center is present in its low-spin ferric form in the resting state of the enzyme (1). Upon binding of the substrate (2), the iron changes from a low- to high-spin electronic configuration, and is subsequently reduced to its ferrous state (3). The nicotinamide cofactor NADPH (or NADH) is utilized as an electron source. Molecular oxygen binds to the iron (4), and undergoes reductive scission. In the process, the center is again reduced, and after the uptake of two protons, the oxygen-oxygen bond is cleaved. One oxygen atom is released as a water molecule, forming the green ferryl-oxo intermediate "Compound I" (7) with its oxidized iron(IV) center. This state responsible for

the actual conversion step had long been elusive, and could only be isolated and characterized in 2010 by RITTLE and GREEN.[170] Hydrogen atom transfer from the substrate yields Compound II (8), which then transfers its hydroxyl group to the substrate radical in a rebound mechanism. Thus, the ferric iron state is regenerated (9), allowing the oxidized product to dissociate and be replaced by water, returning the enzyme to its resting state (1).[171]

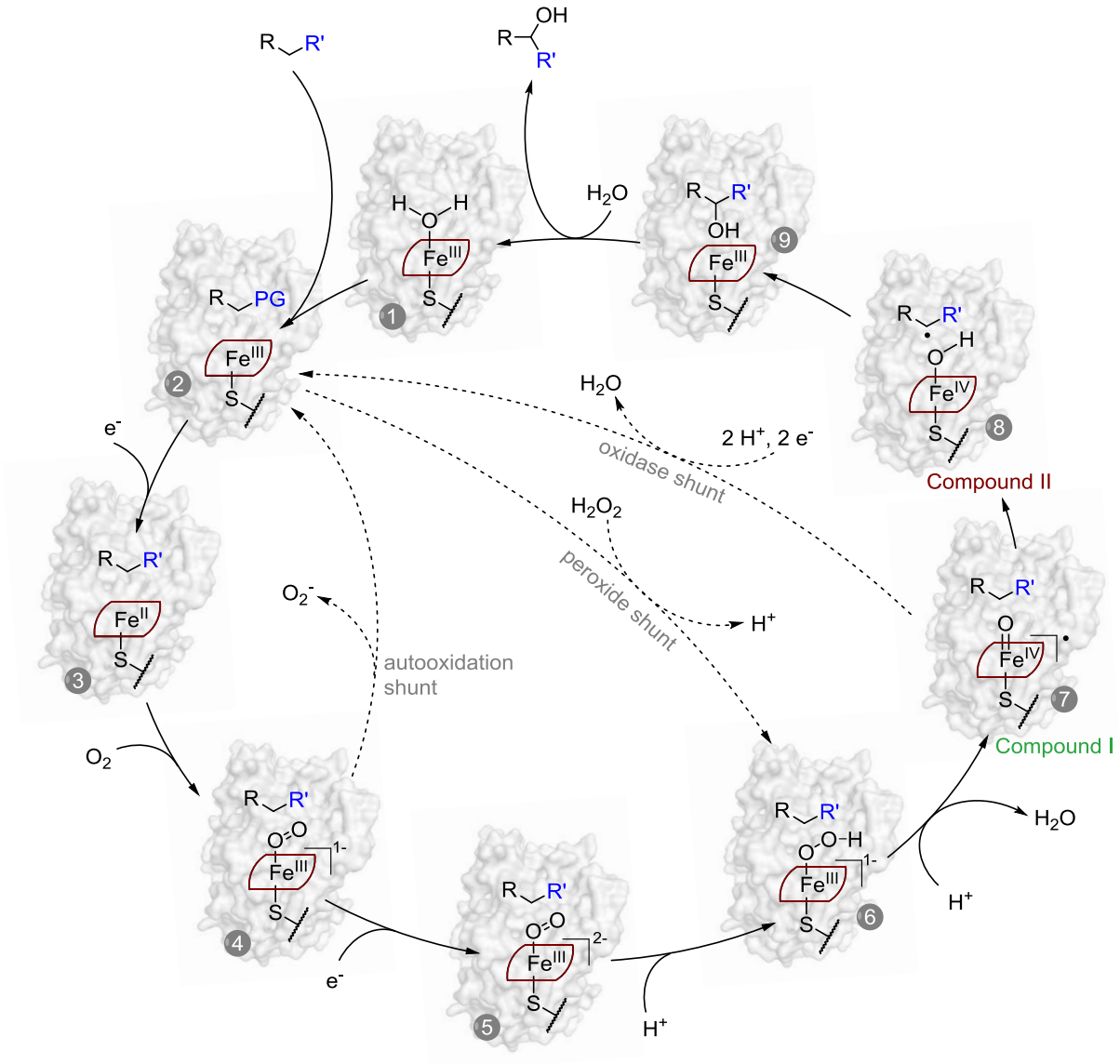

Figure 1-7. Catalytic cycle of mono-oxidation by CYPs. The substrate replaces water upon binding to the active site with its heme group. Under reduction by NADPH, a dioxygen molecule is cleaved and one atom liberated as water, while the other is transferred to the substrate in a radical rebound mechanism.

Three shunt pathways exist, cutting through the catalytic cycle. Two of these undermine the efficiency of substrate turnover: a superoxide anion can be released after the first reduction step (autooxidation shunt), or Compound I can be reduced, releasing the bound oxygen

atom as water (oxidase shunt), in both cases without any reaction with the substrate. However the third pathway, termed peroxidase shunt, allows to generate compound I directly from hydrogen peroxide, without the need for other cofactors. There have even been efforts to increase the feasibility of this shunt to completely replace the additional oxidizing agent and drive product formation purely with H_2O_2.[172]

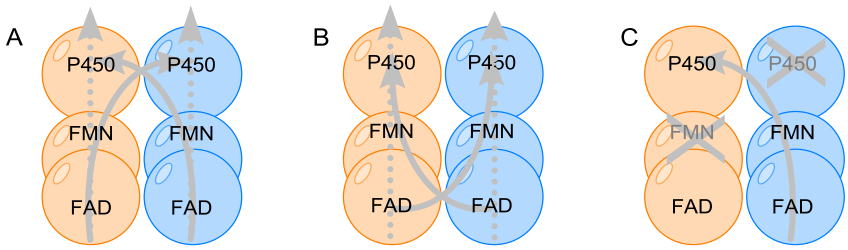

Figure 1-8. Possible electron transfer pathways in $P450_{BM3}$ between monomers and subdomains. A) crossing monomers between FMN and P450 domains; B) crossing monomers between FAD and FMN domains; C) experimental approach for the investigation of the pathway using two mutants with either an inactivated FMN or P450 domain.

The electronic mechanism has long been debated, with three main pathways being discussed (*cf*. Figure 1-8): The first is the intra-monomer electron transfer (dashed lines), from FAD via FMN to heme; but although never fully ruled out, this cannot be the only option, since mutants with one inactivated domain (FMN or heme, as in case C) can regain catalytic activity upon co-incubation.[173,174] This left two options to cross between monomers, either from FMN^1 to $heme^2$ (case A), or from FAD^1 to FMN^2 (case B). Further studies were able to show conclusively that the most likely mechanism involves an electron transfer along FAD^1-FMN^1-$heme^2$ (case A).[165]

In any case, the transfer across multiple centers requires the orchestrated interaction of various sites, making the process vulnerable to side reactions. These leakage or uncoupling processes can occur anywhere on the way from the FAD to the heme center, or inside the catalytic cycle (shunt pathways, see above). Since especially mutants are often prone to higher leak rates,[175] this parameter together with the overall coupling efficiency, are important parts of cytochrome characterization and have been intensely studied.[176]

1.3 Drug Delivery

The first question in drug development is undoubtedly the activity towards the target, closely followed by the need to rule out side effects. However, the next important problem to be solved is always how to get the drug into the body, and to its site of action. A lot of drugs would pass right through the body if given orally, either without being taken up because of low bioavailability or because they are deactivated by digestion. If they do make their way into the blood stream, they first pass through the liver, where most of the enzymes are produced that are responsible for the decomposition of complex compounds – P450s among the most important – so that a high percentage of drugs is already inactivated before they can reach their target. Depending on where the drug's final site of action is located, there can be additional obstacles, for example cell membranes or the blood brain barrier. Some other effects have to be considered, even once the drug has successfully entered the bloodstream, which can be detrimental for its activity, ranging from kidney filtration, uptake by phagocytes, or aggregation with serum proteins, to premature enzymatic degradation.[177,178]

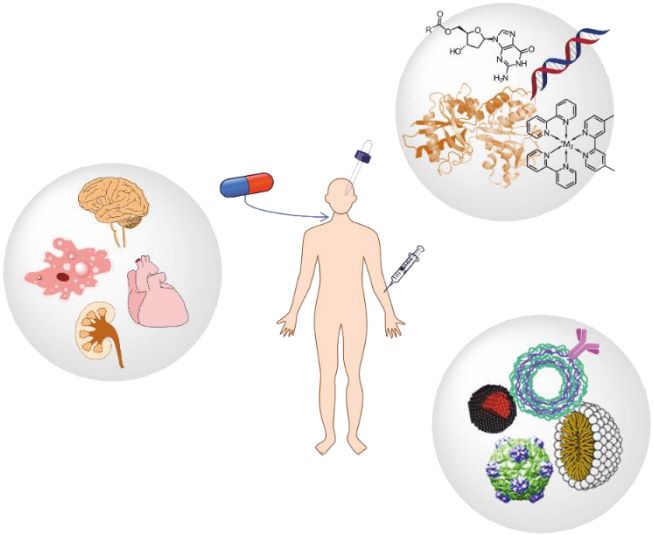

Figure 1-9. Aspects of drug delivery. Around the central aspect of administration, the target tissue (left), the nature of the compound (top) and the molecular delivery system (bottom) are equally important for successful treatment.

To address these issues in cases where the pure drug is not effective enough, different methods have been developed to overcome these issues. The ideal delivery system has a range of characteristic features: it has to be stable in dosage form, protect the active ingredient until it arrives at the site of action, control localization and release, while minimizing toxicity and side effects. At the same time, it has to be biodegradable, and of course should be cheap and easy in its preparation. This important but multi-facetted problem is recognized by the scientific community, and as a result, a vast amount of research is being conducted on this field from very different perspectives – chemistry, biology,

medicine, pharmacy, physics, or material sciences. For every drug and its purpose, the delivery system has to be tailored to suit the particular needs of the affliction and the patient, which is the main reason for ever ongoing developments in the area. Reviews covering the topic of drug delivery in general are available for example by CROMMELIN,[179] MARTINHO[180] or KAPARISSIDES.[181] The most common approaches can be classified according to different principles, which are equally important for medical treatment (*cf*. Figure 1-9). Most obvious for the patient is the mechanism of administration, with different options available, depending on the targeted tissue (e.g. oral, subcutaneous, transdermal, intravenous, pulmonary, or intraocular). The chemical nature and molecular weight of the drug has a large influence on stability and distribution in the body – a small organic molecule will behave inherently different from nucleic acids or a protein. Thus, the packing of the drug on a molecular level has to be tailored accordingly, options ranging from pure solutions via encapsulation to antibody-tagging. Table 1-1 gives on overview over different methods with examples, some of which will be addressed in more detail below.

Table 1-1. Overview and comparison of different drug delivery concepts.

Vesicle Class/ Method	Pro	Con	Examples	References
Prodrugs	specifically tailored, tuning of physico-chemical properties	only suitable for small molecules, usually less stable than parent compounds	*Aspirin*, *Fingolimod*; enhanced solubility and uptake, extra functions	CLAS[182]
Micelles	improved circulation time, use of EPR effect, lowered toxicity	subject to equilibrium – dissolution of micelles, interaction with proteins	*cis*-Platin	NISHIYAMA[183]
Liposomes	tunable physico-chemical properties, functionality, cheap	low encapsulated load, instability in bloodstream, burst release, side effects	siRNA delivery, resulting in hepatic gene silencing	SEMPLE[184]
Polymeric Nanoparticles	tunable, low inter-action with proteins, protection of cargo	slow biodegradation	cytostatic agent *Vinorelbine* against breast cancer	BAHADORI[185]
Polyelectrolyte Capsules	tunable, easy addition of functional elements for targeting or release control	toxicity, low biocompatibility/ degradability, protein interaction	antigen delivery	DE KOKER[186]
Viral Vectors	self-assembly, differently sized packing molecules, evolved for delivery	immune reaction depending on expressed antigens	delivery of a zinc phthalocyanine for PDT	MA[187]

1.3.1 Prodrugs

The most straightforward way to implement improvements to a drug, from a chemist's point of view, is to modify the actual drug on a molecular level, creating a prodrug which is metabolically converted into its active form by the body itself, by either attaching a caging group or using a precursor compound. The prodrug strategy is quite common, with a market share of 15% in 2009,[188] since it allows to improve a wide array of properties. The following examples (*cf.* Scheme 1-1) are only a small glance at the available range of options, but a recent comprehensive review was published by CLAS *et al.*[182]

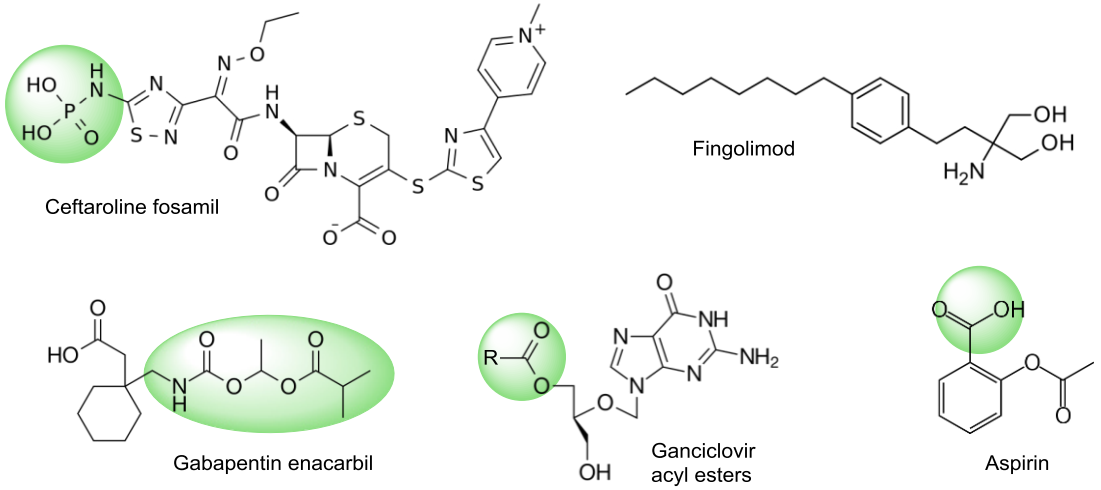

Scheme 1-1. Examples for prodrugs with different changes to crucial parameters. Enhanced moieties compared to their parent compounds are highlighted.

A major issue to be addressed is often solubility or permeability, as in the case of *Ceftaroline fosamil*, an antibiotic against resistant dermal infections.[189] *Fingolimod* was adapted to be activated by the body instead of suffering inactivation, and alleviates multiple sclerosis upon phosphorylation.[190] *Gabapentin enacarbil*, prescribed against restless leg syndrome, was optimized for uptake by directly addressing transporters.[191] Even targeting to tissues is possible at this level, by tailoring metabolic mechanisms as with acyl esters of *Ganciclovir*, which are an ophthalmic antiviral agent. Probably the most common prodrug, and a compound that seldom comes to mind, is *Aspirin*, which adds a secondary function with an additional group: Salicylate by itself only has an analgesic effect. But the common derivative is a lot more potent, adding anti-inflammatory and antipyretic properties. It can covalently transfer an acetyl residue to cyclooxygenase (COX), which is used for prostaglandin biosynthesis, thus irreversibly inhibiting the enzyme, and releasing salicylate in the process.[192]

1.3.2 Nanoparticles

However, the effect of a small side chain can diminish when added to a larger drug. For this reason, larger packaging systems based on nanoparticles are being developed.
The term covers a large family of complex structures (*cf.* Figure 1-10), and basically the only aspect they have in common is their size, which lies between 1 and 100 nm. The simplest ones are inorganic nanoparticles, small spheres of uniform composition of metals, salts or silica. More elaborate versions include defined alloys or core-shell structures. Nanoparticles made from lipids can have two major shapes, depending on the synthesis conditions: single-layered micelles and double-layered liposomes. If polymers are used, especially in the case of block-copolymers, complex formations can be achieved through differences in hydrophobicity. Hollow structures or spheres of polymer matrix, in which drugs can be embedded, or also rod-like shapes, are possible. Polyelectrolytes can be used to create layered hollow capsules, which are easily modified by embedding further functional groups inside the outer membrane. An especially versatile material is carbon, which can form different ordered structures in addition to spherical nanoparticles, like tubes, cones, or fullerenes. Adopted from nature are virus particles, which typically consist of several hundreds to thousands of protein molecules that self-assemble to form a hollow scaffold packaging the viral nucleic acid. These can be emptied and used to deliver various cargoes.
All of these can be tuned by composition and synthesis conditions, or be modified afterwards by attaching functional groups or ligands to their surface. Hybrid particles from different classes can also be formed, often with a layered structure. Due to the immensely active research in the field of applying nanoparticles for medical uses, a large number of review articles on the topic is published every year. Recent examples have been published by COOPER,[193] SUN[194] or LEE.[195]
The simplest nanoparticles that can be used for drug delivery purposes are micelles, which consist of a single lipid layer and can keep hydrophobic molecules inside. In one example, *cis*-Platin loaded micelles showed longer circulation in blood compared with the free drug, and improved accumulation in the tumor when tested on mice with a human lung cancer xenograft.[183] A bit larger, but made from similar compounds, are liposomes. They are already quite common and approved for various treatments.[196] An example of a very successful application of liposomes is the stable nucleic acid lipid particle (SNALP), which can for example be used to deliver strands of small interfering RNAs (siRNA), with a specific sequence designed to silence a liver gene.[184] Instead of lipids, larger constructs like polymers can be used for self-assembling nanoparticles. Since there is a plethora of monomers to choose from, polymeric particles are easily tunable and have been used for a wide range of drug types, from DNA to metal complexes. In comparison with liposomes, they are more stable and not in equilibrium with monomers, which makes it less likely for them to interact with plasma proteins while giving them an even longer half-life. Their dense packing also

protects their cargo against outer influences like changes of pH value or reactive oxygen species. Their long half-life can pose problems in terms of biodegradability, but tailored polymers are already addressing this issue.[197] *Vinorelbine*, an anti-mitotic chemotherapy drug that is used against some types of cancer, showed improved IC_{50} values in a polymer formulation.[185] Charged polyelectrolytes can be used in addition to neutral polymers. They are wrapped around a template, layer-by-layer with opposite charges, before the core is dissolved. The choice of electrolytes determines the properties, but other modifications can be introduced into the layers and add different functions. Unfortunately, their surface charge can put them in danger of interacting with serum proteins.[198] They have been used to deliver antigens for vaccination to dendritic cells.[186]

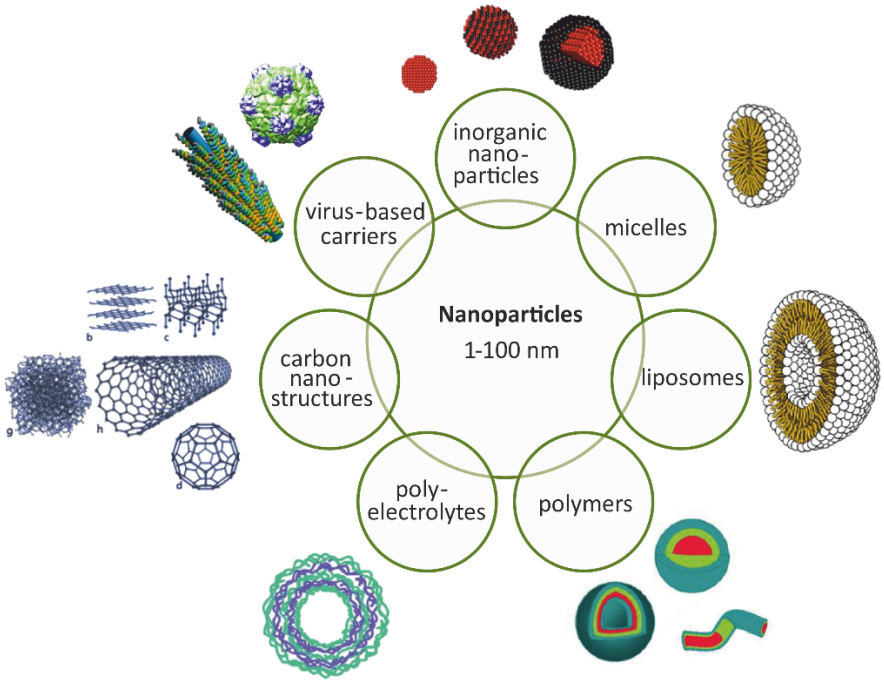

Figure 1-10. Classification of nanoparticles based on their structure and materials.

As always in science, nature already had the idea of using nanoparticles for cellular delivery long before us – we call them viruses. They have been shown to allow dissassembly by pH changes, emptying of the original cargo, and closing them again around other compounds, like hydrophobic drugs or oligonucleotides. For example, a zinc phthalocyanine was packed inside, which generates reactive oxygen species upon irradiation.[187]

The delivery of proteins and enzymes is an especially formidable challenge, due to the size and various sensitivity issues. However, various approaches have been reported, including chitosan-[199] or silica nanoparticles[200], modified nanocapsules,[201] or again virus-based methods.[202] Conjugation to polymers has been suggested to allow oral application of certain enzymes.[203]. A recent review for therapeutic delivery focusing on protein-based nanoparticles was published by HERRERA ESTRADA *et al*.[204]

1.3.3 Targeting

Targeting a drug to its site of action is not a new concept – it dates back to the early 20th century, when PAUL EHRLICH managed to develop a cure for syphilis that selectively attacked *Treponema pallidum* inside its human host:[205] *Salvarsan* was the first chemical compound rationally selected by screening and chosen for the treatment of a specific pathogen. His dream was what he called *Zauberkugel* (magic bullet) in reference to an opera, where a man makes a pact with the devil for a bullet that will automatically find its target, so he could win his task and marry his bride. EHRLICH wanted the same for his research: to find one treatment that could selectively kill all pathogens without having any side effects. Even today, it does not seem likely that this will ever be possible, but progress has been made with selectively targeting certain tissues by attaching ligands to the drug or a vesicle that can be recognized by certain cells. Targeting not only to the right tissue but also to the right compartments inside cells is crucial for the activity of the treatment (*cf.* Figure 1-11).

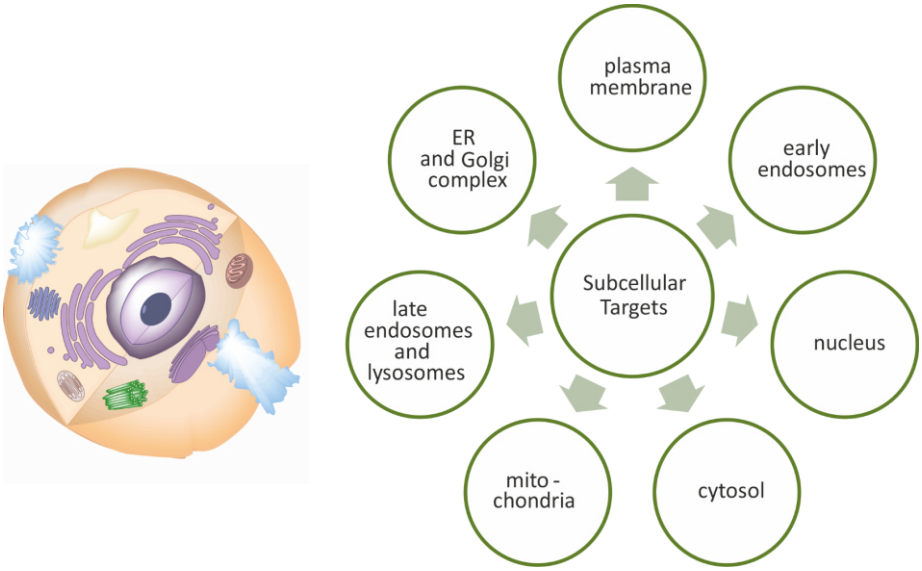

Figure 1-11. Subcellular targets in a eukaryotic cell.

An acid-labile drug for example will be degraded rapidly if it is delivered to the lysosome, and a transcriptional inhibitor cannot fulfil its task if it does not reach the nucleus. For this reason, it depends again on the mechanism of action and the nature of the drug to determine which kind of targeted delivery should be chosen.

A lot of this research is being conducted with regard to cancer, which is the number 2 death cause in developed countries, second only to heart diseases. The special properties of vessels nourishing tumors are very useful, opening a door for medical chemists: Tumors and also inflamed tissue often show an unnaturally high permeability of the vasculature. Macromolecular drugs with a long circulating half-life can accumulate here, depending on the biophysicochemical properties. Especially tumors often lack functional lymphatic

drainage, so that once arrived, the macromolecules will stay in the tissue for prolonged times. This is called the enhanced permeability and retention effect, short EPR.[178,206] This so-called passive targeting relies on the native characteristics of the target tissue to accumulate the drug. Active targeting, on the contrary, adds a structure to the compound or delivery vesicle that can only be recognized by certain cells through selective interaction with receptors, and thus enhances the uptake. This can only be achieved after the compound has reached the tissue in question. Both methods can be beautifully combined, especially since the modification of nanoparticles with their modular build is quite easy. Review articles have been published by BERTRAND,[207] ARIAS,[208] or NARANG.[209] Table 1-2 gives an overview over different methods.

Table 1-2. Overview of targeting methods and examples for their application.

Ligand Class/ Method	**Pro**	**Con**	**Example**	**References**
Small Molecules	small, cheap, robust	little specificity	folate-mediated delivery of anticancer drugs	LICCIARDI[210]
Monoclonal Antibodies (Mab)	high specificity	large, complex, expensive, short half-life, Immune reactions possible	antibody drug conjugates already used in medicine	FIRER[211]
Peptides/ Proteins	specific, small, low immunogenicity, stable, easy synthesis, library techniques established	possible interactions with other proteins	transferrin-linked *Doxorubicin*	ŁUBGAN[212]
Aptamers	selective, tailored (SELEX), suitable for all sizes of targets, easy synthesis and modification, rapid tissue penetration	degradable by RNases and DNases (can be overcome with expanded alphabet -> toxicity?)	aptamers binding thrombine, biotin, cocaine	NIX[213] NEVES[214] LONG[215]
Remotely Controlled Systems	spatial and/or temporal control, monitoring, adaptivity to situation	expensive equipment for treatment, confined to magnetic field shape	magnetic nanoparticles, light triggered release	DEL PINO[216] OCHS[217]

Folic acid for example is a water soluble vitamin, which is essential for nucleotide biosynthesis and one-electron transfer reactions. For this reason, the corresponding folate receptor is highly overexpressed in many malignant tissues. The receptor keeps its high affinity for it even after derivatization via its γ-carboxylic acid group and folate can thus be used to target these tissues. LICCIARDI *et al*. reported the development of a formulation to deliver hydrophobic antitumor drugs bound in polymeric nanoparticles.[210] One effect of

folate as a targeting ligand is the subcellular adressation to a recycling center instead of a lysosome, which reduces the risk of premature degradation of the active compound.
Another class with higher molecular weight are antibodies – they have been used as drugs on their own for some decades, but they are also valuable as targeting agents, and some formulations are already in use or in clinical studies.[211] The problem is that they are complex and expensive, show a short half-life, and sometimes lead to immune reactions.[218] For this reason, antibody fragments are studied, but other proteins and peptides are also promising possibilities.
A different, but highly specific class of compounds are aptamers. They are either DNA- or RNA-oliconucleotides, which fold into unique conformations depending on their sequence, and can be tailored to selectively identify almost any compound, from small molecules to large proteins.[213–215] An important tool for their development is called SELEX (*s*ystematic *e*volution of *l*igands by *ex*ponential enrichment), a screening technique that depends on iterations of amplification from a large combinatorial library.[219] More than 200 aptamers have already been isolated and can be used as targeting ligands in nanoparticle drug delivery. The implications for chemical biology of aptamers in general and this technique in particular have been pointed out repeatedly.[220,221]

Not quite drug-targeting in the sense used above, but too important to leave unmentioned, are so-called gene-targeting techniques:
Antisense oligonucleotides[222,223] or siRNAs[224] (as briefly mentioned above) can be used to regulate protein expression by either directly blocking mRNAs or recruiting cell-internal degradation machinery. A recent comprehensive review on the topic covering current clinical developments was published by McClorey and Wood.[225]
The very promising, more radical gene-targeting technique CRISPR/Cas has been developed recently, which allows the introduction of stable, heritable changes into an organism's genome.[226] Originally, the mechanism is used as a defense strategy against viral DNA, providing bacteria with acquired immunity. The process is based on programmable nucleases like Cas9, which rely on CRISPR RNAs (*c*lustered *r*egularly *i*nterspaced *s*hort *p*alindromic *r*epeats) to guide them to their target sequence. Modifying these guide-RNAs allows the targeted exchange of a sequence in any genomic location, resulting in a versatile gene editing method.[227] With this unique ability to permanently alter genes in a living organism, potential cures for genetic diseases may soon be within reach, although further research and ethical debates are first necessary. An international summit of leading scientists was held in late 2015, with formal ethical guidelines to be expected in 2016.[228] In the meantime, research on the topic is moving fast, and a large number of current reviews can be found across the life sciences. General overviews were published for example by Doudna & Chapentier[229] or Hsu *et al*.[230]

Apart from the last cases, these are all possible ways to attach some type of ligand to the drug or the vesicle, so that it might arrive at the right place. The other option is external control, where the physician can choose where to deliver the drug inside the body and at what time to release it. An interesting approach is the use of magnetic nanoparticles, which can be steered by an external magnetic field. In a report by DEL PINO *et al*., magnetic nanoparticles were loaded with siRNA for gene silencing, and added to a flow reactor with cultured GFP-expressing HeLa cells.[216] When a magnet was brought close to the setup, the particles accumulated there, and caused only cells in proximity to shut down their GFP synthesis.

In a different strategy, light can be used to trigger the release of cargo. For this application, gold nanoparticles are embedded in the shell of polyelectrolyte capsules. They can be excited by IR light of a certain wavelength, and the plasmonic vibrations of the particles will then heat the shell in a sharply defined area, breaking the capsule and releasing its content. This has been demonstrated by PARAK'S group, who showed that they can open two different kinds of capsules sequentially, releasing an enzyme and its substrate and follow the reaction by fluorescence microcopy.[217] Since in photodynamic therapy, irradiation is already used routinely, it would be comparatively easy to implement this kind of reaction in everyday treatments.

With ever more methods being developed, there are virtually no limits on the possible delivery and targeting combinations that can be developed from the different approaches mentioned above, all catering to different specific aspects of the cargo in question. A general overview on active drug release systems was published by KIRYUKHIN *et al*.,[231] while WEISER *et al*. are focusing on limitations and models of the field.[232]

2 Objective

This thesis focuses on the development of an enzyme-based, catalytic bioorthogonal system for the activation of caged compounds *in vivo*, using a modular toolbox (*cf.* Figure 2-1): at the core of the concept are small-molecules (e.g. dyes, probes or pro-drugs) that can be inactivated by caging with a tailored protection group (A). These will be activated using a catalyst (B), which we intend to develop for the efficient turnover in a physiological environment.

Ultimately, we envision to establish a targeted delivery system (C) as a carrier of the catalyst to its intended site of action, so that the method can be used within living cells or organisms. This endeavor can be split into three separate steps, which are described in detail below.

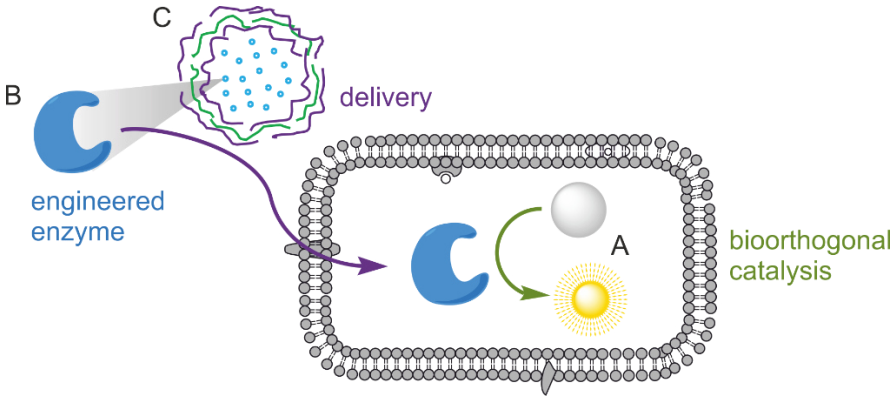

Figure 2-1. Concept of the bioorthogonal enzymatic activation of caged compounds. The substrate A) is activated by uncaging, a reaction which is catalyzed by an engineered enzyme B). Delivery system C) brings the catalyst inside the cell to its intended site of action.

A

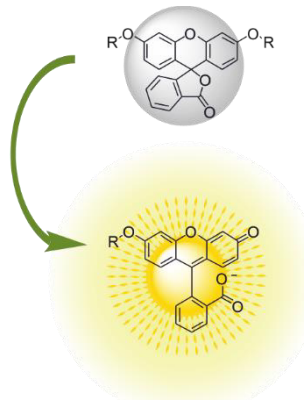

Initially, protection groups have to be identified, ideally featuring bioorthogonality, which means that the protection group is completely stable in the biological environment and is cleaved efficiently and selectively solely by the engineered enzyme of choice. We chose different ether groups as alcohol protection groups, since they are particularly stable under physiological conditions, but can be cleaved by some family members of cytochrome P450 monooxygenases (*cf.* Figure 2-2). An adjacent methylene group of the substrate is subjected to oxygen insertion, yielding an intermediate hemiacetal. This chemical species is hydrolytically unstable and undergoes spontaneous decomposition in aqueous media, liberating the reactivated target molecule R-OH, which carries a free hydroxyl group and exhibits for example fluorescence and/or bioactivity (orange). The protecting moiety (PG, blue) is released with an aldehyde functional group.

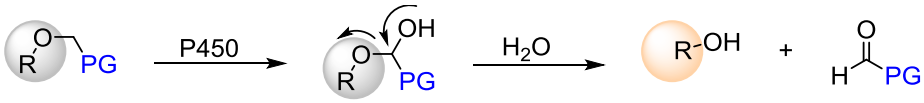

Figure 2-2. Mechanism of the ether-deprotection reaction catalyzed by P450 mutants. The insertion of a single oxygen atom at the methylene group creates an unstable hemi-acetal, which in turn undergoes spontaneous hydrolysis in aqueous media.

Choosing the right substituents for the protection group, we hypothesize that they are not recognized as substrates by natural enzymes but only by engineered CYPs. To further minimize the effort and simplify product analysis, a direct fluorescence read-out will be used. Caged fluorophores will be synthesized, using different protection groups, and these will be tested as substrates for the enzyme variants.

B

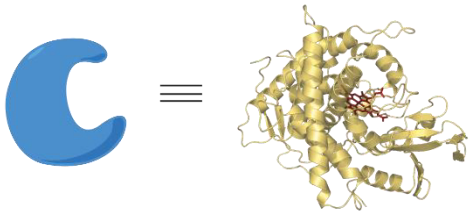

Given the performance issues typically observed in chemically or light-induced uncaging reactions,[18,37,45] our goal is to use an engineered "bioorthogonal enzyme" instead, to keep any interference with the cellular environment to a minimum. For the development of the biocatalyst, a collaboration with the REETZ lab with their long expertise in protein engineering provides the necessary knowledge. The creation of mutant libraries by directed evolution can be achieved much faster now than only a few years ago, due to advances in methodologies[162] and systematic reduction of unnecessary work, for example by using reduced alphabets.[110] Nevertheless, it is in everybody's interest to get as much as possible out of the work involved in the creation of libraries and collections. Our plan, therefore, is to screen already existing libraries of evolved $P450_{BM3}$ variants for our different, formerly unintended application. This allows the reduction of both

time and money spent, especially since in the case of collections statistically occurring duplicates are already ruled out.

C

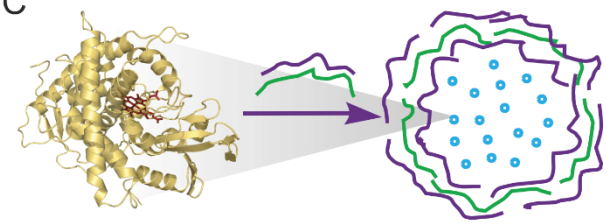

Once the deprotection system is working, we plan to implement a microparticle-based delivery system in collaboration with the PARAK lab. A range of examples for protein delivery to mammalian cells exist,[233–235] and OCHS *et al.* have previously published examples of encapsulation and triggered release.[217] The modular build of these capsules readily allows the fine-tuning of their properties. The stability of the biocatalyst under different conditions will be investigated, so that the delivery system can be adapted to its needs.

3 Results and Discussion

3.1 Substrate Synthesis

For proof-of-principle studies, the well-known fluorescent dye fluorescein (**1**) was used as parent compound for the design of suitable caged substrates to be deprotected by P450$_{BM3}$ mutants.

In solution, fluorescein is present as a complex mixture of seven prototropic forms.[236] At pH values around 3, the non-fluorescent spiro-lactone form is most abundant (left in Scheme 3-1), while at higher pH values above 7 the highly fluorescent dianion is the only species (right). The compound can be fixed in its spiro form by alkylation of both hydroxyl groups, thus suppressing fluorescence.

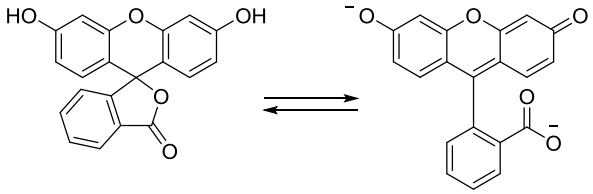

Scheme 3-1. pH-Dependent equilibrium between the colorless spiro-lactone (left) and the fluorescent dianionic species (right) of fluorescein. Alkylation of the hydroxyl groups can lock the compound in its spiro form, thus suppressing fluorescence.

The choice of protection groups is crucial to the success of the concept, so a small selection of different options was chosen as a starting point: allyl and propargyl, since similar positions are known to be favored in hydroxylation reactions by P450$_{BM3}$ but not by other cytochromes.[237–239] Alkynes are also known to act as suicide inhibitors on some P450s,[240,241] which could help to put higher demands on the enzyme, thus reducing the risk of uncaging

by natural variants. Following a recent study by RUFF *et al*. who used coumarin derivatives as P450 probes,[242] benzyl was selected as a third alternative.

Fluorescein derivatives were obtained via a WILLIAMSON ether synthesis, following a protocol by RAJASEKAR *et al*.[243] Reaction conditions are shown in Scheme 3-2: First, the fluorophore was deprotonated with potassium carbonate in dimethyl formamide (DMF), before a primary alkyl bromide carrying the protection group was added to the reaction mixture to yield the desired ether via an S_N2 reaction in moderate yields. Enough substrate for the following screening procedures was obtained, so that no optimization of the synthesis was performed.

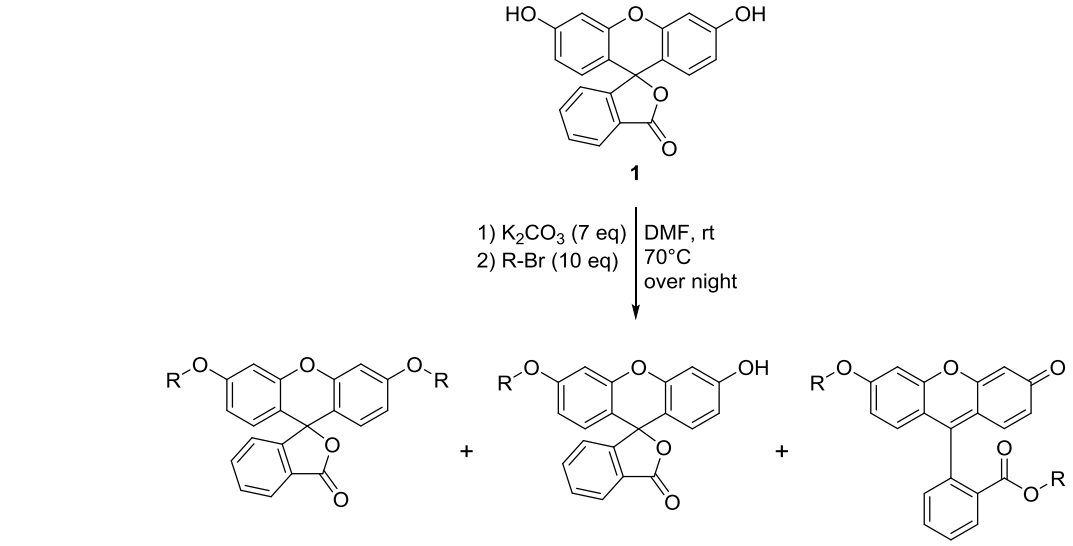

Scheme 3-2. Synthesis of fluorescein diethers **1a-1c** via WILLIAMSON ether synthesis. After deprotonation with carbonate, the hydroxyl groups are coupled to the corresponding bromide in an S_N2 reaction. In the case of the propargyl substituent, side products **1a'** and **1a''** of the alkylation reaction were observed.

In the case of the propargyl caging group, side products were observed, which can be attributed to the reaction with only one equivalent of bromide resulting in the formation of the corresponding mono-ether, and the reaction of the acid moiety instead of one hydroxyl group, leading to the ether-ester derivative. In contrast to the colorless diether, both byproducts are colored and show fluorescence, albeit at lower intensity than the parent compound. Derivatives can readily be separated by flash column chromatography over silica.

3.2 Screening Method

3.2.1 Concept

The screening method was adapted for analysis by fluorescence from known protocols.[161] For the substrate reaction, a cofactor recycling system is employed, generating NADPH *in situ* from $NADP^+$, with glucose dehydrogenase (GDH) as a catalyst and glucose as reducing agent, as shown in Figure 3-1.[244] Not only does this routine lower the cost by preventing the need to handle the unstable and expensive compound NADPH, but this system also ensures a continuous supply of the cofactor in the reaction mix, allowing higher overall turnover and increased signal intensities.

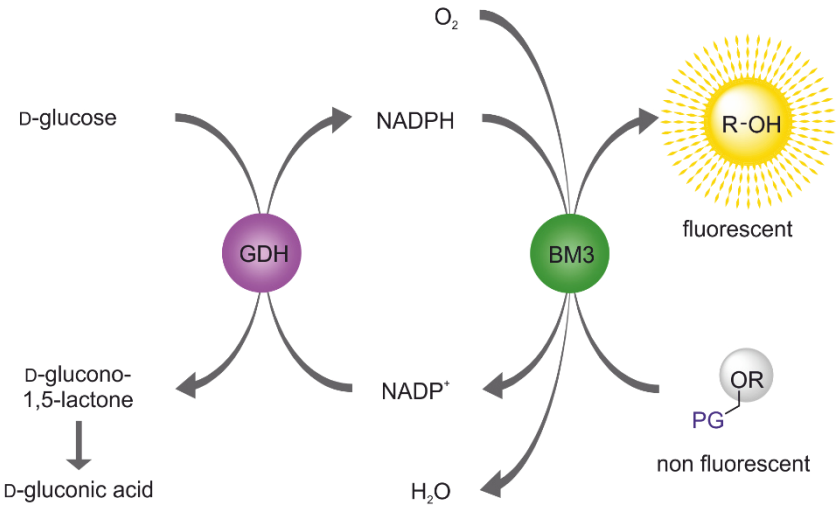

Figure 3-1. Cofactor recycling system for the *in situ* generation of NADPH, for $P450_{BM3}$-catalyzed deprotection reactions. $NADP^+$ is converted to NADPH by GDH, under oxidation of D-glucose. The cofactor can then be used by $P450_{BM3}$ for the hydroxylation of substrates.

Changing the analysis method from chromatography to fluorometry in this case highly reduces cost and workload of the screening, since time-consuming steps such as extraction, filtration and chromatographic separation are replaced by simply transferring the reaction mix into a black flat-bottom 96-well microtiter plate (MTP) and measuring either spectra or single-point results. To find the best conditions for analysis, emission and excitation spectra of the parent compound were measured, maxima determined and a suitable cut-off filter identified. These settings were used in all following experiments, and are shown in Table 5-1.

To identify the most suitable working concentrations of enzyme and substrates, test reactions were carried out on substrates **1a-c** with 11 purified mutants (including the wild type, wt) and lysates of a small collection containing 32 variants from a different project, which were available at the REETZ lab (Figure 3-2, mutant names are either derived from their changed amino acid sites or are numbered according to their original project ID). First, enzyme concentrations of 10 µM and 100 nM were tested at substrate concentrations of 1 mM and

10 µM. These first tests showed that, on one hand, solubility of the substrate was an issue due to precipitation at 1 mM, limiting working concentrations to 100 µM, and on the other hand that it was not necessary to run reactions at high enzyme concentrations. Transferred to lysate reactions and tested on the small one-plate collection, this allows a 1:10 dilution of lysate and thus the screening of multiple substrates from one batch. Immediately, the prevalence of derivative **1a** becomes apparent, especially in the more active mutants.

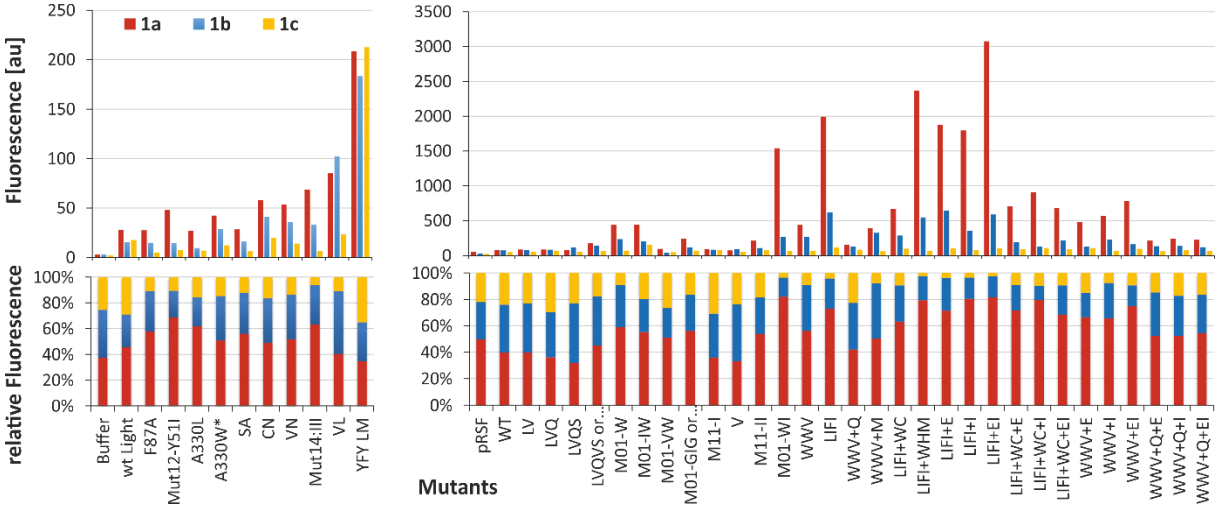

Figure 3-2. Results of the pre-screen of fluorescein derivatives **1a-c** using 11 purified enzymes at 100 nM (left, 10 µM substrate) and a small test collection of 32 variants (right, lysate reaction of 100 µM substrate). Top panels show overall intensity, bottom panels illustrate relative substrate selectivity. Reactions were carried out in Buffer I following standard conditions.

This optimized procedure not only saves time, but also makes the comparison of results obtained from the same batch much more reliable, since errors due to changing levels in protein expression are eliminated. Additionally, the deprotection reaction is extremely fast, reducing reaction times to 90 min instead of the 24 h often applied in P450$_{BM3}$ reactions. With shorter incubation times, volume changes due to evaporation of the buffer are minimized, again leading to lower errors in the screening process.

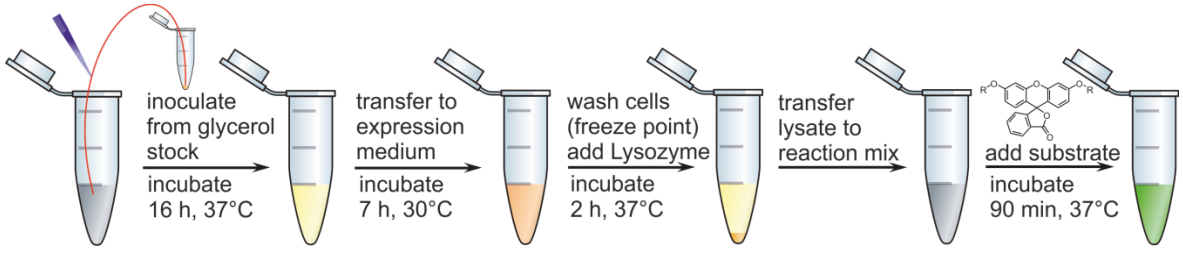

Figure 3-3. Schematic representation of the optimized screening process, from glycerol stock to substrate reaction. No further workup is necessary before fluorometric analysis.

Figure 3-3 gives an overview over the final screening procedure. Library glycerol stocks were used to inoculate over-night cultures. After incubation, an aliquot was transferred to a new

vessel containing expression medium with IPTG. Expressed cells were washed with potassium phosphate buffer (KPi), and could then either be frozen and stored until further use, or directly resuspended in lysis buffer. After incubation, cell debris was pelleted by centrifugation and the supernatant (lysate) was transferred to a new vessel containing reaction buffer I. After 90 min, the reaction was finished and could be analyzed fluorometrically.

3.2.2 Libraries

In order to obtain variant libraries for screening, one can either go through the process of creating a new library for a specifically tailored collection, or use an existing library, reducing the amount of work necessary for first results. In accordance with the First Law of Directed Evolution ("You get what you screen for"),[245] we chose to screen two variant libraries available at the REETZ lab, which had been constructed specifically for enhanced regio- and stereoselectivity in the course of other studies.

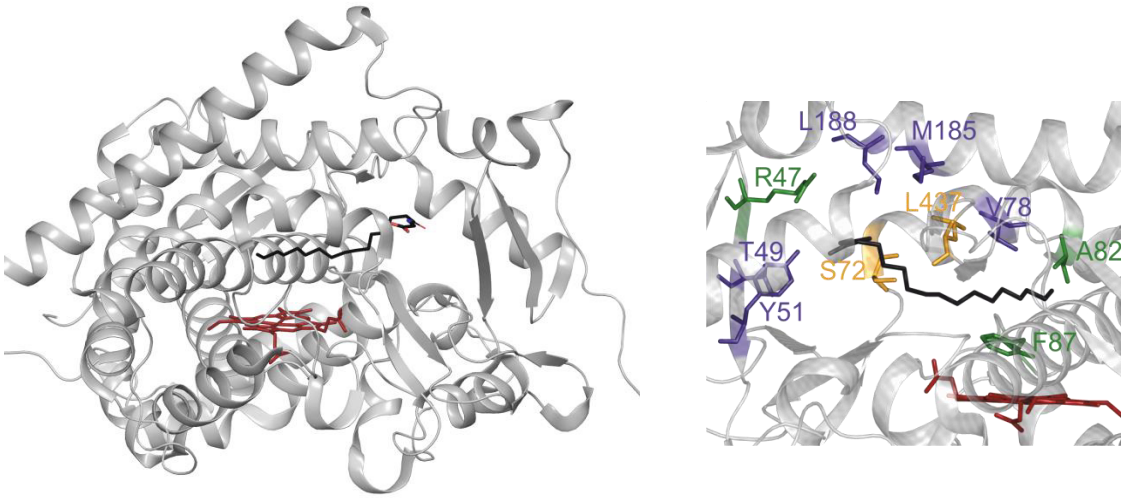

Figure 3-4. PYMOL[246] renderings of $P450_{BM3}$ wt in a co-crystallized structure with *N*-palmitoylglycine (PDB-ID 1JPZ[247]), as full view (left) and zoom into the active site (right). Highlighted are the prosthetic heme group (red) and amino acid residues targeted in SABRINA's Collection (blue), the MegaSite library (orange), or both (green). The substrate is shown in black.

SABRINA's Collection created by SABRINA HOEBENREICH[161,162,248] comprises triplicates of ca. 150 defined variants (list see Appendix 11) arranged in MTPs, which were used for steroid hydroxylation. The second library, termed MegaSite, contains 10 MTPs of unsequenced variants (unpublished work by CARLOS G. ACEVEDO-ROCHA), where five residues were randomized to four different amino acids. Their respective positions inside the active pocket are shown in Figure 3-4. Details regarding library creation and targeted sites are described in Chapter 5.4.2, page 91.

The bacterial strain used here for the inducible expression of proteins in *E. coli* is BL21-Gold(DE3), which carries the gene for T7 polymerase via the phage DE3. Expression of the polymerase is under regulation by a *lac*UV5 promoter, allowing controlled induction with IPTG or lactose. The gene for $P450_{BM3}$ is introduced to the bacteria either on the vector pRSFDuet (Novagen) or pETM11 (EMBL), together with a kanamycin resistance as a selection marker. In some cases, a His-tag for easier purification and a TEV restriction site for removal of the tag are included with $P450_{BM3}$. Both genes are regulated by a T7 promoter that is only transcribed by T7 polymerase, thus practically eliminating expression until induction is performed. Figure 3-5 shows a plasmid map of pRSFDuet, including all motifs and sequencing primers.

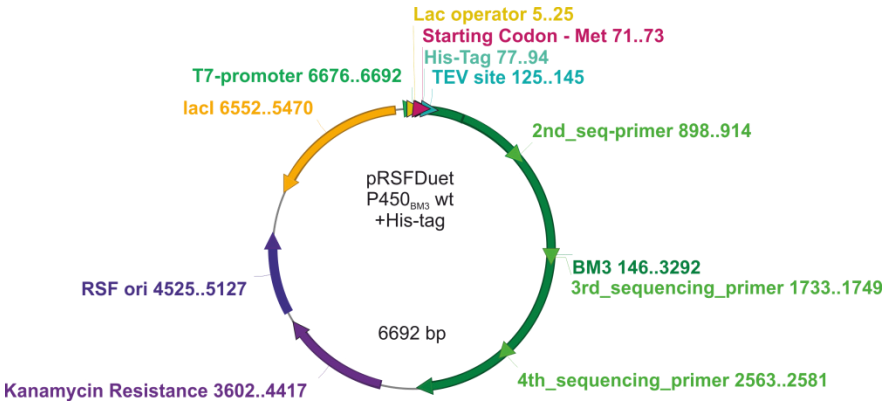

Figure 3-5. Vector map of pRSFDuet-1 as used for creation of the MegaSite library, including all primer sites. Optional His-tag for purification and TEV restriction site are included in the representation.

3.3 Screening Results

3.3.1 Fluorescence Read-out

The examination of these over 1000 mutants against substrates **1a-c** showed that only few mutants are able to convert the allyl diether **1b** with medium activity, while no mutants were found to cleave the benzyl derivative **1c**. However, a number of enzyme mutants displayed remarkably high activity towards the cleavage of the propargylic diether **1a**. The plate exhibiting the highest signal is shown in Figure 3-6. These results are particularly noteworthy since alkynes are known to act as suicide inhibitors, irreversibly inactivating CYPs by alkylation of the heme group in their active center.[240,241,249] However, some of the mutants from this study seem to be able to overcome this threat. Generally, results from SABRINA'S collection were much lower due to a different plasmid with lower copy numbers and thus lower expression levels, so they had to be assessed separately.

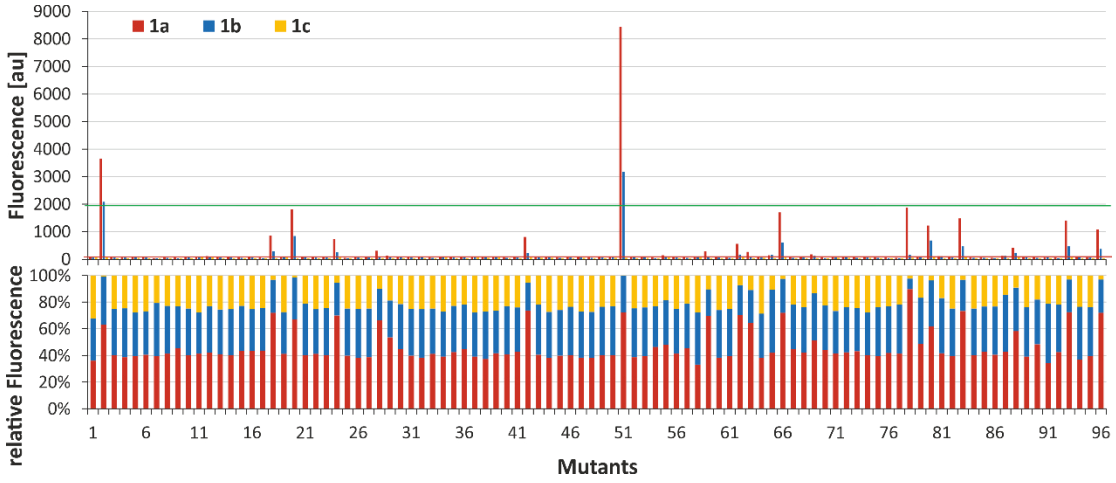

Figure 3-6. Example of screening results for MegaSite plate No. 7, indicating activity (top panel) and relative selectivity (bottom panel). Horizontal lines indicate background intensity (red) and the minimum activity threshold that was chosed for genetic sequencing (green, results *cf.* Appendix 6). Reactions were carried out in Buffer I with lysate at a final substrate concentration of 100 µM.

Those mutants from the MegaSite library showing signals higher than 2000 au (represented by the green threshold line in Figure 3-6), which means roughly 20-fold increased activity over the wild type, as well as the six most active enzymes from SABRINA's collection, were combined to a new plate of 48 variants (present in duplicates) and sent for sequencing to GATC to identify and confirm their mutations.

3.3.2 Sequence Analysis

Genetic sequencing was performed by the company GATC, using two sets of primers to cover the relevant parts of the gene. The resulting sequences were aligned with the wild type sequence in BioEdit 7.2.0 to determine mutations present in the isolated variants, as collected in Table 7-1, Appendix 6.

Upon analyzing the sequence traces, it became clear that some mutants had been isolated up to four times. The differences in their performance between entries are due to varying expression levels in the culture. For further experiments, the most active stock was used. A new collection plate was assembled, containing the 33 different hit variants from this study, as well as hits from other projects, the empty vector and the wt as controls (details see Appendix 12). Reproducibility of the results for this collection plate can be seen in Figure 3-7, showing good correlation across different times and experimenters.

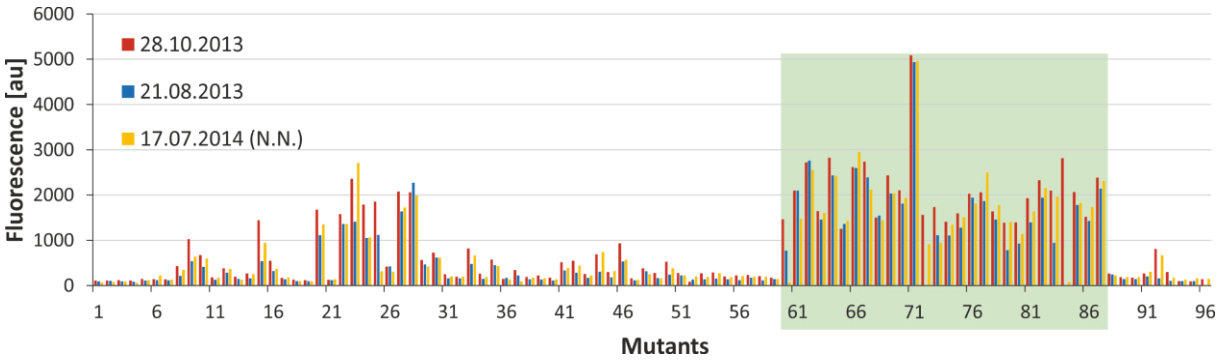

Figure 3-7. Results for the deprotection reaction of **1a** as determined by fluorescence assay on the mixed 96er collection plate (mutant details *cf.* Appendix 12). Hit variants from this project are highlighted. Reproducibility is shown over time and different experimenters (the data row denoted N.N. was generated by NATHALIE NETT). Reactions were carried out in Buffer I with lysate at a final substrate concentration of 100 µM using the NADPH recycling system described in Figure 3-1.

Overall the most prominent example was mutant TFFIS (mutations R47T/S72F/A82F/F87I/L437S), reliably showing almost twice as much activity as any other mutant in the lysate reaction. It shows a strong preference for the activation of the propargylic diether **1a** over **1b** (weak activation) or **1c** (no activation). In contrast, wild type (wt) P450$_{BM3}$ does not activate any of the derivatives, demonstrating a compelling degree of selectivity across the mutants. The mutant which gave the highest overall signal in the first screening, TSFIS (*cf.* Figure 3-6), showed lower apparent selectivity than TFFIS, and did not confirm its activity in repetitions with the collections plate, prompting us to exempt this apparent false positive from further studies. To be able to obtain quantitative results, the most promising hit mutants were purified (*cf.* Chapter 3.5.1, page 43).

3.4 Substrate Modification and Optimization

3.4.1 Modifications of the Propargyl Protection Group

To further investigate the propargylic protection group, NATHALIE NETT prepared a second generation of substrates during her master thesis,[250] comprising of three additional derivatives **1d-f** (*cf.* Scheme 3-3). The necessary bromides were prepared in an APPEL reaction from their corresponding alcohols. Fluorescein derivatives were then synthesized in a WILLIAMSON ether synthesis following the same reaction conditions as described in Chapter 3.1, page 29.

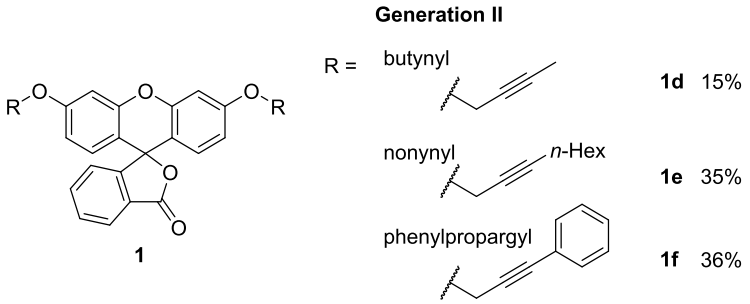

Scheme 3-3. Second generation fluorescein derivatives obtained via WILLIAMSON ether synthesis as shown in Scheme 3-2. Formally, a variation of the propargyl protection groups was introduced.

3.4.2 Coumarin Derivatives

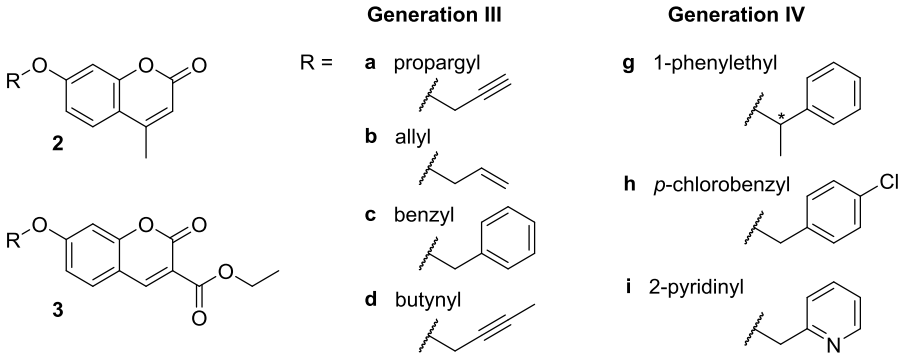

Scheme 3-4. Coumarin derivatives synthesized for deprotection reactions to investigate the applicability of the previously used protection groups for different substrates.

Encouraged by the results based on fluorescein derivatives, a third generation of substrates derived from two coumarin fluorophores (**2** and **3**) was investigated. 4-Methylumbelliferone **2** is an established drug used in bile therapy[251] and has recently been under intense investigation for its activity as an anti-cancer agent effective against various cancer types.[252–

[256] Its ethers are closely related to a known probe for CYP levels in clinical samples.[257] The second compound, 3-carboxycoumarin **3**, is a known substrate for similar reactions catalyzed by P450 variants.[140,242,258] Particularly, derivative **3c** has previously been reported for deprotection reactions by $P450_{BM3}$,[242] and is therefore a useful reference for the evaluation of screening results.

Their propargylic ether derivatives (**2a** and **3a**) were prepared, as well as the respective 2-butynyl (**2d** and **3d**) and benzyl (**2c** and **3c**) ethers. After positive results with these protection groups were obtained, further modifications were made to substituent **c**, to investigate sterical and electronic influences on the deprotection reactions of resulting 4th generation compounds **3g**, **h** and **i**.

Synthesis of Umbelliferone Derivatives

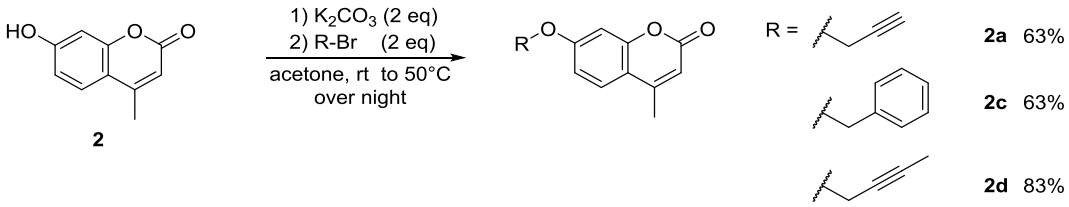

Scheme 3-5. Synthesis of umbelliferone derivatives **2a**, **c** and **d** via WILLIAMSON ether synthesis. After deprotonation with carbonate, the hydroxyl groups are coupled to the corresponding bromide in an S_N2 reaction.

In analogy to the fluorescein derivatives and following literature known methods,[259] methyl umbelliferone was alkylated via a WILLIAMSON ether synthesis. In comparison to the synthesis of fluorescein derivatives, the solvent was changed from DMF to acetone. Lower temperature and reduced equivalents of the reagents were employed. Due to no competing sites, a much cleaner reaction was observed. The resulting products were purified by crystallization from ethyl alcohol to yield a white solid. Reaction conditions are shown in Scheme 3-5.

Synthesis of Carboxycoumarin Derivatives

The synthesis of the unprotected 3-CCE **3** was carried out via a one-step synthesis according to a procedure by RUFF *et al.* (*cf.* Scheme 3-6).[242] 2,4-Dihydroxybenzaldehyde reacted with diethyl malonate in methanol in a KNOEVENAGEL-like reaction catalyzed by morpholine and acetic acid: an ALDOL reaction is followed by elimination of water and decarboxylation, ultimately leading to the formation of an intramolecular γ-lactone. The crude product was recrystallized from methanol to remove traces of byproducts, such as *trans*-coumarinic acid, yielding the unprotected coumarin as a pure colorless solid.

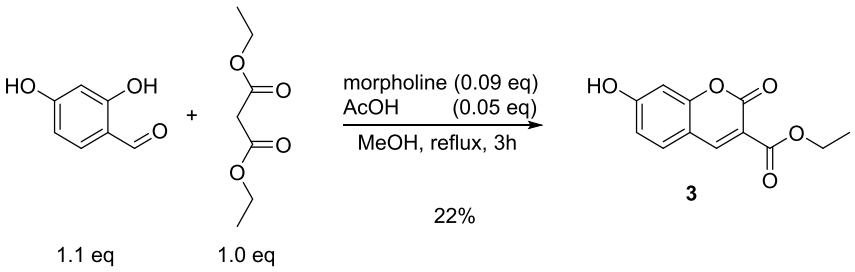

Scheme 3-6. Synthesis of the unprotected carboxy-coumarin **3** in a KNOEVENAGEL condensation reaction.

For the following alkylation via WILLIAMSON ether synthesis, two possible conditions were employed (Scheme 3-7). Method I followed the conditions previously described for parent compounds **1** and **2**. In the second route,[242] the unprotected compound was treated with sodium hydride in toluene as a first step, allowing the isolation of the corresponding sodium salt **3-Na**, before it was reacted with the desired bromides in DMF.

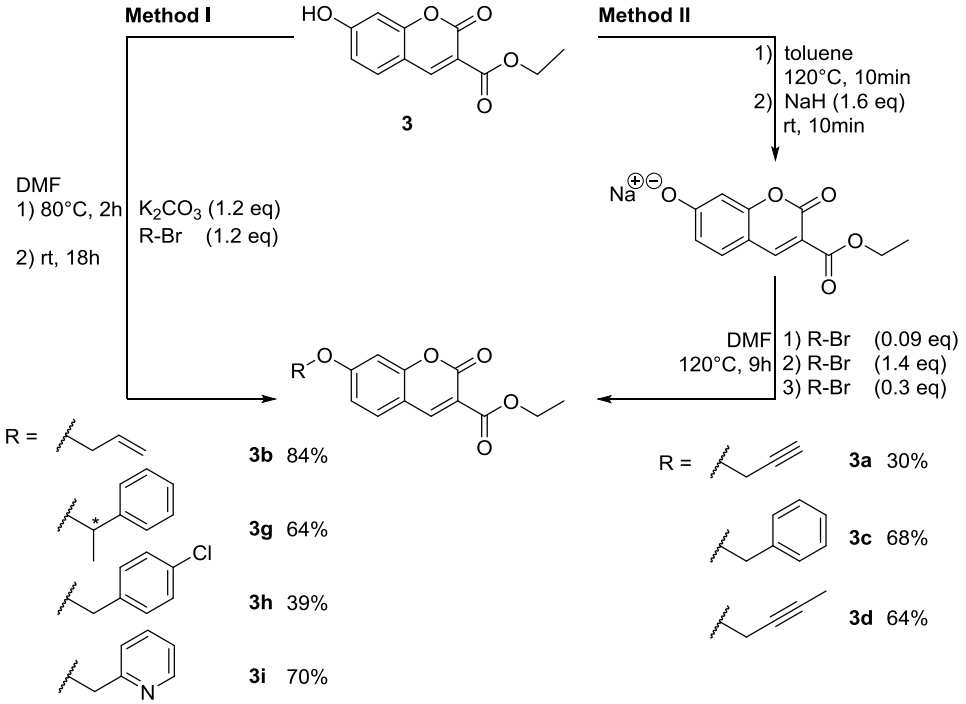

Scheme 3-7. Two methods for the preparation of ether-protected 3-CCE derivatives by WILLIAMSON ether synthesis. Method I follows the same one-pot approach as described before for derivatives of compounds **1** and **2**, while Method II takes a two-step approach with intermediate isolation of the corresponding sodium salt.

Method I tended to yield slightly higher amounts of the raw product, while Method II gave a cleaner reaction, making purification easier. In both cases, flash chromatography over silica afforded the pure derivatives **3a**, **b**, **c**, **d**, **g**, **h** and **i**. Parts of this work were carried out by NATHALIE NETT[250], CHRISTIAN SPRINGER,[260] LISA ENGELSBERGER, KERSTIN MARK, JULIUS WINKLER and JANOSCH KETTLER.

In case of the chiral compound **3g**, chiral resolution was determined. Unfortunately, the chiral center in the protection group racemized during the reaction, most likely during the synthesis of the bromide, so that the enantiomers had to be resolved via chiral reversed phase HPLC for chirality dependent analyses. HPLC traces showing the purity before and after enantiomeric resolution are shown in Figure 3-8, conditions are described in Table 5-4.

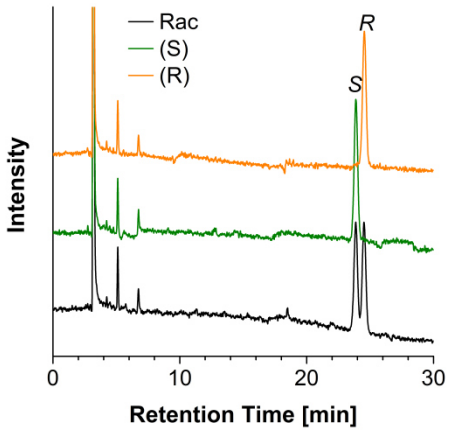

Figure 3-8. HPLC traces of chiral resolution of enantiomers **3g**, before (black) and after semi-preparative purification via HPLC (orange: (*R*)-**3g**; green: (*S*)-**3g**). Separation was conducted on a CHIRALPAK IB column using MeCN : 0.1% TFA/H_2O as solvents, following gradient IV as described in Table 5-4, page 72.

3.4.3 Screening Results of Substrate Generations II-IV

A graphic representation of the results for substrate generations II-IV is shown in Figure 3-9. The distinct suitability of the propargylic protection group was confirmed by experiments with 2nd generation alkyne derivatives **1d**-**f**. Whereas a large number of P450$_{BM3}$ mutants display weak activity for the 2-butynyl diether **1d**, no active mutants could be found for the alkynes **1e** and **1f**. For this reason, investigations towards those protection groups were discontinued. The advantage of 3rd and 4th generation substrates based on coumarin is that they carry only one protection site, rendering kinetics calculations less complex. The disadvantage of these derivatives, however, is that they have their emission maximum in the range of the cofactor NADPH, so that a large fluorescence background impedes the evaluation of the libraries. Nevertheless, we were able to identify hit mutants by subtracting the background from measurements. Parts of these screening experiments were carried out by NATHALIE NETT (**3a**, **c**, **d**),[250] CHRISTIAN SPRINGER (**3g**, **i**)[260] and LISA ENGELSBERGER (**3b**, **h**). Overall, mutant WMV (R47W/A82M/F82V) displayed extremely high activity towards the benzylic ethers **2c** and **3c**, whereas mutant M01 (R47L/F87V/L188Q/E267V/G415S)[19] showed to be capable of selectively activating the propargylic ethers **2a** and **3a**. These were subsequently purified by KATJA KRÄLING (*cf*. Chapter 3.5.1, page 43).

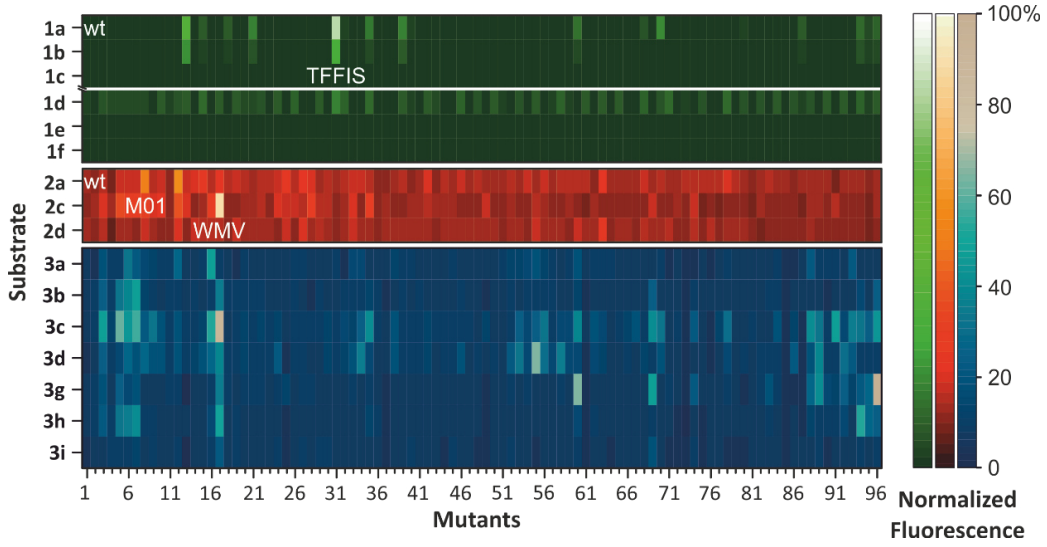

Figure 3-9. Activity of $P450_{BM3}$ mutants towards different caged compounds arranged in an MTP format (96 samples). Fluorescein- **1a-f** (green) and coumarin-based substrates (**2a**, **c**, **d**, red and **3a**, **c**, **d**, blue) were used for library screening. Fluorescence intensities are normalized to the lowest/highest values included in the plates, brighter colors showing higher activity (for original values see Appendix 8). Figure adapted after our publication with permission from JOHN WILEY & SONS LTD.[1]

Coumarin derivate **3b**, carrying an allyl group, was not converted efficiently by any screened mutant. The same is true for pyridinyl derivative **3i**, which is probably due to inhibition: it is possible for the substrate to coordinate to the iron core via its nitrogen atom, as is known for imidazoles.[261] Quite actively, but with very low selectivity, a large number of mutants from SABRINA's collection (data not shown) converted derivative **3h**. Low selectivity, however, is not beneficial to this endeavor, so investigations with regard to this compound was abandoned.

For an outlook towards the design of suitable protection groups, the chiral compound **3g** was used to test for enantioselectivity in our libraries (*cf.* Figure 3-10). In a first step, the racemic compound was screened, directly comparing it with earlier results of **3d**. Some very promising mutants were found, albeit most of them also converted **3d**. The most active ones were selected, and used for reactions with the enantio-pure derivatives **3g**). It became clear that a general preference for (*S*)-**3g** prevailed in all but one selected mutant. Noteworthy is the inverted selectivity upon changing only two residues: mutant LFFA (R47L/S72F/A82F/F87A) behaves like the majority of tested mutants, while LFFFA (R47L/S72F/A82F/F87-/L437A) exhibits a preference for (*R*)-**3g**.

These results are very promising, and found mutants could be used as a starting point for future engineering efforts. However, no extended investigation of 4th generation results was possible in the given timeframe. Future docking studies and modifications towards chiral protection groups could definitely help improve the selectivity of the uncaging system.

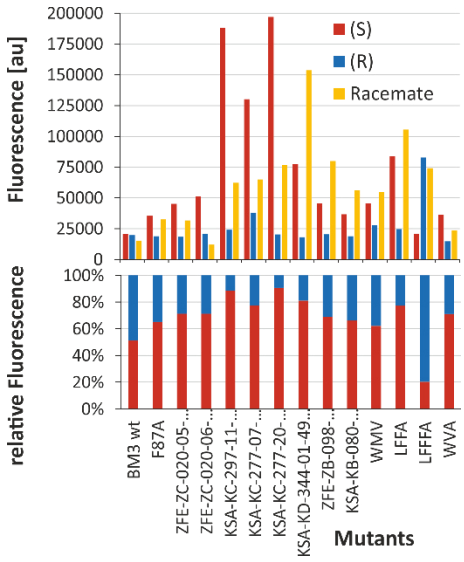

Figure 3-10. Results of the lysate reaction of different mutants towards enantiomers **3g**. All but one tested mutant (LFFFA) favor the S-enantiomer. Top panels show overall intensity, bottom panels illustrate relative selectivity. Reactions were carried out in Buffer I with lysate at a final substrate concentration of 100 µM.

3.5 Mutant Characterization

3.5.1 Purification and Concentration Determination

For enzyme purification, large scale expression cultures were grown in TB medium containing kanamycin. The bacteria were washed with buffer, resuspended and lysed by sonication. The lysate was cleared by centrifugation and filtration before purification. Since most hit mutants did not contain a His-tag, these enzymes were purified over a series of chromatographic steps, starting with a manually operated anion exchange column by increasing the concentration of KCl, followed by a desalting column using HEPES buffer, a second anion exchange column, and last a gel filtration column. The sample was concentrated by ultracentrifugation after each step, and the buffer replaced to KPi after the last column. In case of His-tagged proteins, the raw extract was purified by affinity chromatography (Ni-NTA) and eluted by gradually increasing the competitor concentration in the buffer. Generally, imidazole is used for this step, but in the case of P450s, it can deactivate the enzyme by coordinating to the iron core of the active site, so that histidine was used here instead. In both cases, the sample was then divided into aliquots, frozen in liquid nitrogen and stored at -80°C until further use.

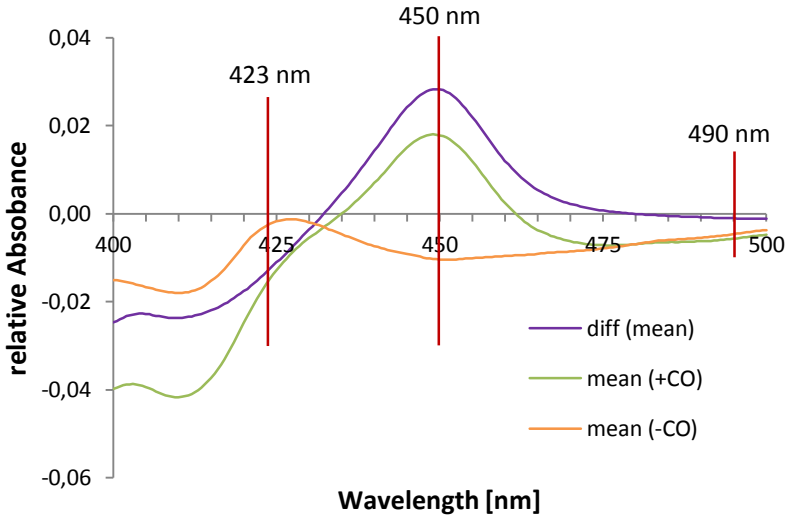

Figure 3-11. Concentration determination of $P450_{BM3}$. Shown are absorption spectra of the reduced enzyme, averaged over three measurements with (green) and without addition of CO (orange), as well as the calculated difference spectrum (purple).

Enzyme concentration was determined using an established method based on spectroscopic measurements of the corresponding CO-heme complexes, allowing to distinguish intact active sites from inactivated ones.[262] Unlike in the literature procedure, no additives for the buffer were needed in this case, since we used a purified, soluble protein, which is not membrane bound and not derived from tissue samples.

A diluted solution of the protein is divided into different cuvettes, half of which are saturated with CO-gas, while the other serve as controls. The gas binds to the ferrous iron core of the active site, inducing an increase of the absorption band at 450 nm. To make sure all iron centers are in their reduced ferrous oxidation state, all cuvettes are treated with sodium dithionite, before measuring spectra or single point absorption at three wavelengths. Protein rendered inactive by loss of its axial cysteine ligand from the iron center experiences a hypsochromic shift, and can be tracked by measuring absorption at 423 nm. As a general background for the presence of other P450 enzymes, a reference measurement at 490 nm is used. This can be particularly useful when measuring concentrations from tissue samples. For analysis of the data, non-CO reference values are subtracted from the values of CO-treated samples to yield a difference spectrum (*cf*. Figure 3-11), and the concentration of active and inactive enzyme can be calculated using the molar extinction coefficients of 91,000 $M^{-1} \cdot cm^{-1}$ at 450 nm and 41,000 $M^{-1} \cdot cm^{-1}$ at 423 nm, respectively. Table 3-1 shows concentrations of purified $P450_{BM3}$ mutants. Their original screening data towards different substrates is collected in Appendix 7.

Table 3-1. Determined concentrations for all purified mutants.

Screen	Mutant Name	Library/Entry		Substrate	His-Tag	Concentration [µM]
	wt+His	-		-	+	97.7
	wt	-		-	-	24.4
	wt	-		-	-	91.5
Gen I	TFFIS	MS	-03-7C	**1a**, **1d**	-	15.5
	TFFIS	MS	-05-A12	**1a**, **1d**	-	17.3
Gen II	YFM-WEI-A	SC	-05-70	**1d**	+	13.6
	PC-A	SC	-05-34	**1d**	+	29.2
Gen III	M01	96er	-08	**2a**	-	13.5
	M11	96er	-12	**2a**	-	18.7
	WMV	96er	-17	**2c**, **3c**	-	2.4
	LV	96er	-05	**3c**	-	121.6
	WWV-MQ'	96er	-55	**3d**	+	42.0

3.5.2 HPLC Analysis

For the analysis of possible side products and quantification of turnover for kinetic calculations, analytical HPLC methods were developed.

Qualitative

First, separation conditions were established: Due to the polarity of the compounds, reversed phase HPLC is the method of choice. Separation of substrates and reaction products is possible using a C18 or C8 column and different gradients of acetonitrile and 0.1% trifluoroacetic acid (TFA) in water (*cf.* Chapter 5.1.4, page 70).

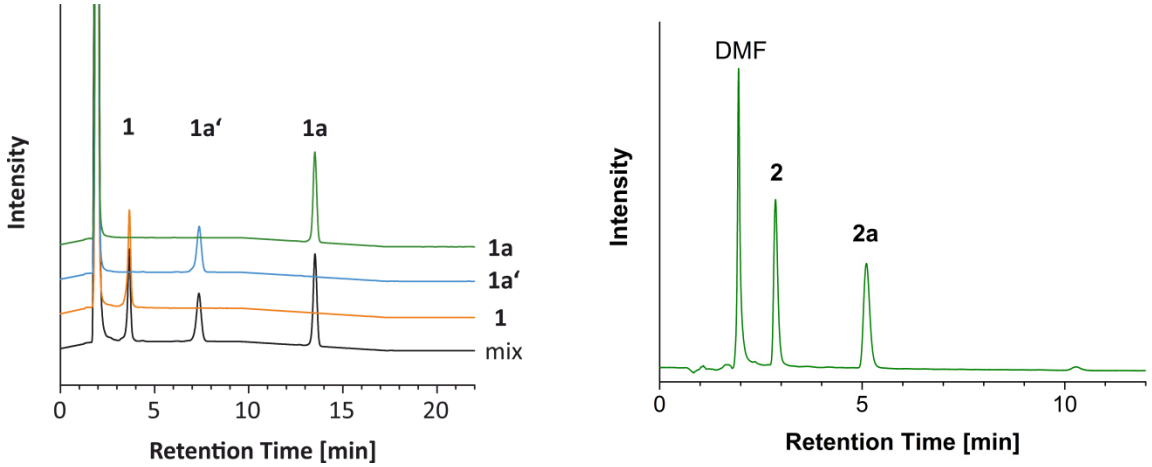

Figure 3-12. HPLC traces of fluorescein (left) and umbelliferone derivatives (right). Separation was conducted on a reversed-phase C18 column using MeCN : 0.1% TFA/H_2O as solvents, following gradient I (left panel) as described in Table 5-4, page 72 or at isocratic conditions (50:50, right panel).

Quantitative

For quantification by HPLC, concentration calibration curves of fluorescein substrates were prepared of direct dilutions and extracts (carried out in triplicates, *cf.* Appendix 5, Figure 7-2). All dilution series show linear correlation of peak area vs. concentration in the working range, and closing in on (0|0) for all substrates apart from free fluorescein, where a y-offset of 473 mAU · s is observed. Below 10 µM, error bars tend to grow beyond 10%. Measurements are prone to solvent change, since samples diluted in water instead of MeCN generally show a lower signal by an average of 24% (denoted by "x" in the graph). Therefore, dilution in the same solvent is mandatory for comparison of results. The next step is the comparison of these data with extracted samples.

To determine the best extraction method, different solvents were tested on derivatives of substrate **1** and **2** (Figure 3-13). Extraction was carried out 3 times, the organic phases combined, evaporated, and the residue redissolved in acetonitrile prior to analysis. Overall,

ethyl acetate proved to be the best choice, retaining the best ratio between different derivatives. Especially in the case of fluorescein derivatives this is not a trivial task, due to the increased polarity of the products, which strongly influences extraction from aqueous phase.

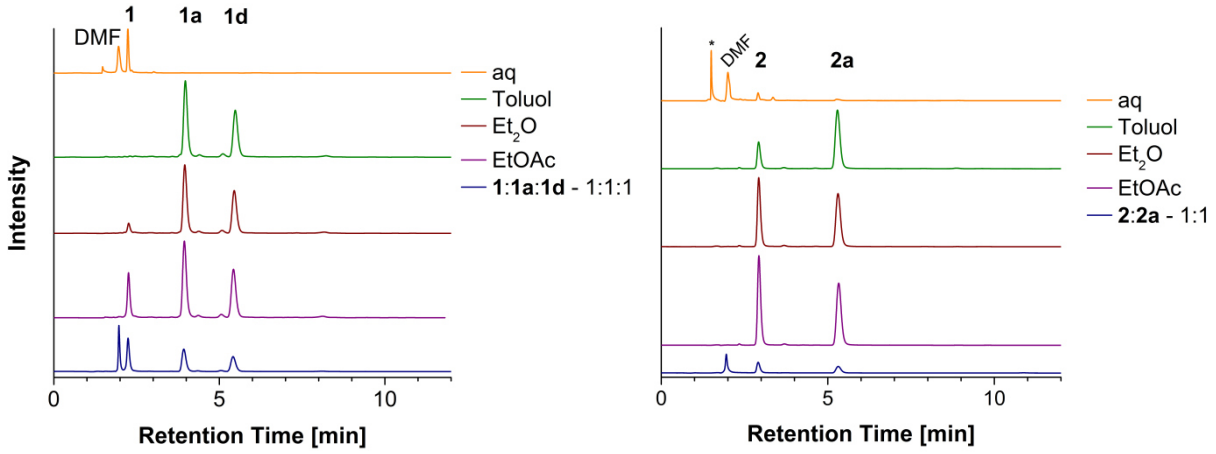

Figure 3-13. Evaluation of extraction solvents on fluorescein und umbelliferone derivatives. Separation was conducted on a reversed-phase C18 column using MeCN : 0.1% TFA/H_2O as solvents at isocratic conditions of 70% (left panel) or 50% acetonitrile (right panel). The peak denoted with an asterisk is due to unidentified water-soluble components.

Additionally, different extraction processes were tested with fluorescein derivatives. When comparing different automated and manual extraction methods (details *cf.* Chapter 5.1.4, page 71), it becomes clear that a large difference in efficiency is observed. Only for the butynyl diether **1d** can equal results be obtained, at around 70% of the intensity of the direct dilution. Even though percentages for the other substrates are even lower, especially in the robot-method, the automation of the results is an immense advantage both in terms of time and reliability. Therefore it is sensible to use the robot for all further extraction steps to keep the error as low as possible.

Dilution series were extracted with the robot (*cf.* Appendix 5, Figure 7-3), and indeed show a linear correlation of peak area vs. concentration, albeit at larger errors than the direct measurements. So even though extraction is not complete, the results clearly show the ability to estimate the total amount of compounds present in solution.

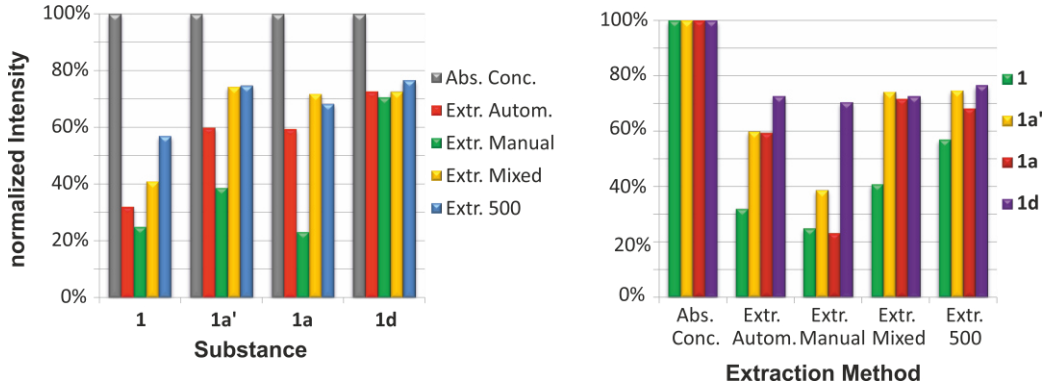

Figure 3-14. Evaluation of extraction methods, normalized to the observed concentrations in corresponding fixed dilution measurements. The left panel emphasizes varying degrees of extraction completeness across the derivatives, while the right panel accentuates the difference between methods. Separation was conducted on a reversed-phase C18 column using MeCN : 0.1% TFA/H_2O as solvents, following gradient I (left panel) as described in Table 5-4, page 72. Corresponding peak areas were then normalized to the value measured for analysis of a solution with known concentration (gray).

3.5.3 Biochemical Analysis

After purification, the most prominent mutants were characterized biochemically using defined enzyme concentrations and the same reaction conditions used for the screening procedure (*cf.* Chapter 5.6.2, p. 97).

Relative Activity

By controlling the enzyme concentration, it was possible to cancel out differences in expression levels present in lysates, allowing the direct comparison of our most promising hit mutants as shown in Figure 3-15. In the case of substrate **1a**, the most active mutant TFFIS yields a 52-fold higher fluorescence response than the wt. None of the other hits was able to convert any of the fluorescein substrates. While the highly active mutant WMV converted all coumarin-derived substrates (**2a**, **2c**, **3c**, and **3d**), the more selective mutant M01 showed activity towards substrates **2a** and **2c** only, at about 4-fold higher than the wt. This means that compounds even with very similar core structures can be differentiated by certain mutants, but this gain in selectivity comes with an activity penalty, e.g.: WMV shows 16-fold higher activity than M01 towards substrate **3d**. Previous reports for **3c**[18c] using other $P450_{BM3}$ mutants achieved only a 7-fold increase at similar concentrations in a different buffer[21] after one round of random directed evolution, which differs from our library mutants where the active site was targeted using recommended guidelines.[22]

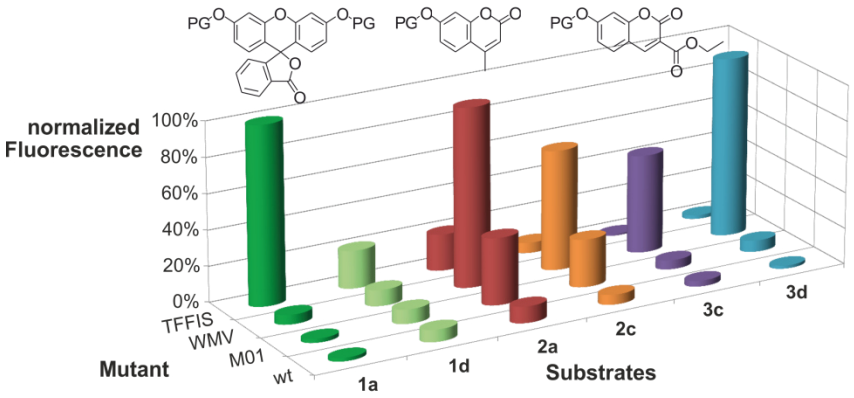

Figure 3-15. *In vitro* characterization. Enzymatic activity of $P450_{BM3}$ hit mutants towards caged compounds, normalized to the largest observed fluorescence response for each substrate (original data: *cf*. Appendix 9). Reactions were carried out in Buffer I, generally following standard conditions at final concentrations of 0.1 µM and 100 µM for enzyme and substrate, respectively. Figure reproduced from our publication with permission from JOHN WILEY & SONS LTD.[1]

To further investigate the reaction, real time fluorescence analysis of the reaction of TFFIS with **1a** was conducted (Figure 3-16), in which the mono-deprotection of **1a** was revealed. The observation was later easily confirmed by HPLC analysis, as shown below in Figure 3-18.

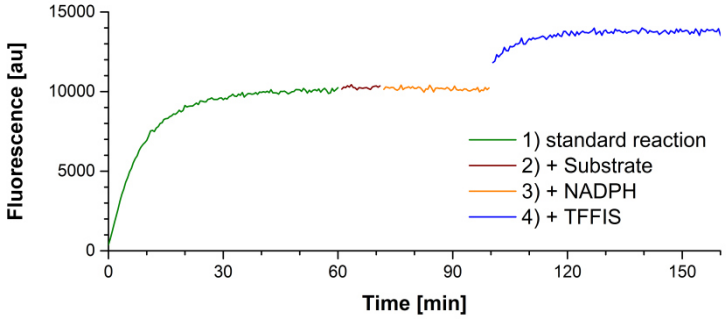

Figure 3-16. Real-time fluorescence monitoring of the reactions TFFIS/**1a**. The reaction was carried out in Buffer I, following standard conditions at final concentrations of 0.1 µM and 100 µM for enzyme and substrate, respectively. Completion of the reaction is observed after ca. 40 min (stage 1, green). Functionality of the enzyme was checked by a second addition of substrate (stage 2, red), and NADPH (stage 3, orange). A second addition of enzyme (stage 4, blue) showed some conversion, but significantly lower than before, pointing towards an inactivation of $P450_{BM3}$.

A two-step deprotection should be visible in the fluorometric trace, with a first, smaller increase in signal intensity, since the mono-ether is less fluorescent than free fluorescein, which would only be generated in a second deprotection step. To gain some insight into what caused the reaction to stop, more substrate was added, but to no avail. Therefore, either the enzyme was inactivated or the cofactor was depleted, meaning the recycling system had failed. To distinguish between those two possibilities, NADPH was added to the system, again resulting in no change in fluorescence. This confirmed that enzymatic activity had been

affected. Adding more enzyme to the reaction resulted in some turnover, but not at the full previously observed activity, suggesting that something in solution was affecting the enzyme after a certain number of turnovers. However, no further investigations were conducted in this study as to what the inhibitory effect might be.

Selectivity and Orthogonality

By choosing highly selective catalysts, it may be possible to have two independent reactions in the same system without interference from one another, which could reveal possibilities for further applications. Not only could this be of advantage in bio-imaging,[263] but also for classical organic synthesis of complex molecules, where the independent cleavage of different protection groups is of great importance. Therefore, to determine the orthogonality of different mutants towards each other, their behavior in a mixed system was investigated. Real-time monitored reactions containing two enzymes added simultaneously or successively were conducted under standard reaction conditions in buffer I, towards substrate **1a** at a concentration of 100 µM. Similar measurements with coumarin-based substrates were not possible because of the interference of NADPH fluorescence.

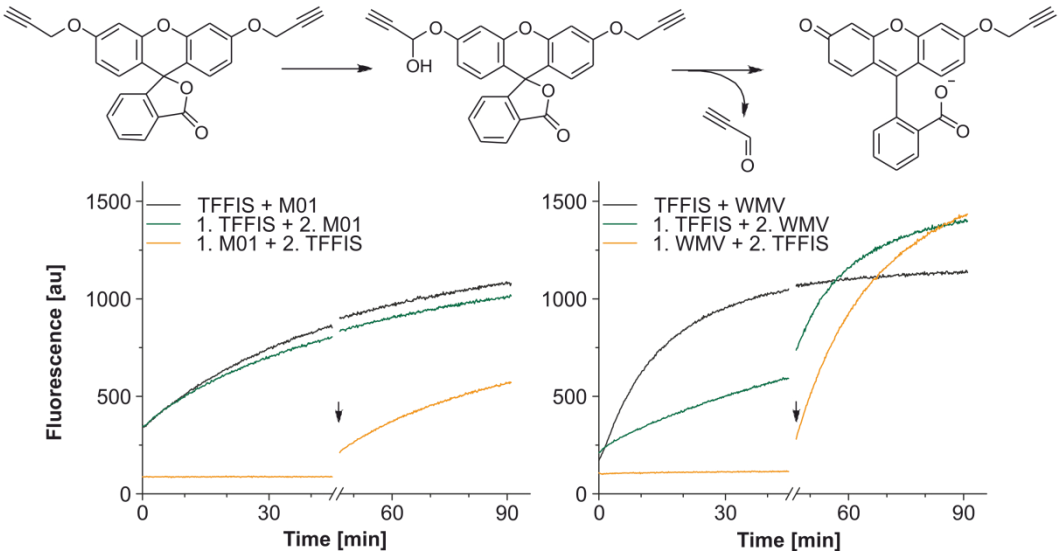

Figure 3-17. Orthogonality test with different mutants in the case of substrate **1a**. Both enzymes were either added at the same time (black lines) or successively (colored lines, addition time marked by arrows). Left: TFFIS and M01; Right: TFFIS and WMV. The TIFFIS/M01 pair shows expected orthogonality, whereas the data of the TFFIS/WMV pair provides evidence for the formation of mixed dimers with changed catalytic properties. Reactions were carried out in Buffer I, generally following standard conditions at a final substrate concentrations 100 µM. The final enzyme concentration was 0.1 µM for TFFIS and M01, and 0.01 µM for WMV, to account for the difference in performance.

This mixed approach was found to work well *in vitro* for some combinations of P450$_{BM3}$ mutants (*cf.* Figure 3-17, left panel), where activity is only seen when the corresponding

mutant TFFIS suitable for substrate **1a** is added to the reaction mix, as expected. The observation does not change when M01 is present, which does not show activity for substrate **1a**. However, this is not true for every combination of mutants. In the example of WMV, depicted on the right panel of Figure 3-17, higher activity is achieved when both enzymes are mixed, exceeding the activity of the active mutant by itself. This observation could be attributed to the particularly complex case of P450$_{BM3}$, which is only active as a dimer and thus subject to cooperative changes in substrate turnover. The activity gain could be due to conformational changes, but more likely is a result of the electron transfer pathway bridging both monomers,[264] so one mutant would take over substrate conversion while the other excels at cofactor turnover. Therefore, it is recommended that the behavior of every pair of suitable mutants be tested carefully in regard to the properties of mixed P450$_{BM3}$ systems for future projects based on the concept of orthogonality.

Kinetic Parameters

For further applications, characterization of the kinetic parameters of the found mutants is of importance. A combination of two methods was used as a basis for kinetic evaluation: photometric analysis of NADPH consumption allowed the tracking of changes in cofactor concentration in real time, while HPLC analysis of products, as described in Chapter 3.5.2, p. 45, was used for endpoint quantification of products.

Leak- and Consumption Rate

First, the leak rate (LR) was determined. This value describes the amount of cofactor that is used by the enzyme in absence of a substrate. Upon addition of enzyme to a NADPH solution in buffer, the depletion can be directly followed. The observed change of absorption over time ($\Delta A/\Delta t$) was used to calculate the change of NADPH concentration Δc, following LAMBERT-BEER's law (Eq. 1), where ε is the extinction coefficient and d is the cuvette diameter. This value Δc_{NADPH} was then normalized by the concentration of enzyme c_{BM3}, to yield the amount of cofactor consumed by one mole of enzyme per time (Eq. 2):

$$A = \varepsilon \cdot c \cdot d \qquad (1)$$

$$LR = \frac{\Delta c_{NADPH}}{c_{BM3} \cdot t} \qquad (2)$$

The NADPH consumption rate (CR) is determined in the same way, albeit in the presence of substrate. These reactions are followed until the slope flattens to a horizontal line, marking the end of turnover.

Product Formation Rate

Using HPLC analysis of extracts obtained from finished CR measurements (*cf.* Figure 3-18), the overall product formation rate (PFR) can be determined according to known protocols.[161] Since as described above, we observed differences in extraction efficiency, it would be most useful in future work to use such a correlation as a basis for calculations. However, to keep this study comparable to earlier works, the same established method was used for determining kinetic characteristics, where all substrate/product integrals are added to determine the assumed 100% mark, and fractions thereof are calculated accordingly for the individual compounds.

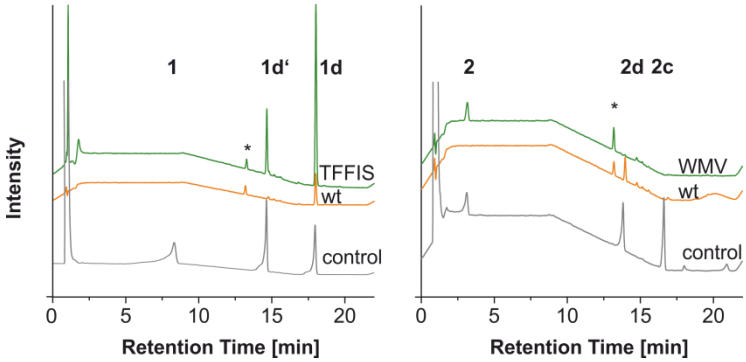

Figure 3-18. HPLC traces of reactions as used for quantification. Hit mutants are shown in green, clearly showing product formation – in case of substrate **1d**, mono-deprotected fluorescein **1d'** is formed by mutant TFFIS (left). WMV (right) shows total conversion of substrate **3d**. No conversion occurs in wt reactions (orange). Grey lanes show a control of chemically synthetized derivatives. The substance marked * is an unidentified compound present in all enzyme reactions, independent of the substrate. Separation was conducted on a reversed-phase C18 column using MeCN : 0.1% TFA/H_2O as solvents, following gradient I as described in Table 5-4, page 72.

Multiplying the observed conversion (%C) with the initial substrate concentration c_S and dividing by the reaction time t_R, normalized to the concentration of enzyme, yields the amount of product formed per mole enzyme over time (*cf.* Eq. 3).

$$PFR = \frac{\%C \cdot c_S}{c_{BM3} \cdot t_R} \qquad (3)$$

Coupling Efficiency

To determine coupling efficiency (CE), a measure of the catalytic efficiency describing the ratio of cofactor used for product formation, the overall NADPH consumption rate (CR_{tot}) over the full reaction time was first determined following Eq. 1 and 2, to then calculate the CE:

$$CE = \frac{PFR}{CR_{tot}} \qquad (4)$$

Turnover Number

An important measure for catalytic performance is the turnover number (TON), describing the number of substrate molecules converted per molecule of catalyst. Since the measurements described above were limited by the total amount of cofactor present, the TON was determined using the NADPH recycling system (Buffer II). After the reaction was finished, products were extracted and analysed by HPLC to calculate the conversion %C as described above. Multiplying %C with the initial substrate concentration c_S and dividing by the concentration of enzyme, yields the maximum amount of product formed per mole enzyme.

$$TON = \frac{\%C \cdot c_S}{c_{BM3}} \quad (5)$$

MICHAELIS-MENTEN Kinetics

Classical MICHAELIS-MENTEN kinetics were analyzed by determining initial reaction rates as described above for different substrate concentrations c_S, then linearly plotted as a function of c_S (*cf.* Figure 3-19). In the case of substrate **1a**, a direct approach for following substrate conversion was used and the reaction analysed in real time via fluorescence.

$$v = \frac{v_{max} \cdot c_S}{K_M + c_S} \quad (6)$$

$$k_{cat} = \frac{v_{max}}{c_{BM3}} \quad (7)$$

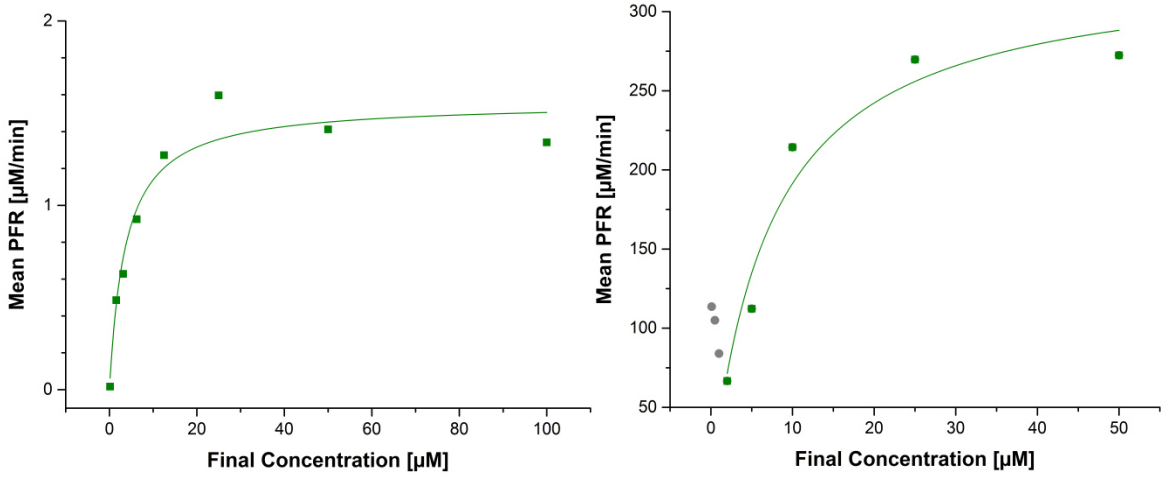

Figure 3-19. MICHAELIS-MENTEN plots for TFFIS with **1a** (left) and WMV with **3d** (right). At lower concentrations (grey data points), the high leak rate of WMV without substrate interferes with the measurement.

The program ORIGIN was used for non-linear curve fitting to match the MICHAELIS-MENTEN Equation (6), where v_{max} is the maximum reaction velocity at saturation substrate concentration and K_M is the MICHAELIS constant (describing substrate concentration at half maximum velocity). Knowing the enzyme concentration, the enzymatic turnover number or catalytic constant, k_{cat}, can be determined and used to calculate the catalytic efficiency k_{cat}/K_M (Eq. 7).

Results

The results of determined kinetic parameters are summarized in Table 3-2. In the case of substrate **1a**, the most active mutant TFFIS yields a 52-fold higher fluorescence response than the wt, corresponding to a turnover number (TON) of 425. MICHAELIS-MENTEN parameters of K_M and k_{cat} were determined to be 3.7 µM and 0.26 s^{-1}, respectively (k_{cat}/K_M = 70.3 $mM^{-1} \cdot s^{-1}$). None of the other hits was able to convert any of the fluorescein substrates. By far the highest performance is shown by mutant WMV, which shows full substrate conversion already at a low enzyme concentration of 0.01 µM with remarkable MICHALIS-MENTEN values of K_M = 7.2 µM, k_{cat} = 550 s^{-1}, and $k_{cat}/K_M = 7.6 \cdot 10^4$ $mM^{-1} \cdot s^{-1}$ against substrate **3d**. This respectively translates into a turnover number over 5000 (assay limit), an excellent value that is seldom reported for $P450_{BM3}$ mutants.[147] However, another important parameter for CYP enzymes besides turnover and activity is their leak rate. The WMV-mutant was found to have the highest leak rate, resulting in the wasting of valuable resources (NADPH) if left without the opportunity to use them productively. Still, about 15 and 21% of the NADPH electrons are directed to product formation in the case of TFFIS and WMV, respectively.

Table 3-2. Biochemical characterization of different $P450_{BM3}$ mutants. Given are values for leak rate (LR), NADPH consumption rate (N), product formation rate (PFR), coupling efficiency (CE), turnover number (TON), catalytic constant k_{cat}, Michaelis constant K_M, and catalytic efficiency k_{cat}/K_M.

Mutant	Substrate	LR	N	PFR	CE	TON	k_{cat}	K_M	k_{cat}/K_M
TFFIS¤	**1a**^	620	861	131	15%	425	0.26	3.7	70.3
wt¤		106	182	*	*	*	*	*	*
WMV§	**3d**~	26608	18643	3845	21%	>5000	549.8	7.2	$7.6 \cdot 10^4$
wt¤		106	81	*	*	*	*	*	*
M01¤	**2a**^	119	81	3	4%	47	*	*	*

Leak rate and NADPH consumption rate are given in µmol NADPH · µmol $BM3^{-1} \cdot min^{-1}$ and were calculated as initial rates over 10s in presence of 1% DMF. Product formation rate is given in µmol · µmol $BM3^{-1} \cdot min^{-1}$. The MICHAELIS constant K_M is given in µmol · L^{-1}, k_{cat} in s^{-1} and k_{cat}/K_M in mmol · $L^{-1} \cdot s^{-1}$. Reactions were carried out in Buffer I or II (for TON) at enzyme concentrations of 0.1 µM (¤) or 0.01 µM (§) and maximum substrate concentrations of 100 µM (^) or 50 µM (~). Entries marked * could not be determined due to low activity.

While the highly active mutant WMV activated all coumarin-derived substrates (**2a**, **2c**, **3c**, and **3d**), the more selective mutant M01 showed activity towards substrates **2a** and **2c** only, at about 4-fold higher than the wt (TON = 47). This means that compounds even with very similar core structures can be differentiated by various mutants, but this gain in selectivity comes with an activity penalty, as discussed above (page 47).

3.5.4 Consideration of Individual Site Influences

For a better understanding of the observed selectivities, it is sensible to combine *in silico* models and empirical data. Therefore, docking and molecular dynamics (MD) simulations of the three most interesting variants TFFIS, WMV and M01 with their respective substrates (**1a**, **3d** and **2a**) were performed by RICHARD LONSDALE.[1] Mutations were introduced *in silico* to the wt crystal structure (PDB-ID 1BU7[265]), and the simulations led to stable binding modes of the substrates in their corresponding mutants close enough to enable hydroxylation by the oxidizing iron-oxo species (Compound I). These results are shown in Figure 3-20, and can be compared with literature-known data on the influence of mutations at certain sites, a lot of which have been reviewed by WHITEHOUSE *et al.*,[149] while key mutations have been pointed out by BUTLER *et al*.[266]

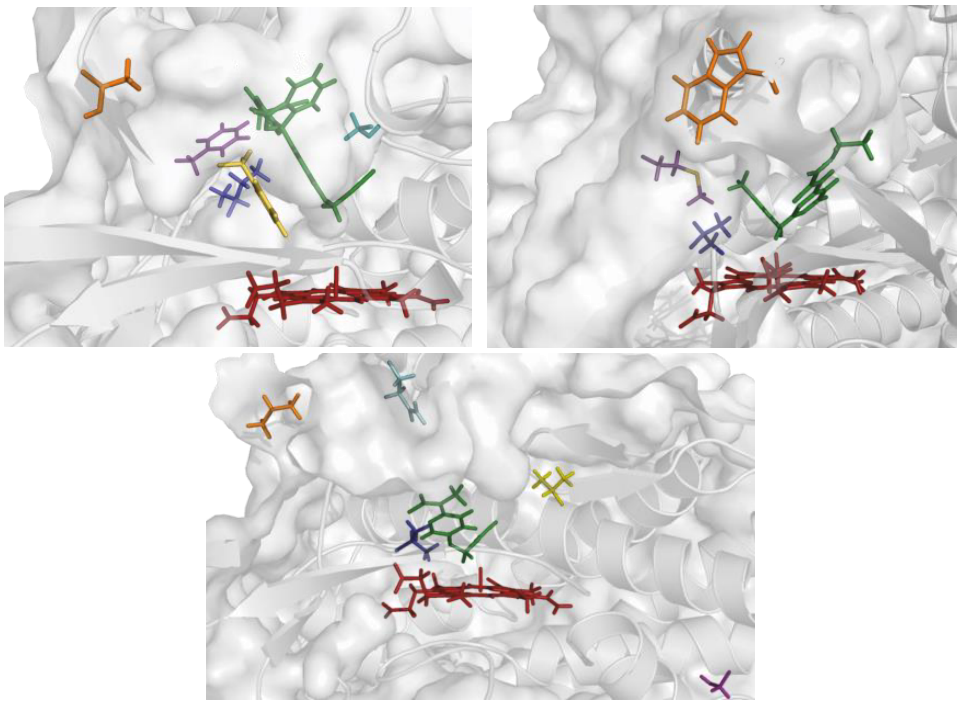

Figure 3-20. *In silico* results. Docking poses for (a) substrate **1a** in TFFIS, (b) substrate **3d** in WMV and (c) substrate **2a** in M01. Highlighted are the oxidized prosthetic heme groups (red), substrate (green) and mutated residues (orange: R47x, blue: F87x).

TFFIS shows a change at position S72F (yellow), where a small polar residue is replaced by a bulky one. This position is known to dramatically affect stereoselectivity, so we can expect this radical change to have an influence on substrate binding.[267] And indeed, it forms a π-stacking interaction with the substrate, fixing it in proximity to the iron core to allow conversion. Likewise, substrate binding is known to be influenced via direct or water-mediated hydrogen bonds by changes of L437 to polar residues.[132] However, serine here does not show any apparent direct interaction in the docked structure.

In the case of WMV, the substrate can enter deep into the active site, positioning the protection group closely to the heme, which can account for the extremely fast turnover observed in the kinetics measurements. Additionally, substrate positioning of **3d** is facilitated by a hydrogen bond between the carbonyl oxygen and S72.

L188, which is mutated in M01, is located on the F-helix of the enzyme. This structure, together with the G-helix, can influence substrate admission,[136,268,269] because they cover the active site and are able to restrict or grant access in a sliding mechanism. Mutations at E267, also present in M01, can be expected to interfere both with substrate binding and proton shuttling, by disturbing a highly conserved hydrogen bond pattern. However, changing it for valine in the case of this mutant can reportedly improve coupling efficiencies for some substrates.[270]

All three mutants have changes of R47 and F87 in common, and especially the latter shows a pattern of being replaced by a small hydrophobic residue (valine or isoleucine, blue). It is known that F87 is close to the substrate in the active site,[136,269,271] restricting access to the iron core, especially in the case of bulky substrates. It is also highly conserved in naturally occurring homologues, but changing it to alanine can reportedly influence selectivity.[149] Our found mutants do not show alanine, but similar changes to small hydrophobic residues (isoleucine for TFFIS and valine for both WMV and M01). R47, on the other hand is the only charged residue in the binding pocket, and crucial for substrate binding and affinity, often appearing in a mutation dyad with Y51.[268,269,271–273] Here we cover a wide range of mutations (orange), from small, polar protic threonine in TFFIS, favoring fluorescein substrates, over small, hydrophobic leucine in M01 to large, hydrophobic tryptophan in WMV. The latter two are most puzzling, since the smaller, supposedly less restrictive residue is present in the more selective mutant. That is a clear reminder that individual residues can never account for the observed performance of an enzyme, but that it is important to look at the bigger picture.

3.6 Reactions inside Living Cells

For the investigation of the deprotection system as a means for possible prodrug activation, the implementation into living cells is an important milestone. TFFIS/**1a** was used as deprotection system for all following experiments, unless otherwise stated.

3.6.1 HeLa Cells

A cervical cancer cell line isolated in 1951 and named HeLa after the original donor HENRIETTA LACKS, was used here.[274] Being the first stable human cell line that allowed culturing over multiple generations, it is widely used across various scientific fields. However, it should be noted that due to changes in chromosome numbers and different additional mutations obtained over the years, the comparability with healthy human tissue is debated. Nevertheless, HeLa cells are still an invaluable tool for investigations *in vivo*, not least because their genome has been sequenced,[275] but also because their behavior has been extensively studied, allowing direct comparisons with different findings and between research groups.
First of all, cytotoxicity of the substrate had to be ruled out, by subjecting the cells to the compound and comparing their activity in a photometric resazurin conversion assay. The experiments carried out by MIKHAIL ZYUZIN confirmed no changes in cell viability at substrate concentrations ranging from 100 nM to 100 µM (*cf.* Figure 3-21).

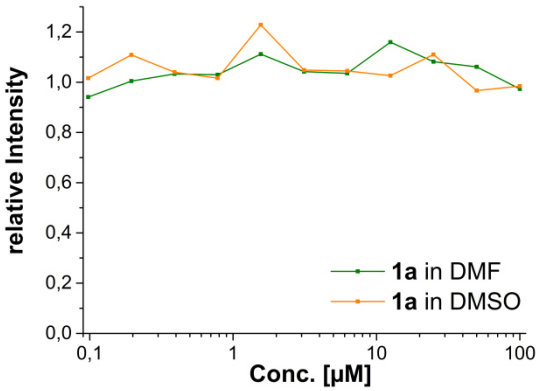

Figure 3-21. Cytotoxicity of substrate **1a** against HeLa cells, with DMF and DMSO as co-solvents, as determined via a resazurin fluorescence assay. Adherent cells were incubated with varying concentrations of the substrate (0.1-100 µM) for 7 h before treatment with resazurin, and the signal was normalized to a control of cells treated with the same co-solvent but no substrate.

Direct Transfection

For a first straightforward qualitative estimation of the deprotection performance inside a living system, commercially available kits allow the direct transfection of cells. This can be done by either using the pure protein or mRNA, which is then used as a translation template by the cell's protein synthesis machinery. Another option is microinjection, which eliminates the need of additional reagents. All three methods were investigated.

Purified Protein

The purified protein was transfected using the commercially available kit TURBOFECT.[276] The enzyme is first mixed with the transfection agent to allow complex formation. Then the cells are treated with the mix and incubated for complex uptake. Upon addition of substrate stock solution to the cells, very low activity of fluorescence was observed along with considerable cytotoxicity (*cf.* Figure 3-22). Experiments were carried out in collaboration with MIKHAIL ZYUZIN.

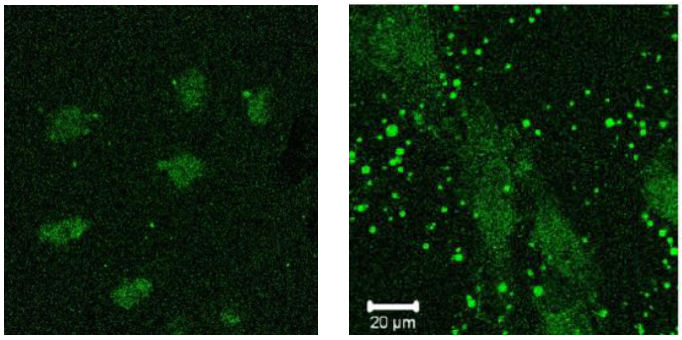

Figure 3-22. Transfection of HeLa cells with purified TFFIS using TURBOFECT at 0.8 (left) and 1.6 µL/µg protein (right). Toxicity of the treatment is easily visible by the round shape of the cells, indicating detachment from the plate, and the formation of vesicles.

Two different complexation ratios were tested, 0.8 or 1.6 µL/µg of the agent per total protein. Cells are dead in both cases, and at increased contrast settings low fluorescence can be seen at the lower concentration, while at higher TURBOFECT ratio the cells are surrounded by a number of TURBOFECT-TFFIS particles. Toxicity of the treatment is easily visible by the formation of vesicles and the round shape of the cells, indicating detachment from the plate. To investigate the cause of this toxicity, the cells were observed over time upon incubation with the complex, and after the addition of the substrate (*cf.* Figure 3-23). The samples showed no difference regarding the incubation time with the reagent, but after addition of the substrate apoptosis was quickly induced in all of the cells. Since substrate toxicity had been ruled out, the reason for the apoptosis of transfected cells has to be attributed to a different effect. A possible explanation is the sudden activation of the enzyme upon addition of substrate, and the following NADPH depletion, which might cause too much stress for the cells. Possible solutions are the optimization of the enzyme amount delivered to each cell, to allow a regeneration of the intracellular NADPH pool while the reaction is taking place.

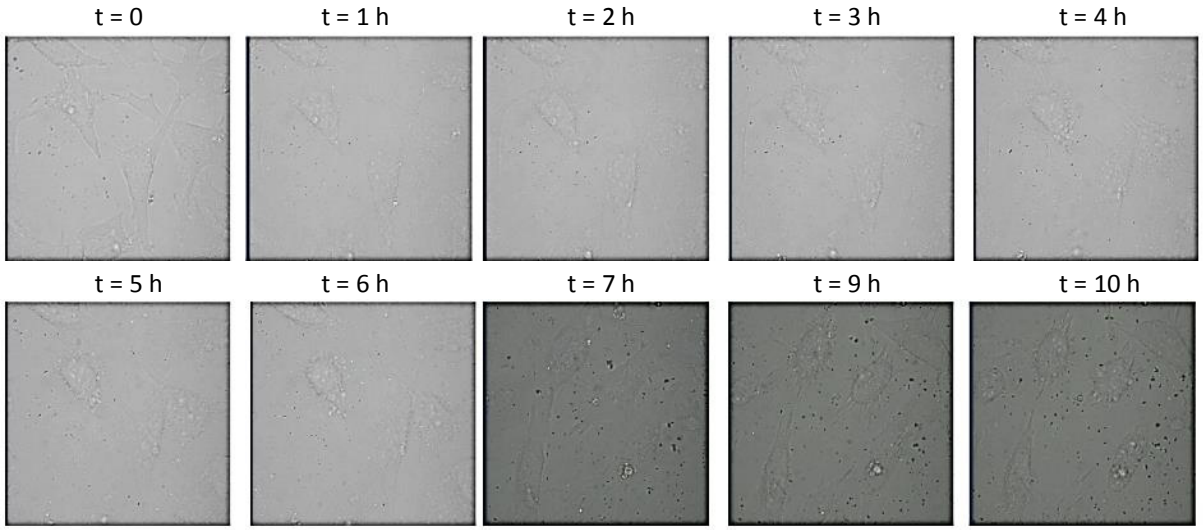

Figure 3-23. Apoptosis of HeLa cells upon addition of substrate **1a** after TURBOFECT transfection of TFFIS.

mRNA

To overcome enzyme deactivation after delivery to lysosomes, a different approach was made to transfect HeLa cells with the corresponding mRNA. Experiments were carried out by JOANNA REJMAN. The general method involves the linearization of plasmid DNA, followed by *in vitro* transcription. The mRNA was subjected to the addition of a poly-A tail, to increase its lifetime inside the cell. It is then transfection into HeLa cells in a process similar to protein transfection, using LIPOFECTAMINE.[277]

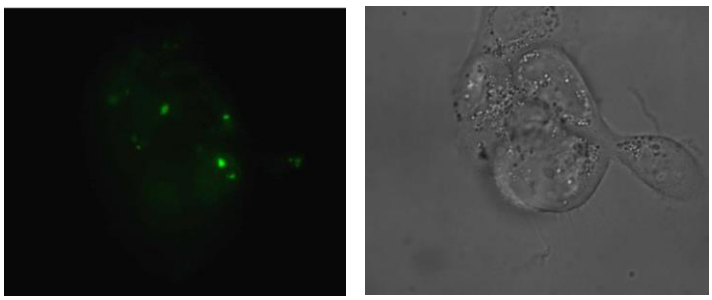

Figure 3-24. Transfection of HeLa cells with mRNA encoding for TFFIS, using LIPOFECTAMINE (left: fluorescence channel, right: bright field). The treatment is toxic for the cells (round shape, formation of vesicles). This has to be attributed to this particular mRNA, since a control with GFP did not show any toxicity (data not shown).

Unfortunately, the achieved fluorescent activity was extremely low, and some toxicity was observed. Since a control experiment using the same method, but mRNA coding for GFP, the toxicity might be due to the protein itself or to the use of bacterial mRNA. To determine which of these, it is suggested to clone the gene to a human vector. However, this approach was not followed any further during the course of this project.

3.6.2 Encapsulation

Ultimately, delivery of the protein to mammalian cells was planned via encapsulation into polyelectrolyte microparticles, which can be taken up via endocytosis and then opened by irradiation.[278] The PARAK group has experience with this procedure, and MIKHAIL ZYUZIN worked on the adaptation of the synthesis for the P450$_{BM3}$ system.

Pre-Tests

In a first step, the enzyme was subjected to a range of different conditions to investigate its stability in the process of encapsulation. Previously published studies[279,280] already showed the susceptibility of the protein to buffer components and environmental conditions, showing the importance of these experiments.

Additives

The performance of the enzyme in presence of different additives used in capsule synthesis was tested at standard conditions in Buffer II: Total P450$_{BM3}$-concentration was kept at 0.1 µM, and the reactions were carried out using NADPH instead of the GDH recycling system, to prevent interactions of the additives with GDH from influencing the results. To evaluate the activity of the enzyme in cell-like environment, HeLa lysate was also used instead of reaction buffer for one reaction. Results are shown in Figure 3-25.

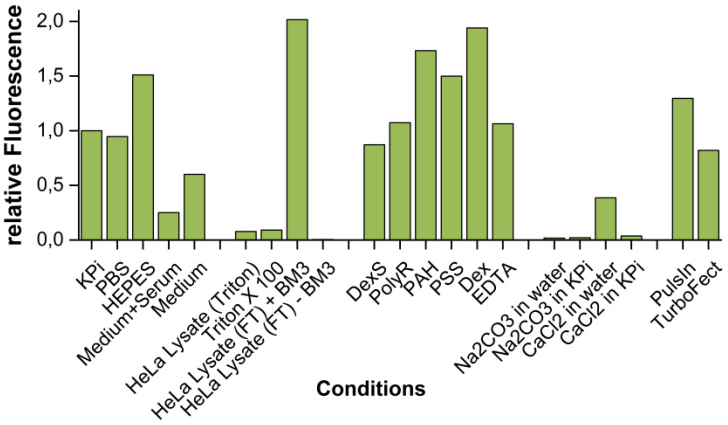

Figure 3-25. Stability of TFFIS in presence of different additives, normalized to the signal in KPi buffer. Reactions were carried out in Buffer II following standard conditions at final concentrations of 0.1 µM and 100 µM for enzyme and substrate, respectively.

Different buffer systems (KPi, PBS) are not an issue, neither are all tested polyelectrolytes. Some of them (PAH, PSS) even increase enzyme activity. HeLa lysate prepared using the detergent Triton X 100 deactivates the protein, while lysate prepared by a cycle of freeze and thaw leads to higher fluorescent responses. Native proteins do not seem to be the cause, so that one possible explanation could be the presence of cell-derived NADPH in the lysate,

because higher cofactor concentration is directly related to product formation. Unfortunately, medium, especially with serum, diminishes enzymatic activity. The biggest issue can be seen in reactions with sodium carbonate or calcium chloride solutions, which reduce activity almost completely. Both tested transfection agents are safe, with PULSIN seemingly being the better choice.

pH-Stability

Since P450$_{BM3}$ is known to be pH sensitive,[145,281] performance of TFFIS was tested at different pH values by ROBERT GIESSMANN. A primary screen showed loss of function between pH 4 and 5, so that a detailed, time dependent profile could be determined (*cf.* Figure 3-26). Below a pH of 4.5, the enzyme is inactivated irreversibly. Time-dependent stability also decreases with falling pH values, so that a pH of 4.0 the enzyme starts deteriorating quickly after ca. 20 min. This can pose a particular problem for intracellular delivery, since many transfection methods first direct their cargo to endosomes, which are often acidified by the cell to become lysosomes with a pH below 5.[282]

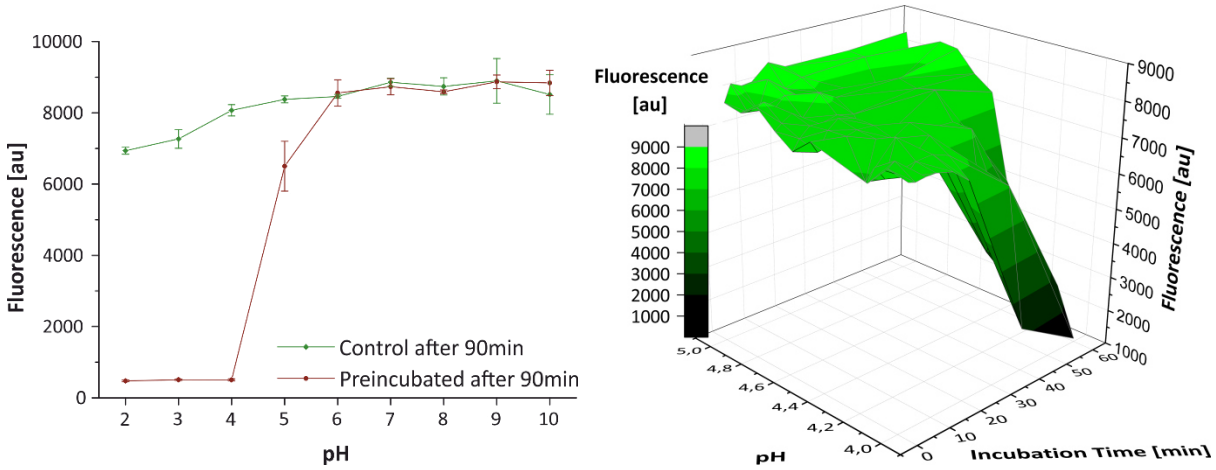

Figure 3-26. Stability of TFFIS at different pH values across a wide range of 2-10 (left), and in a time dependent analysis of a narrow range of 4-5 (right). Reactions were carried out at pH 7 after incubation of the enzyme at the specified pH for 60 min or the specified amount of time. Reactions were carried out in Buffer I following standard conditions at final concentrations of 0.1 µM and 100 µM for enzyme and substrate, respectively.

Ionic Strength

Another important factor in enzymatic activity is ionic strength, known to affect dimerization in P450$_{BM3}$, which is necessary for the enzyme to be active.[264] This parameter can also affect reaction rates.[283] Thus, the performance of TFFIS in potassium and sodium phosphate buffers was analyzed at varying ionic strength between 100 mM and 1 mM.

Even though potassium seems to be the preferred cation for the enzyme, its performance in sodium is still very good and a little less prone to effects from dilution (*cf.* Figure 3-27, top panel). Recommended ionic strength is above 30 mM.

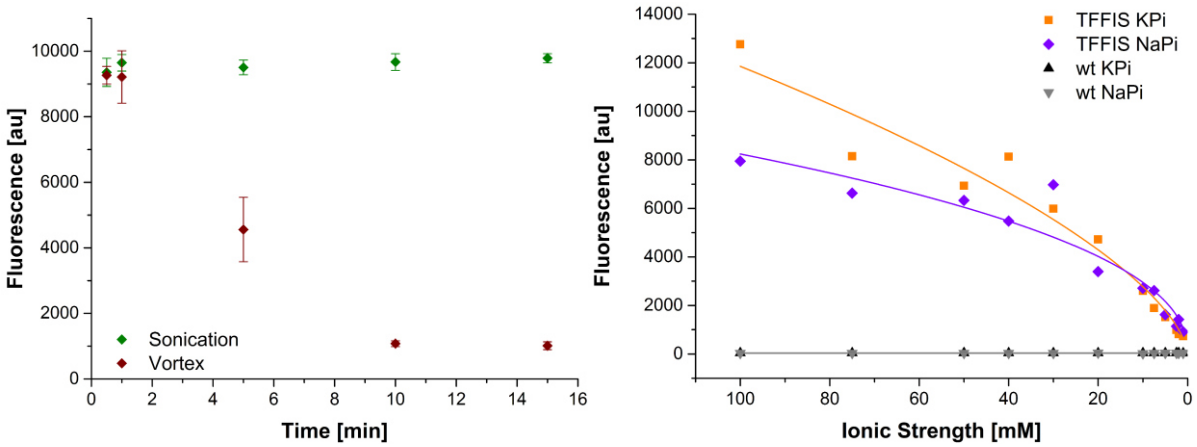

Figure 3-27. Activity test of TFFIS. Left panel: Activity after subjecting the enzyme to different mechanical disturbances for varying amounts of time. Reactions were carried out in Buffer I. Right panel: activity in presence of different cations at varying ionic strength. Reactions were carried out in analogy to Buffer II. All reactions followed standard conditions at final concentrations of 0.1 µM and 100 µM for enzyme and substrate, respectively.

Mechanical Disturbance

The original capsule synthesis protocol requires agitation both by vortex and sonication. For this reason, the endurance of TFFIS was tested after subjecting it to mechanical disturbance for times from 1-15 min. Vortexing for 5 min already reduces activity by around 50%, while sonication is safe even for prolonged periods of time and should thus be favored (*cf.* Figure 3-27, bottom panel).

Modification of Capsule Synthesis

After stability studies (*cf.* Figure 3-28) showed incompatibility of the enzyme with various methods and compounds used in capsule synthesis, modifications were made to diminish these detrimental effects. The general approach is shown in Figure 3-29. First, a calcium carbonate template is precipitated from solution, and then coated in a layer-by-layer technique with alternating layers of anionic and cationic polyelectrolytes.

Once the desired thickness of the wall is reached, the inner core is dissolved using EDTA as a calcium chelating agent. Incorporation of the protein can occur either at the first step (co-precipitation) or after removal of the template (post-loading). Neither method yielded loaded capsules with active enzyme, no matter whether buffered solutions or different mixing methods were applied. Different approaches for the preparation of loaded templates were followed. However, no active capsules could be synthesized so that this means of delivery could not be pursued any further.

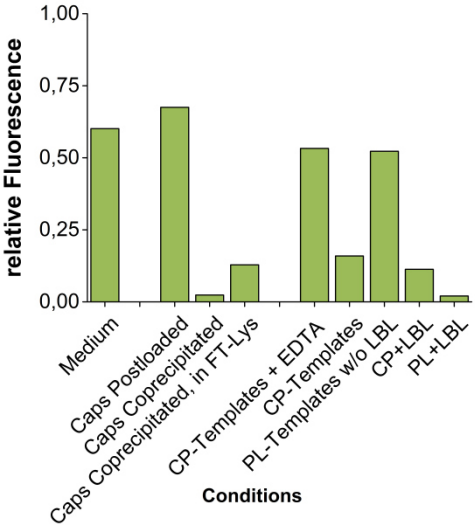

Figure 3-28. Stability of TFFIS during different steps of capsule synthesis. Reactions were carried out in Buffer II following standard conditions at final concentrations of 0.1 µM and 100 µM for enzyme and substrate, respectively.

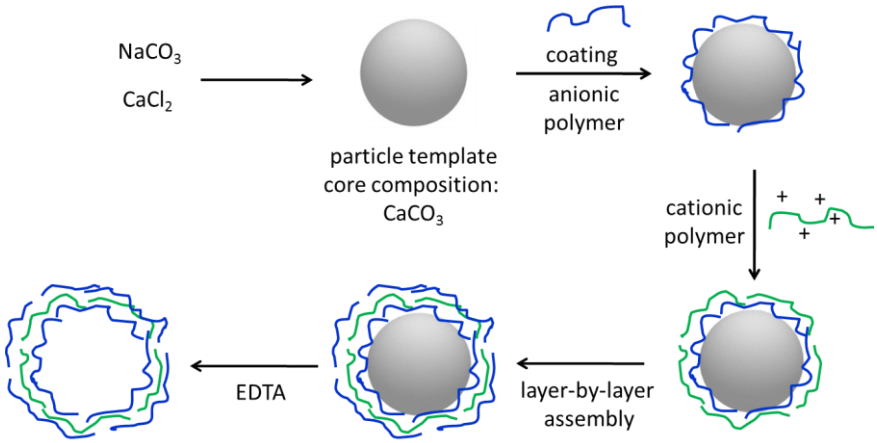

Figure 3-29. Schematic description of capsule synthesis. Solutions of sodium carbonate and calcium chloride are combined and mixed, forming a finely distributed precipitate. These particles are used as templates for a layer-by-layer approach. Treatment of the cores is alternated between anionic and cationic polymers, until the desired thickness is reached. The core can then be dissolved using EDTA as a calcium chelate agent.

3.6.3 Escherichia coli

In order to investigate general enzymatic performance inside living systems, bacterial cells were used as a host, analogous to previous results by RUFF *et al.*[242] In collaboration with NATHALIE NETT, *E. coli* expressing different variants were treated with substrates, and product formation was analyzed either by fluorescence microscopy (measurements by FELIX DEMPWOLFF) or fluorometrically.[1] For TFFIS/**1a**, the resulting signal was easily monitored under a fluorescence microscope, as shown in Figure 3-30. However, the other tested

substrates could not be monitored in that way, since background fluorescence was too high for good contrast imaging. Instead, the supernatants were removed, the cells washed and lysed, before fluorometric analysis using a plate-reader. The results are shown in Figure 3-31, and show clearly that the reaction takes places in the case of all corresponding hit mutant/substrate pairs, but is counteracted by active transport of the product from the cells into the supernatant. Only cells carrying TFFIS keep the majority of the uncaged fluorophore inside.

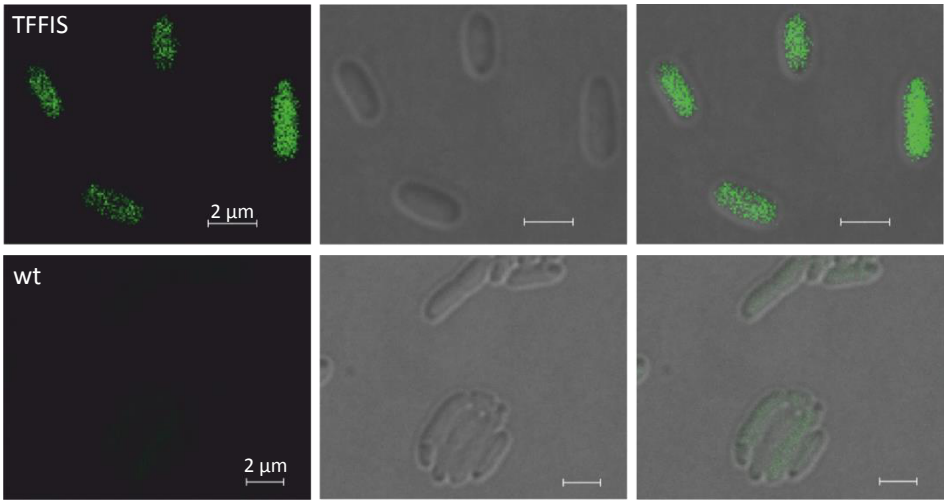

Figure 3-30. Live cell experiments. *E. coli* expressing TFFIS (top) show a high fluorescence signal after treatment with substrate **1a**, indicating successful deprotection**.** No significant signal level is observed in the wt (bottom). Shown are fluorescence channel (left), optical channel (middle) and overlay of both channels (right). Scale bars indicate 2 µm. Figure adapted after our publication with permission from JOHN WILEY & SONS LTD.[1]

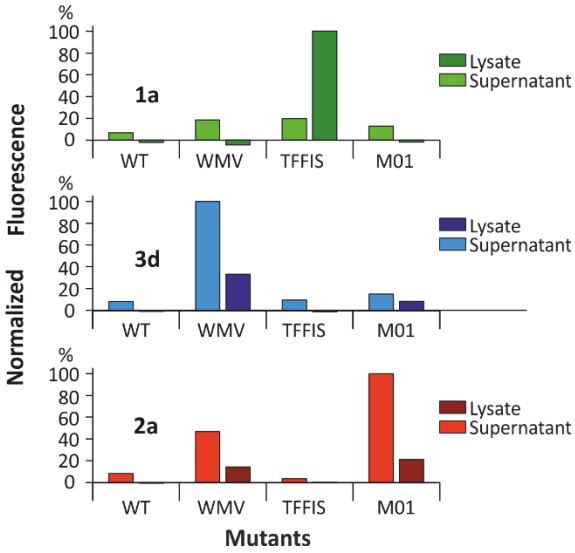

Figure 3-31. Results of fluorescence read-out of supernatants and lysates of whole cell reactions. Signals are normalized to the maximum activity observed for the corresponding fluorophore in this assay, negative signals are due to unrelated substances present in medium or lysate (original data see Appendix 10).

4 Summary and Outlook

Caged compounds have been successfully applied in various fields from chemical biology to medicinal chemistry. For their activation, two main approaches are used: attaching a photolabile substituent, which can be cleaved by irradiation; or using the target organism's own enzymes to remove the group, usually attached via an ester- or amide bond. However, those options suffer from certain disadvantages: The former method often relies on tissue-damaging UV light, and is necessarily confined to the proximity of the light source.[12,35] The latter approach, on the other hand, does not allow any control over the time and site of activation at all. A solution might be the use of artificial catalysts in combination with bioorthogonal protecting groups, but classical metal catalysts are easily deactivated in a cellular environment.[44,45] Fortunately, nature provides us with an invaluable alternative – enzymes are biocatalysts, evolved for selectivity and perfectly adapted to physiological conditions. For that reason, they have been extensively used in medicine and industry.[78,88] However, sometimes their native functionality is not enough for specific applications, giving rise to the flourishing field of protein engineering that allows us to tailor enzymes to our needs.[109,111,112]

Another growing area of research is the controlled delivery and release of a compound inside an organism or even to subcellular destinations. The most versatile option for large biomolecules like a protein are probably nanoparticles, which allow a large range of variation in their composition and can for example be tagged with antibodies for tissue targeting.[284] Thus, we reasoned that engineered enzymes could expand the toolbox of bioorthogonal chemistry by selectively catalyzing the cleavage of an artificial protection group *in vivo*, and that nano- or microparticles could be used to deliver the biocatalyst to its site of action. Specifically, we intended to use caged fluorophores for this proof-of-concept study, to be activated by engineered P450$_{BM3}$ variants available in the REETZ lab, and transported into living cells after encapsulation in collaboration with PARAK's group.

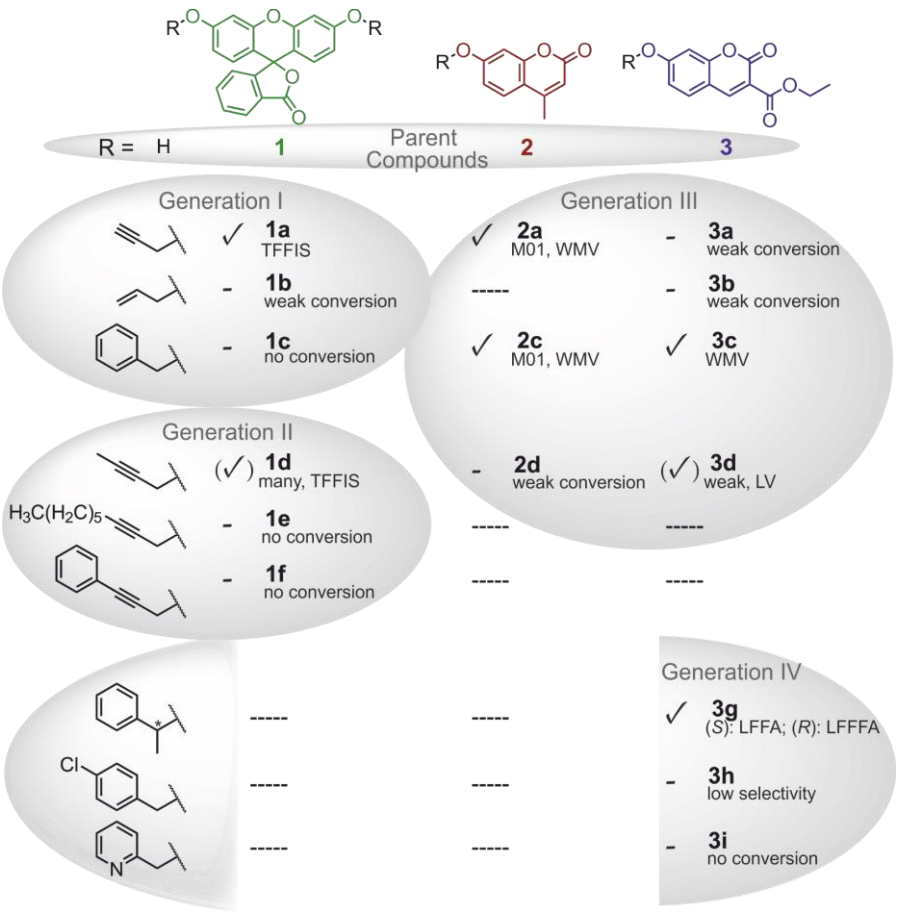

Scheme 4-1. Overview over screened model compounds and their respective hit mutant. First and second generation compounds are fluorescein derivatives (**1**), whereas third generation ones are based on coumarins (**2** and **3**). Further influences were investigated using fourth generation protection groups. Color codes for substrates derived from parent compounds **1** (green), **2** (red) and **3** (blue) are used throughout this study. Figure adapted after our publication with permission from JOHN WILEY & SONS LTD.[1]

As alcohol protection groups, we chose non-native ethers. In the first stage of the project, three fluorescein diethers (Generation I, *cf.* Scheme 4-1 for an overview over all tested substrates) were successfully synthesized. Based on known protocols,[161] a fluorescence-based medium throughput bioassay was developed (*cf.* Figure 3-3). Existing libraries and collections of engineered cytochrome P450$_{BM3}$ variants expressed in *E. coli* (a total of over 1000 variants), which were available from the REETZ lab from previous studies,[161,162,248] were screened for activity in regard to deprotection of these three substrates. The propargyl derivative **1a** proved to be the most suitable option for this fluorophore. After the screening progress, hit variants with unknown mutations were sent for sequencing, and the mutation sites identified. Duplicates were removed, and the mutations of 33 remaining hit variants collected (Table 7-1). Positions of the mutations in the active site are shown in Figure 3-20. The most active mutant is TFFIS, which was purified alongside the wild type for further characterization. Glycerol stocks of active variants, together with others that showed promising activity in different projects (REETZ group) were combined in a collection plate (*cf.*

Appendix 12) to reduce screening effort in the following stages. Results and reproducibility for the conversion of **1a** are shown in Figure 3-7.

In the second stage of the project (Generation II), modifications were introduced at the propargyl residue of the substrate, to test if an improvement in activity could be achieved, but for fluorescein no better protection group was found.[250] Notably, the most active mutant was again TFFIS for the closest related derivative that only differed in a methyl group (butynyl diether **1d**). Furthermore, different fluorescent substrates derived from coumarin were protected with the now established protection groups (Generation III): methyl umbelliferone (**2**), a drug used in bile therapy,[251] and a literature known substrate for similar reactions, 3-carbyxycoumarin ethyl ester (**3**).[242] Their similar core structure can pose a problem for selectivity, since the most active mutant WMV is able to reliably activate both benzyl derivatives **2c** and **3c**. However, it was possible to find mutants that are able to distinguish them (M01), albeit at a lower level of activity. They could be used as starting point for directed engineering to reach better performance. Another set of protection groups (Generation IV) was used to investigate the influence of sterical, electronical, and chiral differences on the deprotection reaction. One interesting aspect was the sensitivity to stereo-information, offering a valuable opportunity to fine-tune selectivity in future designs of caging groups.

After the screening, it was possible to assemble activity profiles like the example shown in Figure 3-9. For every tested parent compound at least one suitable pair of protection group and enzyme was successfully identified in the end, and the corresponding proteins were expressed in a larger culture and purified for further characterization. First, the enzyme concentration was determined to eliminate differences in expression levels that appear in lysate assays. Afterwards, a range of kinetic characteristics and MICHAELIS-MENTEN parameters were measured, highlighting the large differences in performance that are present between mutants. A better understanding on the influence of the involved mutated residues was achieved by combining empirical data from literature known studies with theoretical investigations in docking/MD experiments. An interesting aspect is added by an experiment with two different enzymatic reactions in the same system, which showed that it is possible to create fully orthogonal P450/protection group pairs, but that the issue of mixed dimers has to be closely monitored in such cases (*cf*. Figure 3-17).

To investigate the behavior of the system under the conditions present in encapsulation procedures, TFFIS/**1a** was used as a reliable model reaction and tested against a multitude of different influences: stability against additives and chemicals, changes of pH values, ionic strength, and mechanical disturbance. Unfortunately, it was not possible in the given timeframe to modify the encapsulation protocol sufficiently, so that no functional loaded capsules could be prepared and delivered to mammalian cells. Tests with commercially available techniques to transfect HeLa cells either directly with the protein or the

corresponding mRNA showed only weak activity while at the same time exhibiting a certain level of toxicity.
However, the reaction was successfully implemented inside living *E.coli* with all tested substrates, proving the enzyme active in a cellular environment and thus representing an encouraging support for the general concept (*cf*. Figure 3-30).

Conclusion

In summary, a system for the enzymatic bioorthogonal uncaging of small organic molecules was successfully developed. A range of caged fluorophores carrying ether protection groups were synthesized, which can be cleaved selectively by different identified P450$_{BM3}$ mutants, without the immediate need for mutagenesis experiments. All identified pairs of enzyme and protection group were fully characterized, and the influence of mutations was rationalized based on empirical and theoretical studies. External influences on the performance were examined. Furthermore, it is shown that carefully selected enzyme pairs are able to perform orthogonally in the same system. The scope of different transfection methods into mammalian cells was investigated. Finally, the activity of the P450$_{BM3}$ biocatalysts inside living bacterial cells was proved, and the findings were published and can be accessed at ANGEWANDTE CHEMIE[2] and its international edition.[1]

Outlook

The reported results pave the way for future applications of enzyme-mediated deprotection reactions, which can be used in medicinal chemistry, for the activation of prodrugs at the target location. In chemical biology, carefully selected orthogonal reactions could be used as general tools, or for cellular probes of different compounds, which then result in distinct signals, e.g. for imaging purposes. Another possible use could be the application in crucial steps of organic synthesis, where tailored orthogonal protection groups have a long history in the production of structurally complex compounds. Combined approaches merging chemical and biological synthesis are a much valued concept.[285,286]
To further increase the performance and versatility, it could be promising to transfer the concept to a different system, possibly by choosing a smaller, less complex enzyme that works without the need for a cofactor. Lipases for example are a well-studied class of enzymes, with a long history of engineering, the results of which are listed in an online database.[287]
To address the challenge of protein delivery, other options apart from polyelectrolyte capsules could be investigated. One approach by SÁNCHEZ-SÁNCHEZ *et al*. uses virus-like particles to deliver a functional P450$_{BM3}$ variant into the cytosol of living cancer cells for prodrug activation.[202] A collaboration with their group is currently being established to combine this approach with our enzymatic deprotection system.

5 Experimental Part

5.1 Analytical Equipment

5.1.1 NMR Spectroscopy

NMR spectra were measured at room temperature on a BRUKER AVANCE 300 system (^{1}H-NMR resonance: 300.1 MHz, ^{13}C-NMR resonance: 75.1 MHz), equipped with an autosampler BACS-60 and analyzed using MESTRENOVA V6.0.2 software.
Chemical shifts are given in ppm on the δ scale, and were determined after calibration to the residual signals of the solvents, which were used as an internal standard.[288,289]

$CDCl_3$	^{1}H: δ = 7.26 ppm	^{13}C: δ = 77.16 ppm
DMSO-d_6	^{1}H: δ = 2.50 ppm	^{13}C: δ = 39.52 ppm
Aceton-d_6	^{1}H: δ = 2.05 ppm	^{13}C: δ = 206.26; 29.84 ppm

Coupling constants *J* are given in Hertz and were calculated by the program. Multiplicities of the signals are assigned as observed in the spectra, not according to theoretical expectations. They are denoted as follows: s = singlet, m = multiplet, d = doublet, t = triplet, q = quartet. Assignment of the signals was performed based on coupling constants, 2D spectra (COSY; HMQC) or comparison with literature known compounds.

5.1.2 Mass Spectrometry

Mass spectrometric analysis of the compounds was performed by members of the service department of the PHILIPPS-UNIVERSITÄT MARBURG. HR-ESI mass spectra were acquired with an LTQ-FT Ultra mass spectrometer (THERMO FISHER SCIENTIFIC). Ionic masses are given in units of m/z for the isotopes with the highest natural abundance.

5.1.3 Fluorometric and Spectrophotometric Measurements

Photometric absorption analyses were measured on a JASCO V-650 spectrophotometer equipped with a PAC-743 Peltier temperature control unit and analyzed using SPECTRAMANAGER V2 software or ORIGIN 2015. Fluorescence measurements were performed in black 96-well flat bottom plates on a MOLECULAR DEVICES SpectraMax M5 using SOFTMAX Pro V5.2 software and analyzed using ORIGIN 2015. The settings used for the detection of different substrate classes are shown in Table 5-1.

Table 5-1. Settings for fluorescence read-out of different substrate classes, determined from their respective excitation and emission maxima.

Substrate Class		Excitation Wavelength λ_{ex} [nm]	Emission Wavelength λ_{em} [nm]	Cut-off filter λ_{CO} [nm]
Fluorescein	**1**	490	520	515
Methylumbelliferone	**2**	370	450	420
Carboxycoumarin	**3**	400	440	420

Linearity in the observed ranges of fluorescence was confirmed for all fluorophores (*cf.* Figure 7-1).

5.1.4 HPLC Measurements

HPLC Analysis of Reactions

HPLC analyses were performed on an AGILENT 1200 system equipped with a quaternary pump, autosampler, column oven and variable wavelength detector (220 nm) and analyzed using CHEMSTATION B03.01 software.

Run conditions are shown in Table 5-2. All separations were performed at 30°C, on a reversed-phase C18 column (AGILENT Eclipse XD8-C18, d = 4.6 mm, l = 150 mm, particle size 5 µm) in MeCN : 0.1% TFA/H_2O with 15 µL injection volume. Retention times for all derivatives are given in Table 5-3 and an example chromatogram for a typical reaction of TFFIS on substrate **1a** is shown in Figure 3-18.

Table 5-2. HPLC conditions for analysis of reaction products in MeCN : 0.1% TFA/H_2O, at a flow rate of 1.5 mL/min.

Time [min]	Gradient I	Gradient II
0	30-70	50-50
7	30-70	50-50
15	60-40	70-30
20	60-40	50-50
22	30-70	50-50

Table 5-3. Retention times for substrate derivatives as determined from the conditions described in Table 5-2, Gradient I.

Compound		Retention Time /min	Area for 100 µM /mAU*s
Fluorescein	**1**	8.7	8030
Propargyl Diether	**1a**	18.1	10033
Propargyl Monoether		14.7	6190
Carboxycoumarine	**3**	3.1	1053
Butynyl Ether	**3d**	13.9	1061
Benzyl Ether	**3c**	16.9	1140
Methylumbelliferone	**2**	2.7	582
Propargyl Ether	**2a**	10.7	693

Calibration Curves

For a calibration curve using integrated HPLC signals, DMF stocks of fluorescein derivatives in concentrations ranging from 10 to 0.1 mM were diluted 100-fold, either in water or MeCN. MeCN-tests were carried out in triplicates. The solutions were prepared in a NUNC round-bottom PP 96-well plate in a total volume of 200 µL (water, added one by one using a manual pipette) or 202 µL (MeCN, added in rows of 6 using a manual 8-channel pipette), then sealed with a NUNC rubber lid that can be perforated by the HPLC autosampler. Gradient II was used for all runs on the same machine. Tested substrates were **1**, **1a**, **1a'**, and **1d**.

Concentration Tests

Extraction tests were carried out (results *cf.* Chapter 3.5.2, page 45, Figure 3-14): Substrates and product stocks of substrates and fluorescein in concentrations ranging from 10 to 0. 1 mM were diluted 100-fold in buffer in deep well plates, to yield a total volume of 500 µL. These were extracted using the TECAN Pipetting robot. After the first addition of 200 µL EtOAc and centrifugation for 10 min at 4000 rpm, ~50 µL of the organic phase were transferred to a NUNC round bottom PP 96-well plate, and a second extraction step (150 µL) followed. Organic phases were combined, and evaporated under air overnight. Redissolution in 300 µL MeCN was achieved using an 8-channel pipette, and plates were immediately sealed with a NUNC rubber lid. Samples were prepared in triplicates.

For evaluation of the extraction method and reproducibility, samples of 500 µL at a concentration of 100 µM were extracted manually:

1. copying the robot-procedure exactly (R, Robot)
2. copying the robot-procedure, but adding a step of thorough mixing by pipetting before each centrifugation step (M, Mix)
3. extracting twice with 500 µL EtOAc, combining org. phases (300+500 µL), and redissolving in 500 µL MeCN (500)

Enantiomeric Separation

Separation conditions are shown in Table 5-4. Analytical measurements were performed at 30°C on a DAICEL CHIRALPAK IB column (d = 4.6 mm, l = 250 mm, particle size 5 µm) using gradient IV, and separation of the enantiomers for isolation was performed on a semi-preparative version of the same column (d = 10 mm, l = 250 mm, particle size 5 µm) using gradient III. Example chromatograms are shown in Figure 3-8, page 40.

Table 5-4. HPLC conditions for enantiomeric resolution in MeCN : 0.1% TFA/H_2O.

Time [min]	Gradient III flow: 3 mL/min	Time [min]	Gradient IV flow: 1 mL/min
0	45-55	0	45-55
50	50-50	27	52-48
60	50-50	29	45-55
70	45-55	39	45-55

5.2 Buffers and Stock Solutions

Media and chemicals for bacteria were ordered from FLUKA and ROTH. High-purity water was generated from the institute's deionized water supply using a TKA MICROLAB water purification system.

LB-Medium (Lysogeny Broth)

Tryptone	10 g
Yeast Extract	5 g
NaCl	10 g

Water was added to a total volume of 1000 mL, components mixed until dissolved. The pH was then adjusted to 7 before sterilization by autoclaving.

TB-Medium (Terrific Broth)

Tryptone	12 g
Yeast Extract	24 g
Glycerol	4 mL

Water was added to a total volume of 900 mL, components mixed until dissolved, then sterilized by autoclaving. Before use, 100 mL of phosphate salt solution was added (see below).

Phosphate Salts for TB-Medium (10x)

K_2HPO_4 Trihydrate	164.3 g	(720 mM)
KH_2PO_4	23.1 g	(170 mM)

Water was added to a total volume of 1000 mL, components mixed until dissolved, then sterilized by autoclaving.

Power Mix (100x)

Glycerol	40%	
Glutamate	saturated	in 100 mM KPi, pH 7.4

Components were mixed and sterilized by autoclaving.

Transition Trace Metal Mix (TTM-Mix, 1000x)

Protocol modified from STUDIER et al.[290] by KILLE.[248]

$FeCl_3 \cdot 6\ H_2O$	675.75 mg	(50 mM)
$CaCl_2$	110.99 mg	(20 mM)
$MnSO_4 \cdot H_2O$	84.51 mg	(10 mM)
$ZnSO_4 \cdot 7\ H_2O$	143.77 mg	(10 mM)

$CoCl_2 \cdot 6\ H_2O$	23.79 mg	(2 mM)
$CuCl_2 \cdot 2\ H_2O$	17.05 mg	(2 mM)
$NiCl_2 \cdot 6\ H_2O$	23.77 mg	(2 mM)
$Na_2MoO_4 \cdot 2\ H_2O$	24.19 mg	(2 mM)
H_3BO_3	6.18 mg	(2 mM)
con. HCl	312.5 µL	

The final volume was adjusted with purified water to 50 mL.

TB-Medium (Terrific Broth) with Phosphate Salts for $P450_{BM3}$ Expression

TB-Medium	900 mL
Phosphate Salts	100 mL
Power Mix	10 mL
TTM-Mix	1 mL
Kanamycin	1 mL

10x Phosphate Buffer (KPi) 1 M, pH 7.4

K_2HPO_4 Trihydrate	160 g
KH_2PO_4	40.9 g

Water was added to a total volume of 1000 mL, components mixed until dissolved, then the pH value was confirmed using a pH meter and adjusted with KOH or HCl if necessary.

Phosphate Buffer (KPi) 100 mM, pH 7.4

10x Phosphate Buffer	100 mL
Water	900 mL

Both components were mixed and filtered sterile prior to use. Storage at 4°C.

Stock Solutions of Additives

Individual stocks were prepared by dissolving the specified amount of substance in water[a], KPi[b] (100 mM pH 7.4) or DMF[c] and stored at -20°C, with the exemption from NADPH-stocks, which were freshly prepared before use. Final dilution factors for use are given.

Kanamycin[a] (Kan)	50 mg/mL		x1000
Isopropyl-β-D-1-thiogalactopyranoside[a] (IPTG)	23.83 mg/mL	(100 mM)	x1000
Nicotinamide adenine dinucleotide phosphate monosodium salt[b] ($NADP^+$)	78.74 mg/mL	(100 mM)	x100
Reduced nicotinamide adenine dinucleotide phosphate tetrasodium salt[b] (NADPH)	20.0 mg/mL	(24 mM)	x100

Glucose Monohydrate[b]	180.16 mg/mL	(1 M)	x10
Glucose Dehydrogenase[b] (Codexis GDH-105) (GDH)		133 U/mL	x133
Substrates[c]		(0.01-10 mM)	x100

P450 Washing Buffer

Glycerol	5%	in 100 mM KPi, pH 7.4

P450 Reaction Buffer I

Glucose	100 mM	in 100 mM KPi, pH 7.4
$NADP^+$	1 mM	
GDH	1 U/ml	

The NADPH recycling system used here is described in Figure 3-1.

P450 Reaction Buffer II

NADPH	300 μM	in 100 mM KPi, pH 7.4

BRITTON-ROBINSON Buffers

H_3BO_3	0.04 M
H_3PO_4	0.04 M
Acetic Acid	0.04 M

The aqueous solution was filtered, and titrated to the desired pH value with 0.2 M NaOH.

Lysis Buffer

Lysozyme	1 mg/mL	in 100 mM KPi, pH 7.4

Elution Buffer

KCl	1 M	in 100 mM KPi, pH 7.4

HEPES Buffer

HEPES	20 mM, pH 7.5

DEAE Buffers

Buffer A:	HEPES	20 mM, pH 7.5
Buffer B:	HEPES	20 mM, pH 7.5
	KCl	1 M

His-Trap Buffers

Buffer A:	NaCl	800 mM	in 100 mM KPi, pH 7.4
	L-Histidine	2 mM	
Buffer B:	L-Histidine	80 mM	in 100 mM KPi, pH 7.4

4x SDS Running Buffer

TRIS	25 mM
Glycine	192 mM
SDS	0.1%

SDS Sample Buffer

Tris/HCl	100 mM
SDS	100 mM
β-Mercaptoethanol	2 mM
Glycerol	40%
Bromophenol Blue	1%

SDS Resolving Gel

For 12 gels:

Acrylamide	32 mL	12% in H_2O
Tris/HCl	8.75 mL	0.5 M, pH 8.4
H_2O	19.86 mL	
SDS	350 µL	10% in H_2O
APS	175 µL	10% in H_2O
TEMED	35 µL	

SDS Loading Gel

For 12 gels:

Acrylamide	5.83 mL	5%, H_2O
Tris/HCl	20 mL	1.5 M, pH 6.8
H_2O	27 mL	
SDS	800 µL	10% in H_2O
APS	400 µL	10% in H_2O
TEMED	40 µL	

SDS Gel Stain

Ethanol	50%	in H_2O
Acetic acid	10%	
Coomassie Brilliant Blue	250 mg/L	

5.3 Substrate Synthesis and Characterization

5.3.1 General Methods

Commercially available chemicals were ordered in highest available purity from ACROS, MERCK, SIGMA ALDRICH, TCI CHEMICALS, THERMO FISHER SCIENTIFIC and VWR, and used without further purification unless otherwise specified. Analytical grade solvents for reactions and HPLC were purchased from VWR, ACROS, FISHER SCIENTIFIC or MERCK, if necessary dried using standard protocols.[291] Solvents for chromatography were used from the institute's supply after distillation. Compressed air, liquid and gaseous nitrogen were used from the institutes supply without further purification. High-purity water was generated from the institute's deionized water supply using a TKA MICROLAB water purification system.

Chemical syntheses were performed under inert nitrogen gas atmosphere unless otherwise specified, using SCHLENK technique and flasks dried by repeated heating and flushing with inert gas. Transfer of solvents and liquid compounds was achieved using syringes and septa.

For analysis by thin layer chromatography (TLC), commercially available silica gel sheets were used (Alugram Xtra SIL G/UV$_{254}$ from MACHEREY-NAGEL). Detection of the substances was performed under UV light at wavelengths of 254 or 366 nm, or by staining with a potassium permanganate dip. Purification by flash column chromatography was carried out using silica gel 60 (particle size of 40-63 μm, from MERCK), and under increased pressure from the house air supply.

5.3.2 Fluorescein Derivatives

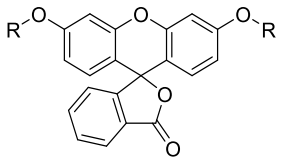

General Method for Protected Fluorescein Derivatives

Adapted from RAJASEKAR *et al.*[243] potassium carbonate (2.93 g, 21.0 mmol, 7.0 eq) and fluorescein (**1**, 1.00 g, 3.0 mmol, 1.0 eq) were dissolved in DMF (3 mL) and purged with nitrogen for 15 min. The corresponding bromide (30 mmol, 10 eq) was added, upon which a reddish precipitate formed, making stirring difficult. An additional ~2 mL of solvent were added to allow for proper stirring. The slurry was heated to 70°C and stirred overnight under air. The resulting mixture was diluted with ethyl acetate (25 mL) and extracted with

5% HCl (25 mL). The aqueous phase was washed twice with ethyl acetate. Combined organic phases were washed with saturated sodium bicarbonate solution and dried over sodium sulfate. The solvent was evaporated and the orange solid raw product purified via column chromatography.

Fluorescein Propargyl Derivatives (1a, a', a'')

The solid raw product was purified via column chromatography (silica; DCM/MeOH 50:1), and isolated as an off-white solid (600 mg, 9.45 mmol, 45%). The mono-ether **1a'** and ether ester **1a''** derivatives were obtained as solid, sticky, orange side products (129 mg, 2.52 mmol, 12% and 330 mg, 3.78 mmol, 18%, respectively).

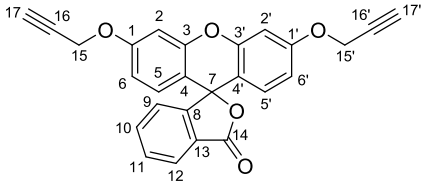

Analytical Data for **1a**

TLC R_f = 0.69 (DCM/MeOH 50:1)
R_f = 0.91 (EtOAc)

^{1}H-NMR (300 MHz; $CDCl_3$): δ 8.02 (d, ^3J = 7.6 Hz, 1H, C12-*H*), 7.73 – 7.56 (m, 2H, C10/11-*H*), 7.16 (d, ^3J = 7.6 Hz, 1H, C9-*H*), 6.88 (d, ^4J = 1.9 Hz, 2H, C2-*H*), 6.72 (dd, ^3J = 8.8, ^5J = 0.4 Hz, 1H, C5-*H*), 6.67 (dd, ^3J = 8.8, ^4J = 2.3 Hz, 1H, C6-*H*), 4.72 (d, ^4J = 2.4 Hz, 4H, C15-*H*), 2.56 (t, ^4J = 2.4 Hz, 2H, C17-*H*) ppm.

^{13}C-NMR (75 MHz; $CDCl_3$): δ 169.4 (*C*14), 159.3 (*C*1), 153.2 (*C*8), 152.5 (*C*3), 135.2 (*C*10), 129.9 (*C*11), 129.3 (*C*5), 126.9 (*C*13), 125.2 (*C*12), 124.1 (*C*9), 112.3 (*C*6/4), 102.3 (*C*2), 83.0 (*C*7), 78.0 (*C*17), 76.29 (*C*16), 56.19 (*C*15) ppm.

HRMS (ESI) m/z: calcd. for $C_{26}H_{16}O_5$ $[M+H]^+$: 409.1076, found: 409.1072.

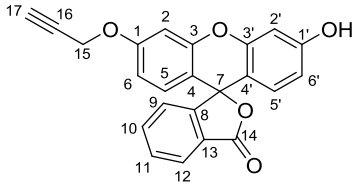

Analytical Data for **1a'**

TLC R_f = 0.00 (DCM/MeOH 50:1)
R_f = 0.79 (EtOAc)

^{1}H-NMR (300 MHz; Acetone-d_6): δ 9.07 (s, 1H, C14-O*H*), 7.99 (td, ^3J = 7.5 Hz, ^4J = 1.0 Hz, 1H, C12-*H*), 7.81 (td, ^3J = 7.5, ^4J = 1.3 Hz, 1H, C10-*H*), 7.74 (td, ^3J = 7.4 Hz, ^4J = 1.1 Hz, 1H, C11-*H*), 7.30 (dt, ^3J = 7.6 Hz, ^4J = 1.0 Hz, 1H, C9-*H*), 6.96 (t, $^{4,5}J$ = 1.5 Hz, 1H, C2-*H*), 6.78 (dd, ^3J = 2.1 Hz, ^4J = 0.7 Hz, 1H, C6'-*H*), 6.77 (d, $^{4,5}J$ = 1.4 Hz, 2H, C5/6), 6.67 (d, J = 0.7 Hz, 1H, C2'-*H*), 6.64 (d,

^3J = 2.1 Hz, 1H, C5'-*H*), 4.89 (d, ^4J = 2.4 Hz, 2H, C15-*H*), 3.15 (t, ^4J = 2.4 Hz, 1H, C17-*H*) ppm.

^{13}C-NMR (75 MHz; Acetone-d_6): δ 160.3, 153.9, 136.1 (C10), 130.8, 130.2, 130.0, 125.4 (C12), 124.9 (C9), 113.5, 113.4, 113.2, 103.4, 103.3, 102.7, 79.2, 77.6, 56.7 (C15) ppm.

HRMS (ESI) m/z: calcd. For $C_{23}H_{14}O_5$ [M-H]$^+$: 371.0914, found: 371.0908.

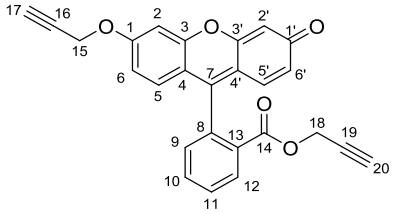

Analytical Data for **1a''**

TLC R_f = 0.00 (DCM/MeOH 50:1)

R_f = 0.39 (EtOAc)

^{1}H-NMR (300 MHz; $CDCl_3$): δ 8.27 (dd, 1H, ^3J = 7.8 Hz, ^4J = 1.2 Hz, 1H, C12-*H*), 7.77 (td, 1H, ^3J = 7.5 Hz, ^4J = 1.5 Hz, 1H, C10-*H*), 7.69 (td, 1H, ^3J = 7.5 Hz, ^4J = 1.5 Hz, 1H, C11-*H*), 7.33 (dd, 1H, ^3J = 7.5 Hz, ^4J = 1.5 Hz, 1H, C9-*H*), 7.07 (d, ^4J = 2.5 Hz, 1H, C2-*H*), 6.94 (d, ^3J = 9.0 Hz, 1H, C5'-*H*), 6.89 (d, ^3J = 9.7 Hz, 1H, C5'-*H*), 6.82 (dd, ^3J = 9.0 Hz, ^4J = 2.5 Hz, 1H, C6-*H*), 6.61 (dd, ^3J = 9.7 Hz, ^4J = 1.8 Hz, 1H, C6'-*H*), 6.57 (s, 1H, C2'-*H*), 4.80 (d, ^4J = 2.5 Hz, 2H, C15-*H*), 4.60 (dd, ^2J = 15.5 Hz, ^4J = 2.4 Hz, 2H, C18-*H*), 2.61 (t, ^4J = 2.4 Hz, 1H, C20-*H*), 2.33 (t, ^4J = 2.5 Hz, 1H, C17-*H*) ppm.

^{13}C-NMR (75 MHz; $CDCl_3$): δ 164.6, 162.0, 159.0, 154.3, 134.7, 133.2, 131.5, 130.7, 130.3, 130.1, 130.0, 118.3, 115.7, 114.0, 106.0, 101.7, 76.9, 75.3, 56.5 (C15), 52.9 (C18) ppm.

HRMS (ESI) m/z: calcd. for $C_{26}H_{16}O_5$ [M-H]$^+$: 409.1071, found: 409.1067.

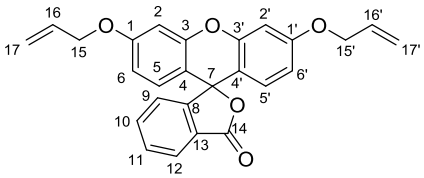

Fluorescein Allyl Diether (1b)

The solid raw product was purified via column chromatography (silica; hexanes/ethyl acetate 5:1 → 3:1), and isolated as a colorless solid (539 mg, 9.03 mmol, 43%).

TLC R_f = 0.34 (Hex:EE 3:1)

^{1}H-NMR (300 MHz; $CDCl_3$): δ 8.02 (d, ^3J = 7.1 Hz, 1H, C12-*H*), 7.65 (ddd, ^3J = 7.4 Hz, ^4J = 1.5 Hz, 1H, C10-*H*), 7.62 (ddd, ^3J = 7.4 Hz, ^4J = 1.4 Hz, 1H, C11-*H*), 7.16 (d,

^{3}J = 7.7 Hz, 1H, C9-*H*), 6.78 (d, ^{4}J = 2.3 Hz, 2H, C2-*H*), 6.68 (d, ^{3}J = 8.8 Hz, 2H, C5-*H*), 6.62 (dd, ^{3}J = 8.8 Hz, ^{4}J = 2.4 Hz, 2H, C6-*H*), 6.04 (ddt, $^{3,trans}J$ = 17.3 Hz, $^{3,cis}J$ = 10.5 Hz, ^{3}J = 5.3 Hz, 2H, C16'-*H*), 5.42 (dq, $^{3,trans}J$ = 17.2, ^{4}J = 1.6 Hz, 2H, C17-*H*), 5.31 (dq, $^{3,cis}J$ = 10.5 Hz, ^{2}J = 1.4 Hz, 2H, C17-*H*), 4.56 (dt, ^{3}J = 5.3 Hz, ^{4}J = 1.5 Hz, 4H, C15-*H*) ppm.

^{13}C-NMR (75 MHz; $CDCl_3$): δ 169.5, 160.2, 153.3, 152.6, 135.1, 132.8, 129.8, 129.2, 127.0, 125.1, 124.1, 118.3, 112.3, 111.6, 101.9, 83.4, 69.2 ppm.

HRMS (ESI) m/z: calcd. for $C_{26}H_{20}O_5$ $[M+H]^+$: 413.1389, found: 413.1384.

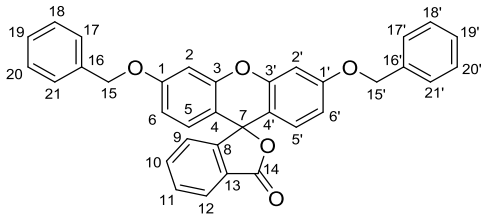

Fluorescein Benzyl Diether (1c)

The solid raw product was purified via column chromatography (silica; DCM/MeOH 10:1) and isolated as a colorless solid (1173 mg, 15.96 mmol, 76%).

TLC R_f = 0.30 (Hex:EE 3:1)

^{1}H-NMR (300 MHz; $CDCl_3$): δ 8.02 (d, ^{3}J = 6.9 Hz, 1H, C12-*H*), 7.88 – 7.53 (m, 2H, C10/11-*H*), 7.53 – 7.31 (m, 10H, C17-C21-*H*), 7.16 (d, J = 7.3 Hz, 1H, C9-*H*), 6.84 (s, 2H, C2-*H*), 6.69 (s, 4H, C5/6-*H*), 5.09 (s, 4H, C15-*H*) ppm.

^{13}C-NMR (75 MHz; $CDCl_3$): δ 169.5 (C14), 160.6 (C1), 153.3 (C8), 152.6 (C3), 136.4, 135.1 (C5), 129.8, 129.3, 128.8, 128.4, 127.6, 127.0, 125.2 (C12), 124.1(C9), 112.4 (C6), 111.7 (C4), 102.0 (C2), 70.5 (C15) ppm.

HRMS (ESI) m/z: calcd. for $C_{34}H_{24}O_5$ $[M+H]^+$: 513.1702, found: 513.1697.

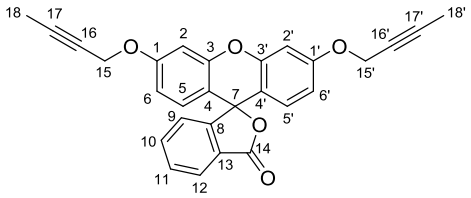

Fluorescein Butynyl Diether (1d)

This synthesis was carried out by NATHALIE NETT.[250]

The solid raw product was purified via column chromatography (silica; DCM/MeOH 50:1) and isolated as a colorless solid (255 mg, 0.58 mmol, 15%).

TLC R_f = 0.57 (DCM: MeOH 50:1)

^{1}H-NMR (300 MHz; $CDCl_3$): δ 8.02 (dd, ^{3}J = 7.2 Hz, ^{4}J = 1.0 Hz, 1H, C12-*H*), 7.64 (td, ^{3}J = 7.4 Hz, ^{4}J = 1.4 Hz, 1H, C10-*H*), 7.61 (td, ^{3}J = 7.4 Hz, ^{4}J = 1.2 Hz, 1H, C11-*H*), 7.16 (dt, ^{3}J = 7.3 Hz, ^{4}J = 1.0 Hz, 1H, C9-*H*), 6.86 (d, *J* = 2.4 Hz, 2H, C2-*H*), 6.75 (dd, ^{3}J = 8.8 Hz, ^{4}J = 2.4 Hz, 2H, C6-*H*), 6.69 (d, ^{3}J = 8.8 Hz, 2H, C5-*H*), 4.67 (q, ^{5}J = 2.2 Hz, 4H, C15-*H*), 1.87 (t, ^{5}J = 2.3 Hz, 6H, C18-*H*) ppm.

^{13}C-NMR (75 MHz; $CDCl_3$): δ 162.7, 159.7, 153.2, 152.6, 135.1, 129.8, 129.2, 127.0, 125.2, 124.1, 112.3, 112.0, 102.2, 84.6, 77.4, 73.6, 56.9, 3.9 ppm.

HRMS (APCI) m/z: calcd. for $C_{38}H_{20}O_5$ $[M+H]^+$: 437.1383, found: 437.1384.

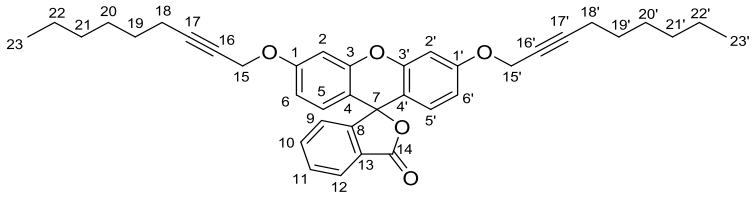

Fluorescein Nonynyl Diether (1e)

This synthesis was carried out by NATHALIE NETT.[250]

The solid raw product was purified via column chromatography (silica; DCM) and isolated as a beige solid (306 mg, 0.75 mmol, 35%).

TLC R_f = 0.64 (DCM)

^{1}H-NMR (300 MHz; $CDCl_3$): δ 8.02 (dd, ^{3}J = 6.6 Hz, ^{4}J = 1.3 Hz, 1H, C12-*H*), 7.64 (m, 2H, C10/11-*H*), 7.16 (dd, ^{3}J = 6.6 Hz, ^{4}J = 1.0 Hz, 1H, C9-*H*), 6.87 (dd, ^{4}J = 2.0 Hz, ^{5}J = 0.7 Hz, 2H, C2-*H*), 6.68 (m, 4H, C5/6-*H*), 4.70 (t, ^{5}J = 2.1 Hz, 4H, C15-*H*), 2.22 (ddd, ^{3}J = 7.1 Hz, ^{5}J = 4.5 Hz, ^{5}J = 2.0 Hz, 4H, C18-*H*), 1.27 (m, 16H, C19-C22-*H*), 0.86 (m, 6H, C23-*H*) ppm.

^{13}C-NMR (75 MHz; $CDCl_3$): δ 159.7, 153.3, 152.6, 135.1, 129.8, 129.2, 127.5, 127.1, 125.2, 124.1, 112.4, 112.0, 102.3, 89.2, 83.3, 74.4, 57.0, 31.4, 28.6, 28.5, 22.7, 18.9, 14.2 ppm.

HRMS (APCI) m/z: calcd. for $C_{38}H_{40}O_5$ $[M+H]^+$: 577.2947, found: 577.2949.

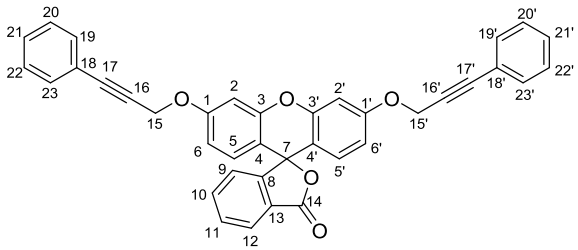

Fluorescein Phenylpropargyl Diether (1f)

This synthesis was carried out by NATHALIE NETT.[250]

The solid raw product was purified via column chromatography (silica; DCM) and isolated as a beige solid (434 mg, 0.77 mmol, 36%).

TLC R_f = 0.77 (DCM)

^{1}H-NMR (300 MHz; $CDCl_3$): δ 8.02 (dd, ^3J = 6.5 Hz, ^4J = 1.1 Hz, 1H, C12-*H*), 7.70 – 7.59 (m, 2H, C10/11-*H*), 7.47 – 7.44 (m, 4H), 7.39 (s, 1H, C9-*H*), 7.34 – 7.29 (m, 5H, C_{arom}-*H*), 7.15 – 7.08 (m, 1H, C_{arom}-*H*), 6.90 – 6.85 (m, 2H, C_{arom}-*H*), 6.65 (d, ^4J = 1.1 Hz, 4H, C_{arom}-*H*), 4.87 (s, 4H, C15-*H*) ppm.

^{13}C-NMR (75 MHz; $CDCl_3$): δ 169.5, 159.6, 153.3, 152.6, 135.1, 132.0, 129.9, 129.3, 129.0, 128.5, 127.0, 125.2, 124.2, 122.2, 112.4, 112.2, 102.4, 87.9, 83.3, 83.1, 57.1 ppm.

HRMS (APCI) m/z: calcd. for $C_{38}H_{24}O_5$ $[M+H]^+$: 561.1695, found: 561.1697.

5.3.3 Methyl-Umbelliferone Derivatives

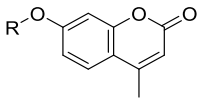

General Method for Protected Methylumbelliferone Derivatives

The synthesis protocol was adapted from NAIK et al.[292]
Methylumbelliferone (**2**, 500 mg, 2.84 mmol, 1.0 eq) was dissolved in dry acetone (10 mL), and anhydrous potassium carbonate (5.68 mmol, 2.0 eq) and the corresponding bromide (5.68 mmol, 2.0 eq) were added. The mixture was heated to 50°C overnight while stirring. After cooling to room temperature, the solvent was evaporated. The residue was treated with 20 mL of cold water, and the resulting white solid was filtered and washed with water. Purification by crystallization from 5-10 mL ethanol, slowly cooling to room temperature overnight, yielded the product as a colorless solid.

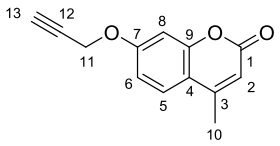

Methylumbelliferone Propargyl Ether (2a)

The purified product was isolated as colorless crystals (385 mg, 63%).

^{1}H-NMR (300 MHz; $CDCl_3$): δ 7.53 (d, ^3J = 8.6 Hz, 1H, C5-*H*), 6.94 (dd, ^3J = 8.6 Hz, ^4J = 2.6 Hz, 1H, C6-*H*), 6.91 (d, ^4J = 2.6 Hz, 1H, C8-*H*), 6.16 (d, ^4J = 1.2 Hz, 1H, C2-*H*), 4.76 (d, ^4J = 2.4 Hz, 2H, C11-*H*), 2.57 (t, ^4J = 2.4 Hz, 1H, C13-*H*), 2.40 (d, ^4J = 1.2 Hz, 3H, C10-*H*) ppm.

^{13}C-NMR (75 MHz, $CDCl_3$): δ 161.2, 160.4, 155.1, 152.4, 125.6 (C5), 114.3, 112.7, 112.5, 102.2, 56.2 (C11), 18.6 (C10) ppm.

HRMS (ESI) m/z: calcd. for $C_{13}H_{10}O_3$ $[M+H]^+$: 215.0708, found: 215.0703.

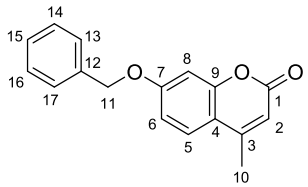

Methylumbelliferone Benzyl Ether (2c)

The purified product was isolated as a colorless solid (628 mg, 63%).

^{1}H-NMR (300 MHz; $CDCl_3$): δ 7.42 (d, ^{3}J = 8.8 Hz, 1H, C5-*H*), 7.39 – 7.23 (m, 5H, C_{arom}-*H*), 6.86 (dd, ^{3}J = 8.8 Hz, ^{4}J = 2.5 Hz, 1H, C6-*H*), 6.80 (d, ^{4}J = 2.5 Hz, 1H, C8-*H*), 6.05 (d, ^{4}J = 1.2 Hz, 1H, C2-*H*), 5.05 (s, 2H, C11-*H*), 2.31 (d, ^{4}J = 1.2 Hz, 3H, C10-*H*) ppm.

^{13}C-NMR (75 MHz; $CDCl_3$): δ 161.7, 161.2, 155.2, 152.5, 135.9, 128.8, 128.4, 127.5, 125.6, 113.8, 112.9, 112.1, 102.0, 70.5 (C11), 18.6 (C10) ppm.

HRMS (ESI) m/z: calcd. for $C_{17}H_{14}O_3$ $[M+H]^+$: 267.1021, found: 267.1016.

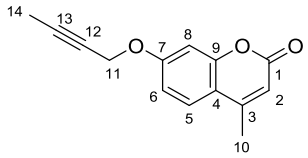

Methylumbelliferone Butynyl Ether (2d)

The purified product was isolated as a colorless solid (539 mg, 83%).

^{1}H-NMR (300 MHz; $CDCl_3$): δ 7.44 (d, ^{3}J = 8.6 Hz, 1H, C5-*H*), 6.90 – 6.79 (m, 2H, C5/6-*H*), 6.08 (d, ^{4}J = 1.2 Hz, 1H, C2-*H*), 4.64 (q,^{5}J = 2.3 Hz, 2H, C11-*H*), 2.33 (d, ^{4}J = 1.2 Hz, 3H, C10-*H*), 1.80 (t, ^{5}J = 2.3 Hz, 3H, C14-*H*) ppm.

^{13}C-NMR (75 MHz; $CDCl_3$): δ 161.20, 160.77, 155.11, 152.46, 125.48 (C5), 113.97, 112.87, 112.21, 102.07, 84.85, 72.98 (C11), 56.89, 18.64 (C10) ppm.

HRMS (ESI) m/z: calcd. for $C_{14}H_{12}O_3$ $[M+H]^+$: 229.0865, found: 229.0860.

5.3.4 Carboxycoumarin Derivatives

The synthesis protocol was adapted from RUFF et. al.[242]

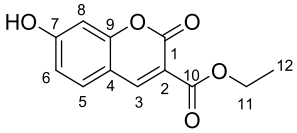

3-Carboxycumarin-ethylester (3)

This synthesis was carried out by NATHALIE NETT.[250]
2,4-Dihydroxybenzaldehyde (2.99 g, 21.6 mmol, 1.1 eq) was dissolved in dry methanol (16 mL), and diethylmalonate (3.15 g, 19.7 mmol, 1.0 eq) was added and heated to boiling. As catalyst mixture morpholine (163 µl, 1.87 mmol, 0.09 eq) and acetic acid (52 µl, 0.90 mmol, 0.05 eq) in 1 ml dry methanol was added to the reaction. After 3 h, the reaction mixture was cooled to room temperature and the yellow solid was filtered and washed with methanol. Purification by crystallization from methanol (ca. 50 mL) yielded the product **3** as a colorless solid (1.03 g, 4.75 mmol, 22%).

^{1}H-NMR (300 MHz, DMSO-d_6): δ 8.67 (s, 1H, C3-*H*), 7.75 (d, ^3J = 8.6 Hz, 1H, C5-*H*), 6.84 (dd, ^3J = 8.6 Hz, ^4J = 2.3 Hz, 1H, C6-*H*), 6.72 (d, ^4J = 2.2 Hz, 1H, C8-*H*), 4.26 (q, ^3J = 7.1 Hz, 2H, C11-*H*), 1.29 (t, ^3J = 7.1 Hz, 3H, C12-*H*) ppm.

^{13}C-NMR (75 MHz, DMSO-d_6) δ 163.5, 157.7, 156.9, 149.8, 132.5, 114.8, 110.7, 102.3, 61.2, 40.6, 40.6, 14.6 ppm.

HRMS (APCI) m/z: calcd. for $C_{12}H_{10}O_5$ $[M+H]^+$: 257.0420, found: 257.0420.

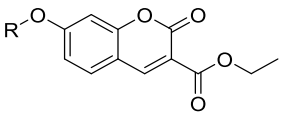

General Method I for Ether-Protected 3-CCE Derivatives

3-CCE (**3**, 1.0 eq), potassium carbonate (1.2 eq) and the corresponding bromide (1.2 eq) were dispersed in a small amount of DMF in a 10 mL round-bottom flask. The mixture was heated for 2 h at 80°C and then stirred without heating for an additional 18 h. The solvent was evaporated *in vacuo*, and the raw product purified by column chromatography.

General Method II for Ether-Protected 3-CCE Derivatives

Following a protocol described by RUFF *et al*.[242]
3-CCE (**3**, 1.0 eq) was suspended in 45 ml toluene and concentrated at 120°C to 5 ml. After cooling the yellow suspension to room temperature, NaH (60% dispersion in mineral oil,

1.6 eq) was added and the solvent was evaporated. The obtained orange salt was dried overnight and directly implemented with the ether protection group: The sodium salt (1.0 eq) was dissolved in dry DMF and heated to 120°C. During heating the corresponding bromide (0.09 eq) was added. After stirring 2 h at 120°C a second batch of bromide (1.4 eq) and after 3 h a third batch of bromide (0.3 eq) were supplemented. The mixture was stirred for further 4 h at 120°C. After cooling to room temperature, the solution was poured into ice water to precipitate the product. The solid was filtered, washed with water and extracted with dichloromethane. The organic layer was dried over Na_2SO_4 and the solvent evaporated *in vacuo*. Purification by column chromatography yielded the product as colorless solid.

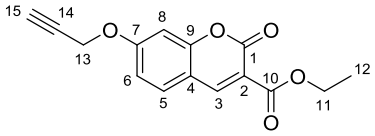

7-Propargyloxy-3-carboxycoumarin-ethylester (3a)

This synthesis was carried out by NATHALIE NETT following Method II.[250]
Starting from 2.84 mmol **3**, the product was purified by column chromatography (silica, DCM/EtOAc 20:1) and isolated as colorless solid (232 mg, 0.85 mmol, 30%).

TLC R_f = 0.5 (DCM:EtOAc 20:1)

^{1}H-NMR (300 MHz, $CDCl_3$): δ 8.51 (s, 1H, C3-*H*), 7.57 – 7.50 (m, 1H, C8-*H*), 6.99 – 6.92 (m, 2H, C5/6-*H*), 4.79 (d, ^4J = 2.4 Hz, 2H, C13-*H*), 4.40 (q, ^3J = 7.1 Hz, 2H, C11-*H*), 2.60 (t, ^4J = 2.4 Hz, 1H, C15-*H*), 1.40 (t, ^3J = 7.1 Hz, 3H, C12-*H*) ppm.

^{13}C-NMR (75 MHz, $CDCl_3$): δ 163.5, 162.9, 157.4, 148.9, 130.9, 115.0, 114.2, 112.4, 101.8, 76.7, 61.9 (C11), 56.6 (C13), 14.4 (C12) ppm.

HRMS (APCI) m/z: calcd. for $C_{15}H_{12}O_5$ $[M+Na]^+$: 295.0580, found: 295.0577.

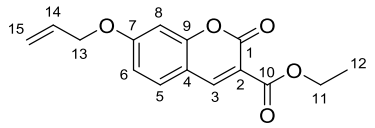

7-Allyloxy-3-carboxycoumarin-ethylester (3a)

This synthesis was carried out by KERSTIN MARK during a lab rotation, following Method I.
Starting from 0.41 mmol **3**, the product was purified by column chromatography (silica, DCM/EtOAc 15:1) and isolated as light yellow solid (93 mg, 0.34 mmol, 84%).

TLC R_f = 0.28 (DCM:EtOAc 15:1)

^{1}H-NMR (300 MHz, DMSO-d_6): δ 8.71 (s, 1H, C3-*H*), 7.84 (d, ^3J = 8.2 Hz, 1H, C8-*H*), 7.07 – 6.98 (m, 2H, C5/6-*H*), 6.06 (ddt, $^{3,trans}J$ = 17.2 Hz, $^{3,cis}J$ = 10.6 Hz, ^3J = 5.3 Hz,

1H, C14-*H*), 5.44 (dd, $^{3,trans}J$ = 17.3 Hz, ^{2}J = 1.6 Hz, 1H, C15-*H*), 5.31 (dd, $^{3,cis}J$ = 10.5, ^{2}J = 1.5 Hz, 1H, C15-*H*), 4.73 (d, J = 6.6 Hz, 2H, C13-*H*), 4.27 (q, ^{3}J = 7.1 Hz, 3H, C11-*H*), 1.30 (t, ^{3}J = 7.1 Hz, 3H, C12-*H*) ppm.

^{13}C-NMR (75 MHz, DMSO-d_6): δ 163.6, 162.8, 156.8, 156.2, 149.0, 132.6, 131.6, 118.3, 113.6, 113.4, 111.5, 101.0, 69.1, 60.9, 14.1 (C12) ppm.

HRMS (ESI) m/z: calcd. for $C_{15}H_{14}O_5$ $[M+H]^+$: 275.0914, found: 275.0923.

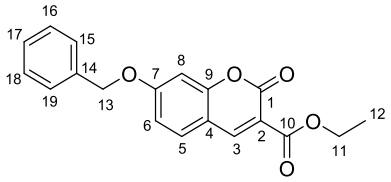

7-Benzoxy-3-carboxycoumarin-ethylester (3c)

This synthesis was carried out by NATHALIE NETT following Method II.[250]
Starting from 4.08 mmol **3**, the product was purified by column chromatography (silica, DCM/EtOAc 20:1) and isolated as colorless solid (1.03 g, 3.17 mmol, 68%).

TLC R_f = 0.5 (DCM:EtOAc 20:1)

^{1}H-NMR (300 MHz; $CDCl_3$): δ 8.50 (s, 1H, C3-*H*), 7.50 (d, ^{3}J = 8.7 Hz, 1H, C5-*H*), 7.45 – 7.35 (m, 5H, C_{arom}-*H*), 6.96 (dd, ^{3}J = 8.7 Hz, ^{4}J = 2.4 Hz, 1H, C6-*H*), 6.88 (d, ^{4}J = 2.2 Hz, 1H, C8-*H*), 5.15 (s, 2H, C13-*H*), 4.40 (d, ^{3}J = 7.1 Hz, 2H, C11-*H*), 1.40 (t, ^{3}J = 7.1 Hz, 3H, C12-*H*) ppm.

^{13}C-NMR (75 MHz; $CDCl_3$): δ 164.3, 163.6, 157.6, 149.0, 135.5, 130.9, 129.0, 128.7, 127.7, 114.4, 112.0, 101.6, 70.9 (C13), 61.9 (C11), 14.4 (C12) ppm.

HRMS (APCI) m/z: calcd. for $C_{19}H_{16}O_5$ $[M+H]^+$: 325.1071, found: 325.1071.

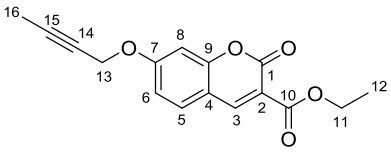

7-Butynyloxy-3-carboxycoumarin-ethylester (3d)

This synthesis was carried out by NATHALIE NETT following Method II.[250]
Starting from 2.17 mmol **3**, the product was purified by column chromatography (silica, DCM:EtOAc 20:1) and isolated as colorless solid (429 mg, 1.4 mmol, 64%).

TLC R_f = 0.5 (DCM:EtOAc 20:1)

^{1}H-NMR (300 MHz; $CDCl_3$): δ 8.51 (s, 1H, C3-*H*), 7.51 (d, ^{3}J = 8.5 Hz, 1H, C5-*H*), 6.98 – 6.91 (m, 2H, C6/8-*H*), 4.74 (q, ^{5}J = 2.3 Hz, 2H, C13-*H*), 4.40 (q, ^{3}J = 7.1 Hz, 2H, C11-*H*), 1.87 (t, ^{5}J = 2.3 Hz, 3H, C16-*H*), 1.40 (t, ^{3}J = 7.1 Hz, 3H, C12-*H*) ppm.

^{13}C-NMR (75 MHz; $CDCl_3$): δ 163.6, 163.4, 157.5, 157.2, 149.0, 130.8, 114.7, 114.4, 112.1, 101.7, 85.5, 72.7, 61.9 (C11), 57.3 (C13), 14.4 (C12) ppm.

HRMS (APCI) m/z: calcd. for $C_{16}H_{14}O_5$ $[M+H]^+$: 309.0734, found: 309.0733.

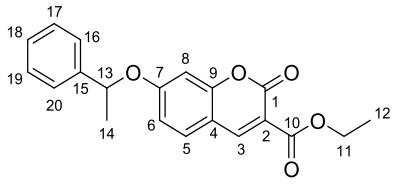

7-(1-Phenylethyloxy)-3-carboxycoumarin-ethylester (3g)

This synthesis was carried out by CHRISTIAN SPRINGER following Method I.[260]

Starting form 0.33 mmol **3**, the product was purified by column chromatography (silica, DCM:EtOAc 20:1) to yield racemic **3g** as crystalline, off-white solid (7.1 mg, 0.21 mmol, 64%). Enantiomeric separation of the amount necessary for mutant screening was achieved via HPLC (see Chapter Enantiomeric Separation, page 72), and yielded ***R*-3g** (4.3 mg, 0.013 mmol, 4%) and ***S*-3g** (3.0 mg, 0.009 mmol, 3%) as slightly yellow oils.

TLC R_f = 0.35 (DCM:EtOAc 20:1)

^{1}H-NMR (300 MHz, $CDCl_3$): δ 8.44 (s, 1H, C3-*H*), 7.42 (d, ^3J = 8.7 Hz, 1H, C5-*H*), 7.32 (m, 5H, C_{arom}-*H*), 6.89 (dd, ^3J = 8.7 Hz, ^4J = 2.4 Hz, 1H, C6-*H*), 6.72 (d, ^4J = 2.4 Hz, 1H,C8-*H*), 5.37 (q, ^3J = 6.4 Hz, 1H, C13-*H*), 4.38 (q, ^3J = 7.1 Hz, 2H, C11-*H*), 1.69 (d, ^3J = 6.4 Hz, 3H, C14-*H*), 1.38 (t, ^3J = 7.1 Hz, 3H, C12-*H*) ppm.

^{13}C-NMR (75 MHz, $CDCl_3$): δ 163.7, 163.6, 157.5, 157.3, 149.0, 141.7, 130.7, 129.1, 128.3, 125.6, 115.0, 114.3, 111.7, 102.6, 77.5 (C13), 61.8 (C11), 24.5 (C14), 14.4 (C12) ppm.

HRMS (ESI) m/z: calcd. for $C_{20}H_{18}O_5$ $[M+Na]^+$: 361.1046, found: 361.1049.

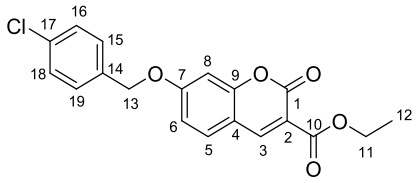

7-(4-Chlorobenzyl)-3-carboxycumarin-ethylester (3h)

This synthesis was carried out by ELISABETH ENGELSBERGER during an internship, following a modified version of Method I.

3-CCE (**3,** 300 mg, 1.28 mmol, 1.00 eq) was dissolved in 4 mL DMF. Potassium carbonate (357 mg, 2.58 mmol, 2.02 eq) was added, and the mixture heated to 80°C, upon which the suspension turned yellow. 1 mL DMF was added to provide proper stirring. 1-(Bromomethyl)-4-chlorobenzene (403 mg, 1.96 mmol, 1.53 eq) was added and stirred at

80°C for 4.5 h, then another 60 h at room temperature. The solvent was removed *in vacuo*, and the raw product purified by column chromatography (hexanes:EtOAc 1:1). Afterwards the product remained slightly yellow and was purified further two times by column chromatography over silica (DCM/MeOH 30:1 and DCM/MeOH 50:1). The product (176.6 mg, 0.49 mmol, 39%) was obtained as a colorless solid.

TLC R_f = 0.50 (hex:EtOAc 1:1)
R_f = 0.31 (DCM/MeOH 30:1)
R_f = 0.23 (DCM/MeOH 50:1)

^{1}H-NMR (300 MHz, DMSO-d_6): δ 8.72 (s, 1H, C3-*H*), 7.86 (d, ^3J = 8.7 Hz, 1H, C5-*H*), 7.60 – 7.41 (m, 4H, C_{arom}-*H*), 7.21 – 6.96 (m, 2H, C6/8-*H*), 5.26 (s, 2H, C13-*H*), 4.27 (q, ^3J = 7.1 Hz, 2H, C11-*H*), 1.30 (t, ^3J = 7.1 Hz, 3H, C12-*H*) ppm.

^{13}C-NMR (75 MHz, DMSO-d_6) δ 164.01, 163.26, 157.31, 156.67, 149.51, 135.51, 133.30, 132.17, 130.28, 129.04, 114.26, 114.08, 112.17, 101.69, 69.79, 61.42 (C11), 14.59 (C12) ppm.

HRMS (ESI) m/z: calcd. for $C_{19}H_{15}ClO_5Na$ $[M+Na]^+$: 381.0500 found: 381.0500.

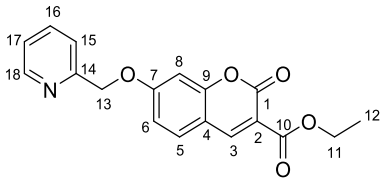

7-(2-Pyridinyl)-3-carboxycumarin-ethylester (3i)

This synthesis was carried out by JULIUS WINKLER and JANOSCH KETTLER during a lab rotation, following Method I.
Starting from 0.85 mmol **3**, the product was purified by column chromatography (silica, DCM:EtOAc 3:2) and isolated as off-white solid (194 g; 0.60 mmol; 70%).

TLC R_f = 0.16 (DCM:EtOAc 3:2)

^{1}H-NMR (300 MHz, DMSO-d_6): δ 8.74 (s, 1H, C3-*H*), 8.62 (ddd, ^3J = 4.9 Hz, ^4J = 1.8 Hz, ^4J = 1.0 Hz, 1H, C18-*H*), 7.94 – 7.82 (m, 2H, C5/16-*H*), 7.58 (dt, ^3J = 7.8 Hz, ^4J = 1.1 Hz, 1H, C15-*H*), 7.39 (ddd, ^3J = 7.6 Hz, ^3J = 4.8 Hz, ^4J = 1.2 Hz, 1H, C17-*H*), 7.16 (d, ^4J = 2.4 Hz, 1H, C8-*H*), 7.13 (dd, ^3J = 8.6 Hz, ^4J = 2.4 Hz, 1H, C6-*H*), 5.35 (s, 2H, C13-*H*), 4.29 (q, ^3J = 7.1 Hz, 2H, C11-*H*), 1.32 (t, ^3J = 7.1 Hz, 3H, C12-*H*) ppm.

^{13}C-NMR (75 MHz, DMSO-d_6): δ 163.5, 162.7, 156.8, 156.1, 155.5, 149.2, 149.0, 137.1, 131.7, 123.2, 122.1, 113.7, 111.7, 101.2, 71.1, 60.9 (C11), 14.1(C12) ppm.

HRMS (ESI) m/z: calcd. for $C_{18}H_{15}NO_5$ $[M+H]^+$: 326.1023, found: 326.1022.

5.3.5 Bromides

General Method for the Synthesis of Bromides from Alcohols

Following a protocol described by HAZRA *et al*.[293]
Triphenylphosphine (1.1 eq) was dissolved in dry dichloromethane and cooled to 0°C. Bromine (1.1 eq) was added dropwise until a yellow suspension was formed. The corresponding alcohol (1.0 eq) was dissolved in dry dichloromethane and added slowly to the suspension. The transparent solution was stirred for 1 h at 0°C. The still slightly yellow solution was then allowed to warm to room temperature, before 150 ml hexanes were added. After 30 min, the colorless solid was filtered through a short silica column and washed with hexane, which yielded the colorless product.

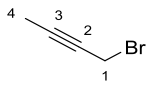

1-Bromo-but-2-yne (d-Br)

This synthesis was carried out by NATHALIE NETT.[250]
Starting from 40.7 mmol of but-2-yn-1-ol, and after purification by filtering over a short silica column (hexanes), the product was isolated as a colorless oil (6.01 g, 35.8 mmol, 89%, in hexane).

^{1}H-NMR (300 MHz; $CDCl_3$): δ 3.90 (q, ^5J = 2.5 Hz, 2H, C1-*H*), 1.88 (t, ^5J = 2.5 Hz, 3H, C4-*H*) ppm.

^{13}C-NMR (75 MHz; $CDCl_3$): δ 83.9, 74.5, 15.8, 4.0 ppm.

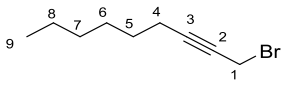

1-Bromo-non-2-yne (e-Br)

This synthesis was carried out by NATHALIE NETT.[250]
Starting from 10.7 mmol of non-2-yn-1-ol, and after purification by filtering over a short silica column (hexanes), the product was isolated as a colorless oil (2.27 g, 10.7 mmol, quant. yield).

^{1}H-NMR (300 MHz; $CDCl_3$): δ 3.93 (t, ^5J = 2.3 Hz, 2H, C1-*H*), 2.23 (ddt, ^2J = 9.4, ^3J = 4.6, ^5J = 2.3 Hz, 2H, C4-*H*), 1.58 – 1.33 (m, 2H, C5-*H*), 1.33 (t, J = 2.2 Hz, 6H, C6,7,8-*H*), 0.89 (t, ^3J = 6.7 Hz, 3H, C9-*H*) ppm.

^{13}C-NMR (75 MHz; $CDCl_3$): δ 88.5, 75.4, 31.4, 28.7, 28.5, 22.7, 19.1, 15.9, 14.2 ppm.

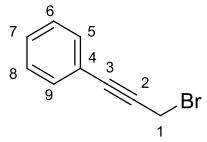

3-Bromo-1-phenylprop-1-yne (f-Br)

This synthesis was carried out by NATHALIE NETT.[250]
Starting from 22.7 mmol of 3-phenylprop-2-yn-1-ol, and after purification by column chromatography (hexanes:EtOAc 29:1) yielded the product as a colorless oil (4.23 g, 95%).

TLC R_f = 0.65 (hex : EtOAc 29:1).
^{1}H-NMR (300 MHz; $CDCl_3$): δ 7.37 (dd, ^3J = 4.9 Hz, ^3J = 2.6 Hz, 2H, C5/9-*H*), 7.25 (m, 3H, C6-C8-*H*), 4.09 (s, 2H, C1-*H*) ppm.
^{13}C-NMR (75 MHz; $CDCl_3$): δ 132.0, 129.0, 128.5, 122.3, 86.9, 84.4, 15.4 ppm.
HRMS (EI) m/z: calcd. for C_9H_7Br $[M+H]^+$: 193.9731, found: 193.9733.

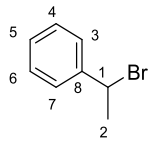

1-Bromo-ethylbenzene (g-Br)

This synthesis was carried out by CHRISTIAN SPRINGER.[260]
Starting from 0.83 mmol of enantiopure (*R*)- or (*S*)-1-phenyl-ethanol, and after purification by filtering over a short silica column (hexanes), the presumably racemic product was isolated as a colorless oil (74 mg, 0.40 mmol, 48%).

TLC R_f = 0.88 (DCM:EtOAc 20:1).
^{1}H-NMR (300 MHz; $CDCl_3$): δ 7.37 (m, 5H, C_{arom}-*H*), 5.22 (q, ^3J = 6.9 Hz, 1H, C1-*H*), 2.06 (d, ^3J = 6.9 Hz, 3H, C2-*H*) ppm.
^{13}C-NMR (75 MHz; $CDCl_3$): δ 143.4, 128.8, 128.5, 127.0, 49.7 (C1), 27.0 (C2) ppm.

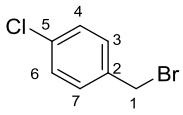

1-(Bromomethyl)-4-chlorobenzene (h-Br)

This synthesis was carried out by ELISABETH ENGELSBERGER during an internship.
Starting from 5.61 mmol 4-chlorobenzylalcohol, and after purification by filtering over a short silica column (hexanes), the product was isolated as a colorless solid (0.985 g, 4.79 mmol, 86%).

^{1}H-NMR (300 MHz, DMSO-d_6): δ 7.56 – 7.38 (m, 4H, C_{arom}-*H*), 4.71 (s, 2H, C1-*H*).

5.4 Screening

5.4.1 General Methods

For liquid handling of single samples and 96-well plates, either standard single- and multi-channel micropipettes (EPPENDORF or THERMOSCIENTIFIC) or dispensers (multidrop, multipette) were used, or an automated approach with a TECAN robotic system equipped with a liquid handling arm (LiHA) and multi-pipette option (Te-MO), which was controlled using GEMINI software V3.50.

5.4.2 Library Information

Targeted Sites and Used Methods

Existing libraries were stored as glycerol stocks (30%) of *E. coli* BL21-Gold(DE3) (MERCK-MILLIPORE) at -80°C in the REETZ lab.

The first library, termed Mega-Site, was constructed by CARLOS G. ACEVEDO-ROCHA in connection to another project (unpublished). Briefly, the P450$_{BM3}$ gene (3,150 bps) was cloned under the T7-promoter of plasmid pRSF-Duet-1 (Novagen) without His-tag, as described earlier.[158] Saturation mutagenesis was applied in two rounds. In the first step, the QuikChange protocol was used to introduce three mutations at position L437S/N/A. After its extraction, the plasmid was used as template to introduce three mutations at four more sites: R47L/W/T, S72V/I/F, A82W/F/M, and F87V/I/M, using overlap extension PCR. Since the wt residue was included as building block in each case, there were 5 residues randomized to 4 different amino acids, which represents a complexity of 1,024 variants. It was transformed into the model *E. coli* BL21-Gold(DE3), before the cells were seeded onto LB agar plates (15 cm) with the right antibiotics. The plates were incubated at 37°C and the next day, 950 colonies were picked into 800 µL of LB media with the proper antibiotic in ten 96-well MTPs. A wt-control was included per plate in well 1A (95 colonies from the library).

The second library, termed "SABRINA's collection", was prepared by SABRINA HOEBENREICH as described before.[161,162,248] Briefly, the P450$_{BM3}$ gene was cloned into the plasmid pETM-11 (EMBL, Heidelberg), which contains an *N*-terminal His-tag and kanamycin marker. The P450$_{BM3}$ F87A variant was used as a template to prepare six libraries: 2x A, 2x B, and 2x C. Library A included residues R47, T49 and Y51; all randomized using the same alphabet consisting of 12 amino acids (R, D, N, C, G, H, I, L, S, V, F, and Y). Library C, which included residues M185 and L188, was randomized using the same amino acid alphabet. Finally, library B included residues V78 and A82; full randomization was either achieved with a nonredundant set of 20 codons or by using the NNK degeneracy (32 codons). The sizes of

libraries A were 5076 and 3864, that of libraries B 3008 and 1222; and that of libraries C 752 and 672 transformants. However, only those mutants identified as "hits" in the original study were combined in triplicates to a smaller collection, composed of ~150 unique mutants, which were used for the screening (full list see Appendix 11).
Finally, a number of M01-derived $P450_{BM3}$ mutants[294] were also available at the REETZ lab, and constructed by site-directed mutagenesis as indicated elsewhere.[295]
Hit mutants from different projects were assembled to a new collection, termed 96er plate (full list see Appendix 12).

Sequencing

Genetic sequencing was performed by GATC and results were analyzed using BIOEDIT Sequence Alignment Editor V7.2.0.[296]

Table 5-5. Primers used for sequencing.

Name	Sequence
T7	ACGCTTGATACAATTGG
2nd	CGAGAACATTCGCTATC
3rd	TTAATTGTAACGGCGTC
4th	ATACCCGGCGTGTGAAATG

5.4.3 Glycerol Stocks

Overnight culture (700 µL) was mixed with 200 µL of 100% glycerol and shock-frozen in liquid nitrogen before being stored at -80°C.

5.4.4 Culture Conditions

Protocol according to KILLE.[248] For pre-cultures, 800 µL LB media containing 50 µg/mL kanamycin (LB^{Kan}) per well were inoculated in a deep-well MTP using a 96-tip comb from library glycerol stocks, covered with gas-permeable seals (SIGMA) and grown overnight at 37°C, shaking at 800 rpm in an HT INFORS MULTITRON Standard shaker equipped with horizontal plate holders. For expression cultures, 100 µL of overnight culture were transferred into 700 µL TB media containing kanamycin, IPTG, Power Mix and TTM-Mix. Expression was performed by shaking for 7 h at 30°C and 230 rpm. They were centrifuged at 1100 g and 4°C for 10 min. The supernatant was discarded, the pellets resuspended by

vortexing with 600 µL P450 washing buffer and centrifuged again for 10 min. The supernatant was removed and the pellets stored at -80°C until use.

5.4.5 Lysate Preparation

Pellets from the MTPs were thawed in a water bath (30-40°C) and resuspended in 430 µL lysis buffer by vortexing. The plates were incubated at 30-37°C for 2 h, shaking at 800 rpm in an HT INFORS MULTITRON Standard shaker equipped with a table containing horizontal plate holders. After closing the plates with a lid, they were centrifuged at 1100 g and 4°C for 10 min and the supernatant was used for screening reactions.

5.4.6 Substrate Reaction

The current protocol was adapted for fluorescent read-out from KILLE *et al*.[161]

Lysate supernatant (50 µL) were transferred into a fresh deep-well MTP containing 445 µL reaction buffer I using the TECAN system. The reaction was started by addition of 5 µL substrate solution. Plates were covered with gas-permeable seals (SIGMA) and incubated for 90 min at 30°C, shaking at 800 rpm. Plates were then centrifuged at 1100 g and 4°C for 10 min, 200 µL of the supernatant transferred to black flat bottom MTPs and analyzed by fluorescent read-out at the appropriate wavelengths for the substrate, which are shown in Table 5-1, page 70.

5.5 Enzyme Purification and Characterization

5.5.1 General Methods

Culture vessels were incubated in an HT INFORS MULTITRON Standard shaker. Cell lysis for protein purification was done using a BANDELIN SONOPULS HD2200 sonicator equipped with a 13 mm sonotrode. Protein purification was performed at 4°C on an AMERSHAM BIOSCIENCES Äkta FPLC system equipped with pump P-920, mixer M-925, sample injection valve INV-907, fraction collector Frac-950, monitor UPC-900 and remote connector CU-950, controlled via UNICORN V5.0 software. The following column materials were used:

Anion Exchange	loose DE52 WHATMANN DEAE cellulose resin
	TOSOH TSK-Gel DEAE-5PW(30) column
Desalting	HiTrap columns by GE HEALTHCARE
Gel Filtration	HiLoad 26/60 Superdex 200 column by GE HEALTHCARE

5.5.2 Expression Cultures

Carried out by KATJA KRÄLING.

$LB^{KAN,tet}$ (5 µg/ml) medium was inoculated from randomly picked colonies or glycerol stocks and grown overnight at 37°C and 230 rpm (16 h). Expression cultures were inoculated by diluting overnight culture 1000-fold in $TB^{30\ µg/mL\ KAN}$ media containing power mix, TTM mix and $MgCl_2$ to a total volume of 1 L. Induction was performed at OD_{600} of 0.6-0.8 by addition of IPTG to a final concentration of 100 µM. After 7 h of expression at 30°C, 230 rpm, cultures were centrifuged at 4000 rpm, 4°C for 60 min. The supernatant was discarded and the cell pellets were resuspended using a pipette with 600 mL P450 washing buffer (100 mM KPi, pH 7.4, 5% v/v glycerin) and centrifuged again for 10 min at 4000 rpm, 4°C. The supernatant was discarded and pellets stored at -80°C until further use.

5.5.3 Lysate Preparation

The resuspended pellet was thawed and subjected to sonication. During the process, the vessel was kept on ice. Three sonication steps at 80% power for 1 min were performed, allowing for cooling breaks of 5 min in between. The slurry was centrifuged for 60 min at 4°C and 17000 rpm and the supernatant was used for purification after sterile filtration via a syringe filter (0.45 µm).
Of this and all following steps, samples were taken for SDS PAGE analysis.

5.5.4 SDS PAGE

Protein expression and purity was checked by sodium dodecyl sulfate polyacrylamide gel electrophoresis (SDS-PAGE).
Gels were prepared by fixing a gel caster with glass and spacer sheets for 12 gels, and checking for leaks with water, before filling in freshly prepared resolving gel mix. The mix was layered with isopropanol to create an even surface, and left to polymerize. The isopropanol was removed, and freshly prepared loading gel mix was added to the caster. Combs for sample pockets were inserted, and the gels left to polymerize completely.
For sample preparation, 15 µL of protein sample were mixed with 5 µL SDS sample buffer in an EPPENDORF tube, and heated to 90°C for 10 min in a Thermocycler.
To run a gel, it was fitted into the running chamber, the comb removed, and the chamber filled with SDS running buffer. A commercially available protein ladder was loaded into the first lane, and an appropriate amount of centrifuged sample solution was added into each following pocket (depending on protein concentration and sample pocket size between 3-10 µL). The gel was then developed at 120 V until the run marker reached the bottom. It was taken out of the chamber, and the glass sheets carefully removed. After rinsing the gel with water, it was covered with SDS gel stain solution, and microwaved for 1 min at maximum power. Repeated rinsing and microwaving in fresh water removed the stain from the gel matrix. After washing, an image was taken of each gel using an electronic camera.

5.5.5 Protein Purification without His-tag

Weak Anion Exchange Column

A glass column with a diameter of 2.5 cm was packed with 20 g of DE52 WHATMAN cellulose resin (suspended in KPi buffer). The sample was loaded onto the column, and fractions were immediately collected in case of unbound protein elution. The column was washed with 30 mL of KPi buffer, before eluting the protein with elution buffer. The volume collected in the last step was concentrated to 10 mL using 100 kDa centrifugation concentrators (MERCK-MILLIPORE).

Desalting Column

Five consecutive HiTrap Desalting columns (5 mL, 71-7154-00 AK by GE HEALTHCARE) were connected to the Äkta system and equilibrated with HEPES buffer, prior to sample loading. Protein elution was monitored via UV detection at 417 nm. Separation was achieved at a flow rate of 1 mL/min and fractions of the eluent were collected in 15 mL Falcon tubes until

UV absorption decreased. Protein-containing fractions were collected and filtered via a syringe filter (0.45 μm).

DEAE Column

A TOSOH TSK-Gel DEAE-5PW(30) column was connected to the Äkta system and equilibrated with Buffer A, before loading the sample. Elution was performed at a flow rate of 1 mL/min with a gradient from 0-100% Buffer B under fractionated collection. Main fractions were combined, concentrated to 2 mL using 100 kDa centrifugation concentrators (MERCK-MILLIPORE) and filtered via a syringe filter (0.45 μm).

Gel Filtration Column

A gel filtration column (HiLoad 26/60 Superdex 200 by GE HEALTHCARE) was connected to the Äkta system and equilibrated with HEPES buffer. The sample was loaded onto the column and purified at a flow rate of 1 mL/min.
Upon elution, main fractions were combined and concentrated using 100 kDa centrifugation concentrators (MERCK-MILLIPORE), changing the buffer to KPi by diluting multiple times. Samples were aliquoted and shock-frozen with liquid nitrogen before storing the protein at -80°C until further use.

5.5.6 Protein Purification with His-tag

Raw extract was purified by affinity chromatography over Ni-NTA His-trap columns by GE HEALTHCARE. Columns were equilibrated with KPi buffer (100 mM), before the extract was loaded with protein and rinsed with Buffer A until the baseline is stable (~40 mL). The enzyme was eluted by gradually increasing the Histidine concentration in the eluent by running a gradient to 100% Buffer B over 20 min at a flow rate of 2 mL/min. Upon elution, main fractions were combined. After washing and concentrating the sample by ultracentrifugation (100 kDA concentrator, MERCK-MILLIPORE), the sample was divided into aliquots, shock-frozen with liquid nitrogen and stored at -80°C until further use.

5.6 Determination of Biochemical Characteristics

5.6.1 Concentration

Cytochrome P450 concentrations were determined using an adapted protocol, running reactions in triplicates.[262]
Purified protein samples were thawed slowly on ice. Per mutant, six stirrable quartz cuvettes were prepared and filled with 980 µL KPi buffer and 20 µL protein, leading to a dilution factor of 50. After activating the auto-zero function of the spectraphotometer, sample temperature was brought to 25°C and blanks were measured at the following wavelengths, corresponding to different species:

490 nm	≙ baseline referene for all P450s
449 nm	≙ active protein
423 nm	≙ inactive protein with Cys detached from heme

Three of the six cuvettes were then treated with CO-gas for 60 s, bubbling through a canule at approximately one bubble per second. One analytical spoon full (~1 mg) of $Na_2S_2O_4$ was added to all six cuvettes, they were covered with parafilm and mixed by inverting them 10 times, until the salt had dissolved completely. Absorption at the above mentioned wavelengths was then measured immediately, and concentrations of active and inactive enzyme calculated following the method described in the literature.

5.6.2 Selectivity and Orthogonality

Reactions for determining steady-state activity were carried out in analogy to screening reactions (see Chapter 5.4.6, page 93) in 500 µL reaction buffer I or II at final enzyme and substrate concentrations of 0.1 µM and 50-100 µM, respectively, unless otherwise specified. Fluorescence read-out was determined after 90 min reaction time at 30°C, centrifugation of the reaction mixture and transfer of 200 µL into black flat bottom MTPs. For HPLC analysis, reaction mixtures were extracted with 3 x 500 µL ethyl acetate, dried and resuspended in 500 µL acetonitrile, unless otherwise specified.

Real-time monitoring of reactions was conducted under standard reaction conditions in buffer II, using the NADPH recycling system and **1a** at a concentration of 100 µM, running the reaction directly in black flat bottom MTPs at a total reaction volume of 200 µL. Coumarine substrates are not suitable for this type of monitoring due to the interference of NADPH at the necessary wavelengths. To study orthogonality, two enzymes were added to the reaction from the start or successively after the first half of the reaction time.

By choosing highly selective mutations, it is possible to have two independent reactions in the same system without interference from one another (*cf.* 5.6.2). This can be an advantage when going towards living cells, and could pave the way for applications in organic synthesis, where the reliable orthogonal removal of protection groups is a valuable asset.

5.6.3 Kinetic Parameters

All measurements were conducted in duplicates or triplicates and carried out in stirrable high precision quartz glass cuvettes (d = 1 cm), stirring with a magnetic stirrer bar at 900 rpm. Before and after each step, cuvettes were cleaned with Virkon and dest. H_2O and dried at 50°C.

NADPH consumption, leak rate and product formation rate were calculated following literature known protocols (results see Table 3-2):[136,161,297]

KPi buffer (965 µL) was brought to 30°C in the cuvettes, and 10 µL DMF or substrate stock in DMF (0.1-10 mM) were added. The auto-zero function of the spectraphotometer was activated, 20 µL of 20 mg/mL NADPH-solution (in KPi) were added and the recording started immediately. At a timepoint of 20 s exactly, the enzyme was added to a specified final concentration (0.1 µM unless otherwise stated), and the decline in absorbance was detected.

For analysis of the initial cofactor concentration, absorption was determined at 15 s (before the addition of $P450_{BM3}$). For analysis of the initial reaction rates, slopes of the initial reaction (measured over a 10 s time starting 5 s after addition) were calculated using the JASCO Spectra Manager V2, kinetics function. In case of substrates, the reaction was followed until the curve flattened completely, before 400 µL of the reaction mix were extracted three times with ethyl acetate. Phase separation can be improved by centrifugation at 4°C. Organic phases were combined and the solvent removed *in vacuo*. Samples were then stored at -80°C until HPLC analysis of conversion and product formation.

Reactions were run at maximum substrate concentration, determining initial rates by time-dependent absorption measurements of NADPH (ε_{340} = 6.22 $mM^{-1} \cdot cm^{-1}$, ε_{320} = 4.37 $mM^{-1} \cdot cm^{-1}$, ε_{360} = 4.25 $mM^{-1} \cdot cm^{-1}$), starting at a NADPH concentration of ca. 0.5 mM. Wavelengths were adjusted for minimal interference with the substrate.

Since coumarin derivatives interfere with measurements at 340 nm, those values were obtained at slightly shifted wavelengths to minimize the effect. Figure 5-1 shows absorption spectra of NADPH and substrates **2** and **3**, indicating the used wavelengths. Extinction coefficients were determined from the spectrum based on the known ε_{340} of 6.22 $mM^{-1} \cdot cm^{-1}$.

For MICHALIS-MENTEN measurements of fluorescein substrate **1a**, it was possible to follow product formation directly by measuring fluorescence development over time (at a reaction volume of 200 µL in black flat bottom 96-well plates). Coumarin substrate **3d**, on the other

hand, had to be measured by NADPH consumption multiplied with the CE, due to the strong background fluorescence at the observed wavelengths.

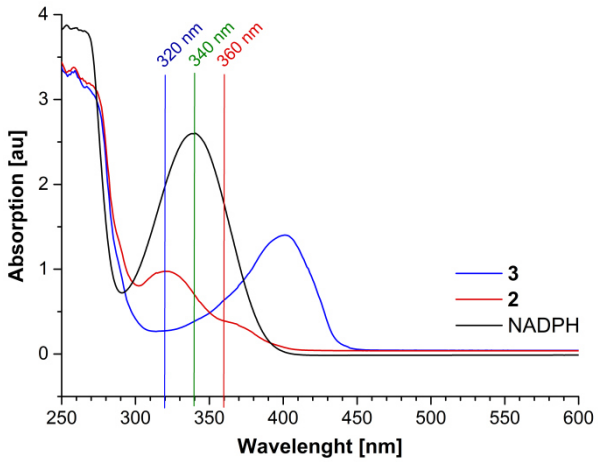

Figure 5-1. Absorption spectra of cofactor NADPH and coumarin compounds **2** and **3**. Both compounds interfere with measurements at the absorption maximum of NADPH (340 nm), but suitable wavelengths are easily found at 320 nm (**3**) or 360 nm (**2**). The absorption coefficient used in calculations was adjusted accordingly.

5.6.4 Stability

All stability reactions were carried out on the mutant TFFIS in analogy to screening reactions (see Chapter 5.4.6, page 93) in 500 µL reaction buffer II at final enzyme and substrate concentrations of 0.1 µM and 100 µM, respectively, unless otherwise specified. Fluorescence read-out was determined after 90 min reaction time at 30°C, centrifugation of the reaction mixture and transfer of 200 µL into black flat bottom MTPs.

pH

This work was partly carried out by ROBERT GIESSMANN.

Reactions were carried out in deep-well MTPs, using Britton-Robinson (B&R) buffers of different pH values or KPi buffer. Three series of experiments were conducted:

- *Reactions at the specified pH*
  Standard reactions were carried out in B&R buffers at pH values of 2-10 and substrate concentration was determined by fluorescence measurements. As a control, fluorescence of **1** was measured at the same pH values.

- *Reactions at pH 7 after pre-incubation*
  The enzyme (3.2 µL) was diluted in B&R buffers (22 µL) at pH values of 2-10 to a concentration of 2 µM, before incubation for 60 min at room temperature. Samples were

then diluted with B&R buffer (pH 7, 465 µL). The reaction was started by the addition of NADPH and substrate stock (5 µL each). As a control, reactions were run in the same buffer mixes with preincubation of the enzyme at pH 7.

- *Time-dependent analysis after pre-incubation*
  The enzyme (11 µL) was diluted in B&R buffers (74.5 µL) at pH values of 4-5 to a concentration of 2 µM, before incubation for different periods of time at room temperature. After the specified time had passed, an aliquot of each solution was transferred to a black flat-bottom MTP containing B&R (pH 7, 186 µL). After the last aliquot was transferred, the reaction was started by the addition of NADPH and substrate stock (2 µL each).

Cofactor Dependence

This work was carried out by ROBERT GIESSMANN.

Reactions were carried out at different starting concentrations of NADPH ranging from 5-300 µM in the reaction mix.

Additives

The performance of the enzyme in different media or presence of different additives was tested. Final BM3-concentration was kept at 0.1 µM, and the reactions were carried out using NADPH (300 µM) instead of the GDH recycling system, to prevent interactions of the additives with GDH from influencing the results. Table 5-6 gives an overview over the experiments.

Table 5-6. Buffers and additives used for stability tests of TFFIS.

Entry	Buffer/Additive	Concentration	Dissolved in	Additional comments
1	HeLa lysate I		-	
2	HeLa lysate II		-	
3	PBS		-	
4	Dex-Sulfate	12 mg/mL	0.5 M NaCl	adjust pH to 6.5 with 0.1 M HCl
5	Poly-Arginine	12 mg/mL	0.5 M NaCl	milky precipitate observed
6	EDTA	0.2 M	H_2O	adjust pH to 6.5 with 0.1 M HCl
7	Triton X 100	1% total	KPi	no incubation time
8	TurboFect	12 and 24 µL	-	≙ 0.8 or 1.6 µL/µg protein
9	Dex-TRITC	10 mg/mL	H_2O	was mixed 1:1 with 12.5 µL TFFIS

To evaluate the activity of the enzyme in cell-like environment, HeLa lysate was also used instead of reaction buffer for one reaction, and directly compared to PBS buffer used during lysis (entries 1-3).

Of entries 4-6, 20 µL were incubated with the protein (TFFIS, 3.2 µL) for 15 min at 0°C, then diluted with KPi buffer to 490 µL before starting the reaction by adding substrate and NADPH. To study the time dependent activity for entry 8, samples were diluted with KPi buffer to a total volume of 500 µL after 30 min, 4 h and 24 h incubation at RT, and reactions started immediately. One batch each was mixed with buffer instead of TURBOFECT for comparison of prolonged incubation at RT.

Ionic Strength

KPi and NaPi buffer (pH 7.4, 100 mM) was diluted to different values ionic strength and the performance of the enzyme was tested under standard conditions (*cf*. CR042, 300µM NADPH instead of recycling system).

Mechanical Disturbance

Protein in buffer solution was vortexed at highest speed or suspended in an ultrasound bath for the given time (30 s - 15 min) at ambient temperatures, then stored on ice until the reaction was started by addition of substrate and NADPH.

Build-up of foam was observed in the vortexed samples, increasing with longer mixing times.

5.7 Docking and MD simulations

MD simulations were performed by RICHARD LONSDALE and details are published.[1] Briefly, the mutant models of $P450_{BM3}$ were constructed using the wt crystal structure as a template (PDB-ID 1BU7[265]), inserting point mutations according to the found variants. Substrates were modelled and then docked into the active site, with the prosthetic heme group in compound I state. Molecular dynamics simulations on the docking poses were used to assess the stability of the observed binding conformations.

5.8 Experiments in Living Cells

5.8.1 Microscopic Imaging

Confocal fluorescent microscopy imaging of *E. coli* was performed by FELIX DEMPWOLFF (GRAUMANN lab) on a LEICA SP8 laser scanning microscope equipped with a 100X HCX PL APO STED Objective (NA 1.4), a white light laser source and LEICA HyD detectors. Images were analyzed using the LAS AF (LEICA) software. *E. coli* were immobilized on coverslips by $S7_{50}$ medium containing agarose pads (1% w/v).

Microscopic imaging of HeLa cells was performed by MIKHAIL ZYUZIN (PARAK lab) on a ZEISS 510 Meta confocal laser scanning microscope equipped with an oil-immersed Plan-Apochromat 63x/1.40 DIC M27 objective, 505-550 nm filter, an argon laser (488 nm, at 60%) as light source and photo-multiplier tube detector. Images were analyzed using ZEN 2009 black edition software.

5.8.2 Escherichia coli

This work was carried out in collaboration with NATHALIE NETT.[250]
E. coli BL21-Gold(DE3) containing the pRSF-Duet1-BM3 plasmid encoding wt or mutant $P450_{BM3}$ were expressed in deep-well MTPs as triplicates for every substrate. Cells expressing the wt were used as negative controls. 800 µL $TB^{KAN50,\ IPTG100\mu M}$ media per well were inoculated with 100 µL of a pre-culture in LB^{KAN50} at 30°C, 220 rpm in an HT Infors Multitron Standard shaker. The cells were expressed for 7 h. To initiate the reaction, 8 µL substrate (100 mM stock solution in DMF) were added to every well and incubated for 16 h at 30°C and 220 rpm in an HT Infors Multitron Standard shaker. After centrifugation of the reaction mixture (4000 rpm, 10 min, 4°C), 200 µL of the supernatant were transferred to black flat bottom MTPs and analyzed by fluorescent read-out at the appropriate wavelength for the substrates (**Fehler! Verweisquelle konnte nicht gefunden werden.**). The pellets were washed with 400 µL KPi buffer (4.000 rpm, 10 min, 4°C) and resuspended again in 200 µL KPi buffer. A sample of the prepared cells was analyzed by confocal fluorescent microscopy (FELIX DEMPWOLFF, AK Graumann, Marburg). Another sample was washed once with KPi buffer, treated with lysis buffer for 2 h at 37°C and 220 rpm, followed by centrifugation and transfer of the lysate to black flat bottom MTPs and analysis by fluorescent read-out (data see Figure 3-31).

5.8.3 HeLa Cells

Growth conditions

The human cervical carcinoma cells (HeLa) were obtained from the AMERICAN TYPE CULTURE COLLECTION (ATCC).
DULBECCO's Modified EAGLE's Medium (DMEM) supplemented with 10% fetal bovine serum (FBS), 2 mM L-glutamine, 100 U/mL penicillin and 100 µg/mL streptomycin was used as growth medium at 37°C in 5% CO_2. Growth vessels were 75 cm^2 cultivation flasks.
In order to keep the cells in their exponential growth rate, it is necessary to periodically decrease the density of the cells every 2-3 days. For this, old cell medium was removed from the cultivation flask using a pipette. Adherent cells were then washed with 6 mL PBS to remove serum from the growth medium. To detach the cells from the bottom of the flask by degrading surface proteins, they were treated with Trypsin-EDTA (0.05%, 3 mL) for 2 minutes at 37°C in 5% CO_2. The enzyme-reaction was stopped by adding 9 mL DMEM, and the detached cells were centrifuged at 1000 rpm for 5 min at room temperature. After decantation of the supernatant, the cells were re-suspended in fresh medium. Cells were counted using a NEUBAUER chamber under a microscope at 100x magnification and $2 \cdot 10^6$ cells were seeded into a new 75 cm^2 cultivation flask with an end volume 15 mL DMEM and grown to a surface coverage of 80-90%.

Lysis

Cells from a 25 mL culture were first cleared of the medium, washed with 6 mL PBS buffer, and then treated with 3.5 mL Trypsin (0.25%) at 37°C for 5 min. The suspension was transferred to a falcon tube and centrifuged at 1000 rpm for 5 min, before being resuspended in 5 mL DMEM. ~0.8 mL were used for inoculation of a new culture. The rest was centrifuged again, the supernatant discarded, and the cells washed with 3 mL PBS.

Lysis Method I

Harvested HeLa cells were lysed by a method adapted from the dissertation of ANNE ADAMS.[298] Lysis was achieved by incubating the cells for 45 min on ice in 4 mL PBS buffer with Triton X (1%). The lysate was shock-frozen in liquid nitrogen and stored at -80°C until further use.

Lysis Method II

Lysation was achieved by freezing the cells at -78°C and subsequently thawing them in a thermocycler (30°C, 800 rpm, 5 min). The cycle was repeated 3 times, before storing the lysate at -20°C until further use.

Toxicity

Carried out in collaboration by MIKHAIL ZYUZIN.

HeLa cells were seeded into a 96-well plate at 15000 cells per well, and incubated for 24 h. Cells were washed, and new medium containing substrate (dissolved in DMF, stock conc. 10 mM) at different concentrations (0-100 μM) was added. To another set of experiments, only DMF was added at different concentrations (0-140 μM). Cells were incubated for 7 h, before the medium with substrate/DMF was removed and fresh medium containing resazurin (10%) was added. After 3 hours of incubation, emission spectra were measured to determine cell viability.

For tests in DMSO (stock conc. 10 mM), the total concentration of DMSO was kept constant over all measurements, and exposure time was extended to 24 h to cover a full cell cycle. These experiments were carried out in duplicates.

Transfection of Purified Protein

Carried out by MIKHAIL ZYUZIN.

A day before the experiment, HeLa cells were seeded in an 8-well-plate at an amount of 20,000 cells/cm^2 in 300 μL DMEM, and grown for 24 h at 37°C with 5% CO_2.

On the day of the experiment, 3.2 μl of TFFIS (15.5 μM) were mixed with either 12 μl or 24 μl (corresponding to 0.8 or 1.6 μL/μg total protein of TURBOFECT Transfection Reagent[276] (from THERMO SCIENTIFIC) and incubated at room temperature for 20 min, before the volume of the mixture was filled up to 100 μl with serum free cell medium.

Cells were washed with PBS, 250 μL of serum free cell medium were added, before adding 50 μL of the TURBOFECT mix to the cells dropwise. Cell were incubated at 37°C with 5% CO_2 for 4 h and 20 h, respectively. After incubation, they were washed with PBS, before 300 μl cell medium with serum containing 1% of substrate **1a** (dissolved in DMF, final concentration of 100 μM) was added.

In the case of 20 h of incubation, 300 μM NADPH co-factor (dissolved in PBS) was also added to the cells. Cells were monitored using an confocal scanning laser microscope, fixing 5 positions per well and taking snapshots of visible light and fluorescence (excitation 488 nm, filter <505 nm, emission >515 nm) every 10 min for multiple hours.

Transfection of mRNA

Carried out by JOANNA REJMAN, Munich.

The isolated plasmid DNA was linearized using one of the following restrictions enzymes or combinations. Resulting DNA concentrations are given in brackets: BlpI (no pellet), XbaI (3.23 μg/μL), DraII (3.58 μg/μL), DraII and XbaI (2.5 μg/μL).

For *in vitro* transcription, a commercially available AMBION LIFE TECHNOLOGIES mMESSAGE mMACHINE kit was used following the standard protocol.[299] mRNA was then modified

with a Poly(A) Tailing kit from APPLIED BIOSYSTEMS, again following standard protocols.[300] Transfection tests of all samples with and without polyA tail were performed using LIPOFECTAMINE[277] and OPTIMEM reduced serum medium (from GIBCO): 2.4 µL LIPOFECTAMINE were mixed with 47.6 µl OPTIMEM; mRNA was diluted to 0.1 µg/µL, before 4 µL of this new stock were mixed with 46 µL of the OPTIMEM solution and incubated at ambient temperature for 10 min, after which another 900 µL OPTIMEM were added. HeLa cells were treated with the solution and incubated at 37°C with 5% CO_2 prior to microscopy.

Microcapsules

Original Capsule Synthesis

100 µL TFFIS were added to a 615 µL of a solution of Na_2CO_3 (0.33 M) and NaCl (0.5 M) in PBS buffer (pH 7.2), and stirred for 30 s at 1000 rpm with a magnetic stirrer at room temperature. A solution of $CaCl_2$ (0.33 M) and NaCl (0.5 M) in PBS (615 µL) was added, mixed for 30 s and incubated for 1-2 min, upon which a cloudy precipitate formed. The mixture was transferred to an Eppendorf tube, centrifuged and the precipitate washed twice with water. For coating, 500-1000 µL dextran sulfate solution (1 mg/mL, 0.5 M NaCl, at pH 6.5) were added, vortexed for 10-15 min, before centrifuging and washing twice with water. This process was repeated with a poly-L-arginine solution (1 mg/mL, 0.5 M NaCl, at pH 6.5).

For multi-layered capsules, the alternating coating steps were repeated another 2-4 times. For trigger-release capsules, 2 mL of 15 nm gold-nanoparticle solution were mixed with 200 µL NaCl (0.5 M), added to the capsule mix and sonicated for 1 min, upon which the precipitate turned blue-black. Another 2.2 mL of gold/NaCl solution was added, the mix centrifuged, and part of the supernatant discarded before the coating process was continued with dextran sulfate and poly-arginine (1 layer each).

After washing of the particles, they were resuspended in EDTA solution (0.2 M, pH 6) and subjected to sonification for 10 min to dissolve the cores. After centrifugation and resuspension in KPi buffer, they were stored at 4°C until use.

Capsule Synthesis Modifications

Based on this protocol and insights from the stability tests (Chapters 5.6.4, page 99, and Chapter 3.6.2, page 59), some modifications were tried to render the synthesis more enzyme-friendly:

- Exchanging each step of vortexing for 30s of sonication
- Reducing stirring speed to 800 rpm instead of 1000 rpm to reduce foam formation
- Washing with KPi instead of water
- Controlling temperatures (4°C instead of room temperature)

For controls, empty capsules or capsules containing a fluorescent marker (Dextrane-Rhodamine, 2 mg/mL in water) instead of the P450 protein were synthesized.

6 References

[1] C. Ritter, N. Nett, C. G. Acevedo-Rocha, R. Lonsdale, K. Kräling, F. Dempwolff, S. Hoebenreich, P. L. Graumann, M. T. Reetz, E. Meggers, *Angew. Chemie (Int. Ed.)* **2015**, *54*, 13440–3.

[2] C. Ritter, N. Nett, C. G. Acevedo-Rocha, R. Lonsdale, K. Kräling, F. Dempwolff, S. Hoebenreich, P. L. Graumann, M. T. Reetz, E. Meggers, *Angew. Chemie* **2015**, *127*, 13640–4.

[3] Nobel Media AB, "List of All Nobel Prizes in Chemistry," accessed 19th Oct. 2015 under http://www.nobelprize.org/nobel_prizes/chemistry/laureates/, **2014**.

[4] Nobel Media AB, "List of All Nobel Prizes in Physiology or Medicine," accessed 19th Oct. 2015 under http://www.nobelprize.org/nobel_prizes/medicine/laureates/, **2014**.

[5] H. C. Hang, C. Yu, D. L. Kato, C. R. Bertozzi, *Proc. Natl. Acad. Sci.* **2003**, *100*, 14846–51.

[6] J. A. Prescher, C. R. Bertozzi, *Nat. Chem. Biol.* **2005**, *1*, 13–21.

[7] E. M. Sletten, C. R. Bertozzi, *Angew. Chemie (Int. Ed.)* **2009**, *48*, 6974–98.

[8] I. Kwon, S. In Lim, *Curr. Org. Chem.* **2015**, *19*, DOI 10.2174/1385272819666150810220630.

[9] A. B. Neef, C. Schultz, *Angew. Chemie (Int. Ed.)* **2009**, *48*, 1498–500.

[10] T.-L. Hsu, S. R. Hanson, K. Kishikawa, S.-K. Wang, M. Sawa, C.-H. Wong, *Proc. Natl. Acad. Sci.* **2007**, *104*, 2614–9.

[11] M. Merkel, K. Peewasan, S. Arndt, D. Ploschik, H.-A. Wagenknecht, *ChemBioChem* **2015**, *16*, 1541–53.

[12] H.-M. Lee, D. R. Larson, D. S. Lawrence, *ACS Chem. Biol.* **2009**, *4*, 409–27.

[13] J. Li, S. Jia, P. R. Chen, *Nat. Chem. Biol.* **2014**, *10*, 1003–5.

[14] C. H. Arrowsmith, J. E. Audia, C. Austin, J. Baell, J. Bennett, J. Blagg, C. Bountra, P. E. Brennan, P. J. Brown, M. E. Bunnage, C. Buser-Doepner, R. M. Campbell, W. J. Zuercher, et al., *Nat. Chem. Biol.* **2015**, *11*, 536–41.

[15] "The Chemical Probes Portal," accessed 30. Nov. 2015 under http://www.chemicalprobes.org/, **2015**.

[16] C. P. Ramil, Q. Lin, *Chem. Commun.* **2013**, *49*, 11007.

[17] J. T. Weiss, J. C. Dawson, C. Fraser, W. Rybski, C. Torres-Sánchez, M. Bradley, E. E. Patton, N. O. Carragher, A. Unciti-Broceta, *J. Med. Chem.* **2014**, *57*, 5395–404.

[18] M. Yang, J. Li, P. R. Chen, *Chem. Soc. Rev.* **2014**, *43*, 6511.

[19] H. C. Kolb, M. G. Finn, K. B. Sharpless, *Angew. Chemie (Int. Ed.)* **2001**, *40*, 2004–21.

[20] J. M. Baskin, C. R. Bertozzi, *QSAR Comb. Sci.* **2007**, *26*, 1211–9.

[21] M. D. Best, *Biochemistry* **2009**, *48*, 6571–84.

[22] P. Thirumurugan, D. Matosiuk, K. Jozwiak, *Chem. Rev.* **2013**, *113*, 4905–79.

[23] C. S. McKay, M. G. Finn, *Chem. Biol.* **2014**, *21*, 1075–101.

[24] E. Saxon, C. R. Bertozzi, *Science* **2000**, *287*, 2007–10.

[25] V. V. Rostovtsev, L. G. Green, V. V. Fokin, K. B. Sharpless, *Angew. Chemie (Int. Ed.)* **2002**, *41*, 2596–9.

[26] C. W. Tornøe, C. Christensen, M. Meldal, *J. Org. Chem.* **2002**, *67*, 3057–64.

[27] H. Koo, S. Lee, J. H. Na, S. H. Kim, S. K. Hahn, K. Choi, I. C. Kwon, S. Y. Jeong, K. Kim, *Angew. Chemie (Int. Ed.)* **2012**, *51*, 11836–40.

[28] M. King, A. Wagner, *Bioconjug. Chem.* **2014**, *25*, 825–39.

[29] D. N. Kamber, Y. Liang, R. J. Blizzard, F. Liu, R. A. Mehl, K. N. Houk, J. A. Prescher, *J. Am. Chem. Soc.* **2015**, *137*, 8388–91.

[30] D. M. Patterson, J. A. Prescher, *Curr. Opin. Chem. Biol.* **2015**, *28*, 141–9.

[31] Y. Lin, Q. Wang, *Chembiochem* **2014**, *15*, 787–8.

[32] B. K. Ruble, S. B. Yeldell, I. J. Dmochowski, *J. Inorg. Biochem.* **2015**, *150*, 182–8.

[33] V. N. Belov, G. Y. Mitronova, M. L. Bossi, V. P. Boyarskiy, E. Hebisch, C. Geisler, K. Kolmakov, C. A. Wurm, K. I. Willig, S. W. Hell, *Chemistry* **2014**, *20*, 13162–73.

[34] U. T. Bornscheuer, R. J. Kazlauskas, *Hydrolases in Organic Synthesis*, Wiley-VCH Verlag GmbH & Co. KGaA, Weinheim, FRG, **2005**.

[35] M. Skwarczynski, M. Noguchi, S. Hirota, Y. Sohma, T. Kimura, Y. Hayashi, Y. Kiso, *Bioorg. Med. Chem. Lett.* **2006**, *16*, 4492–6.

[36] J. P. Casey, R. A. Blidner, W. T. Monroe, *Mol. Pharm.* **2009**, *6*, 669–85.

[37] C. Brieke, F. Rohrbach, A. Gottschalk, G. Mayer, A. Heckel, *Angew. Chemie (Int. Ed.)* **2012**, *51*, 8446–76.

[38] D. Puliti, D. Warther, C. Orange, A. Specht, M. Goeldner, *Bioorg. Med. Chem.* **2011**, *19*, 1023–9.

[39] A. Bhardwaj, J. Kaur, S. K. Sharma, Z. Huang, F. Wuest, E. E. Knaus, *Bioorg. Med. Chem. Lett.* **2013**, *23*, 163–8.

[40] G. B. Cserép, A. Herner, P. Kele, *Methods Appl. Fluoresc.* **2015**, *3*, 042001.

[41] R. M. Versteegen, R. Rossin, W. ten Hoeve, H. M. Janssen, M. S. Robillard, *Angew. Chemie (Int. Ed.)* **2013**, *52*, 14112–6.

[42] J. B. Pawlak, G. P. P. Gential, T. J. Ruckwardt, J. S. Bremmers, N. J. Meeuwenoord, F. A. Ossendorp, H. S. Overkleeft, D. V Filippov, S. I. van Kasteren, *Angew. Chemie (Int. Ed.)* **2015**, *54*, 5628–31.

[43] J. Kim, C. R. Bertozzi, *Angew. Chemie (Int. Ed.)* **2015**, n/a – n/a.

[44] R. M. Yusop, A. Unciti-Broceta, E. M. V Johansson, R. M. Sánchez-Martín, M. Bradley, *Nat. Chem.* **2011**, *3*, 239–43.

[45] T. Völker, E. Meggers, *Curr. Opin. Chem. Biol.* **2015**, *25*, 48–54.

[46] W. a Velema, J. P. van der Berg, W. Szymanski, A. J. M. Driessen, B. L. Feringa, *ACS Chem. Biol.* **2014**, *9*, 1969–74.

[47] J. A. Cowan, *Pure Appl. Chem.* **2008**, *80*, 1799–810.

[48] A. Romero, E. Ramos, C. De Los Ríos, J. Egea, J. Del Pino, R. J. Reiter, *J. Pineal Res.* **2014**, *56*, 343–70.

[49] R. H. Crabtree, *Chem. Rev.* **2015**, *115*, 127–50.

[50] A. P. Silverman, E. T. Kool, *Chem. Rev.* **2006**, *106*, 3775–89.

[51] A. Shibata, T. Uzawa, Y. Nakashima, M. Ito, Y. Nakano, S. Shuto, Y. Ito, H. Abe, *J. Am. Chem. Soc.* **2013**, *135*, 14172–8.

[52] Z. Ma, J. S. Taylor, *Proc. Natl. Acad. Sci.* **2000**, *97*, 11159–63.

[53] K. Gorska, A. Manicardi, S. Barluenga, N. Winssinger, *Chem. Commun.* **2011**, *47*, 4364–6.

[54] C. Gorrini, I. S. Harris, T. W. Mak, *Nat. Rev. Drug Discov.* **2013**, *12*, 931–47.

[55] H. Zhang, P. Limphong, J. Pieper, Q. Liu, C. K. Rodesch, E. Christians, I. J. Benjamin, *FASEB J.* **2012**, *26*, 1442–51.

[56] S. Betanzos-Lara, Z. Liu, A. Habtemariam, A. M. Pizarro, B. Qamar, P. J. Sadler, *Angew. Chemie (Int. Ed.)* **2012**, *51*, 3897–900.

[57] J. J. Soldevila-Barreda, I. Romero-Canelón, A. Habtemariam, P. J. Sadler, *Nat. Commun.* **2015**, *6*, 6582.

[58] D. E. J. G. J. Dolmans, D. Fukumura, R. K. Jain, *Nat. Rev. Cancer* **2003**, *3*, 380–7.

[59] S. G. Bown, *Philos. Trans. A. Math. Phys. Eng. Sci.* **2013**, *371*, 20120371.

[60] S. J. Dougan, A. Habtemariam, S. E. McHale, S. Parsons, P. J. Sadler, *Proc. Natl. Acad. Sci.* **2008**, *105*, 11628–33.

[61] J. J. Soldevila-Barreda, P. J. Sadler, *Curr. Opin. Chem. Biol.* **2015**, *25*, 172–83.

[62] T. Y. Lee, J. Suh, *Chem. Soc. Rev.* **2009**, *38*, 1949–57.

[63] J. Prakash, J. J. Kodanko, *Curr. Opin. Chem. Biol.* **2013**, *17*, 197–203.

[64] W. S. Chei, H. Ju, J. Suh, *J. Biol. Inorg. Chem.* **2011**, *16*, 511–9.

[65] J. C. Joyner, W. F. Hodnick, A. S. Cowan, D. Tamuly, R. Boyd, J. A. Cowan, *Chem. Commun.* **2013**, *49*, 2118–20.

[66] J. Li, J. Yu, J. Zhao, J. Wang, S. Zheng, S. Lin, L. Chen, M. Yang, S. Jia, X. Zhang, P. R. Chen, *Nat. Chem.* **2014**, *6*, 352–61.

[67] M. I. Sánchez, C. Penas, M. E. Vázquez, J. L. Mascareñas, *Chem. Sci.* **2014**, *5*, 1901.

[68] J. T. Weiss, J. C. Dawson, K. G. Macleod, W. Rybski, C. Fraser, C. Torres-Sánchez, E. E. Patton, M. Bradley, N. O. Carragher, A. Unciti-Broceta, *Nat. Commun.* **2014**, *5*, 3277.

[69] P. K. Sasmal, S. Carregal-Romero, W. J. Parak, E. Meggers, *Organometallics* **2012**, *31*, 5968–70.

[70] S. V Chankeshwara, E. Indrigo, M. Bradley, *Curr. Opin. Chem. Biol.* **2014**, *21*, 128–35.

[71] H.-T. Hsu, B. M. Trantow, R. M. Waymouth, P. A. Wender, *Bioconjug. Chem.* **2015**, DOI 10.1021/acs.bioconjchem.5b00469.

[72] D. S. Tawfik, *Curr. Opin. Chem. Biol.* **2014**, *21*, 73–80.

[73] L. Gong, Z. Zhao, Y.-F. Lv, S.-Y. Huan, T. Fu, X.-B. Zhang, G.-L. Shen, R.-Q. Yu, *Chem. Commun.* **2015**, *51*, 979–95.

[74] J. M. Holstein, D. Schulz, A. Rentmeister, *Chem. Commun.* **2014**, *50*, 4478–81.

[75] K. M. Koeller, C. H. Wong, *Nature* **2001**, *409*, 232–40.

[76] A. Wells, H.-P. Meyer, *ChemCatChem* **2014**, *6*, 918–20.

[77] N. J. Turner, A. Wells, *ChemCatChem* **2014**, *6*, 900–1.

[78] M. Vellard, *Curr. Opin. Biotechnol.* **2003**, *14*, 444–50.

[79] A. Payen, J. F. Persoz, *Ann. Chim. Phys.* **1833**, *2*, 73–92.

[80] J. B. Sumner, *J. Biol. Chem.* **1926**, *69*, 435–41.

[81] J. B. Sumner, J. S. Kirk, S. F. Howell, *J. Biol. Chem.* **1932**, *98*, 543–52.

[82] H. S. Olsen, P. Falholt, *J. Surfactants Deterg.* **1998**, *1*, 555–67.

[83] M. J. E. C. van der Maarel, B. van der Veen, J. C. M. Uitdehaag, H. Leemhuis, L. Dijkhuizen, *J. Biotechnol.* **2002**, *94*, 137–55.

[84] L. M. Lods, C. Dres, C. Johnson, D. B. Scholz, G. J. Brooks, *Int. J. Cosmet. Sci.* **2000**, *22*, 85–94.

[85] P. Bajpai, *Biotechnol. Prog.* **1999**, *15*, 147–57.

[86] M. C. Cammarota, D. M. G. Freire, *Bioresour. Technol.* **2006**, *97*, 2195–210.

[87] K. Drauz, H. Gröger, O. May, *Enzyme Catalysis in Organic Synthesis*, Wiley-VCH Verlag GmbH & Co. KGaA, Weinheim, Germany, **2012**.

[88] W. Aehle, *Enzymes in Industry*, Wiley-VCH Verlag GmbH & Co. KGaA, Weinheim, Germany, **2007**.

[89] O. T. Avery, *J. Exp. Med.* **1931**, *54*, 73–89.

[90] P. Ruegsegger, I. Nydick, R. C. Hutter, A. H. Freiman, N. U. Bang, E. E. Cliffton, J. S. Ladue, *Circulation* **1959**, *19*, 7–13.

[91] H. F. Oettgen, L. J. Old, E. A. Boyse, H. A. Campbell, F. S. Philips, B. D. Clarkson, L. Tallal, R. D. Leeper, M. K. Schwartz, J. H. Kim, *Cancer Res.* **1967**, *27*, 2619–31.

[92] J. S. Holcenberg, *Annu. Rev. Pharmacol. Toxicol.* **1977**, *17*, 97–116.

[93] R. O. Brady, R. Schiffmann, *Lancet. Neurol.* **2004**, *3*, 752–6.

[94] R. J. Desnick, E. H. Schuchman, *Nat. Rev. Genet.* **2002**, *3*, 954–66.

[95] R. J. Desnick, E. H. Schuchman, *Annu. Rev. Genomics Hum. Genet.* **2012**, *13*, 307–35.

[96] S. A. Pawar, V. B. Pokharkar, N. R. Solanki, *Pharma Sci. Monit.* **2013**, *4*, 206–51.

[97] R. Kaur, B. S. Sekhon, *J. Pharm. Educ. Res.* **2012**, *3*, 1–13.

[98] S. S. Dewan, K. A. Setia, *Medical Enzymes: Technologies and Global Markets*, BCC Research Market Forecasting, **2011**.

[99] J. Ramundo, M. Gray, *J. Wound, Ostomy Cont. Nurs.* **2008**, *35*, 273–80.

[100] C. Ozcan, O. Ergün, A. Celik, N. Cördük, G. Ozok, C. Özcan, O. Ergün, A. Çelik, N. Çördük, G. Özok, *Burns* **2002**, *28*, 791–4.

[101] V. I. Avramis, *Blood* **2002**, *99*, 1986–94.

[102] H. Takaku, M. Takase, S. Abe, H. Hayashi, K. Miyazaki, *Int. J. Cancer* **1992**, *51*, 244–9.

[103] R. C. Ribeiro, C.-H. Pui, *Clin. Lymphoma* **2003**, *3*, 225–32.

[104] G. Pasut, M. Sergi, F. M. Veronese, *Adv. Drug Deliv. Rev.* **2008**, *60*, 69–78.

[105] K. Knop, R. Hoogenboom, D. Fischer, U. S. Schubert, *Angew. Chemie (Int. Ed.)* **2010**, *49*, 6288–308.

[106] M. Soskine, D. S. Tawfik, *Nat. Rev. Genet.* **2010**, *11*, 572–82.

[107] Y. Xie, J. An, G. Yang, G. Wu, Y. Zhang, L. Cui, Y. Feng, *J. Biol. Chem.* **2014**, *289*, 7994–8006.

[108] A. M. Klibanov, *Nature* **2001**, *409*, 241–6.

[109] M. T. Reetz, *J. Am. Chem. Soc.* **2013**, *135*, 12480–96.

[110] M. T. Reetz, *Angew. Chemie (Int. Ed.)* **2011**, *50*, 138–74.

[111] C. A. Denard, H. Ren, H. Zhao, *Curr. Opin. Chem. Biol.* **2015**, *25*, 55–64.

[112] M. D. Lane, B. Seelig, *Curr. Opin. Chem. Biol.* **2014**, *22*, 129–36.

[113] M. M. Y. Chen, C. D. Snow, C. L. Vizcarra, S. L. Mayo, F. H. Arnold, *Protein Eng. Des. Sel.* **2012**, *25*, 171–8.

[114] J. T. Ngo, D. A. Tirrell, *Acc. Chem. Res.* **2011**, *44*, 677–85.

[115] H. Xiao, A. Chatterjee, S. Choi, K. M. Bajjuri, S. C. Sinha, P. G. Schultz, *Angew. Chemie (Int. Ed.)* **2013**, *52*, 14080–3.

[116] R. Farid, T. Day, R. A. Friesner, R. A. Pearlstein, *Bioorg. Med. Chem.* **2006**, *14*, 3160–73.

[117] W. Sherman, T. Day, M. P. Jacobson, R. A. Friesner, R. Farid, *J. Med. Chem.* **2006**, *49*, 534–53.

[118] W. Sherman, H. S. Beard, R. Farid, *Chem. Biol. Drug Des.* **2006**, *67*, 83–4.

[119] M. J. Grisewood, N. P. Gifford, R. J. Pantazes, Y. Li, P. C. Cirino, M. J. Janik, C. D. Maranas, *PLoS One* **2013**, *8*, e75358.

[120] N. J. Turner, *Nat. Chem. Biol.* **2009**, *5*, 567–73.

[121] U. T. Bornscheuer, G. W. Huisman, R. J. Kazlauskas, S. Lutz, J. C. Moore, K. Robins, *Nature* **2012**, *485*, 185–94.

[122] A. S. Bommarius, *Annu. Rev. Chem. Biomol. Eng.* **2015**, *6*, 319–45.

[123] M. Freichel, K. Mengel, *Antidiabetika* in *Arzneiverordnungs-Report 2014* (Eds.: U. Schwabe, D. Paffrath), Springer Berlin Heidelberg, Berlin, Heidelberg, **2014**, pp. 393–418.

[124] U. M. Zanger, M. Schwab, *Pharmacol. Ther.* **2013**, *138*, 103–41.

[125] V. B. Urlacher, M. Girhard, *Trends Biotechnol.* **2012**, *30*, 26–36.

[126] L. S. Mazzaferro, W. Hüttel, A. Fries, M. Müller, *J. Am. Chem. Soc.* **2015**, *137*, 12289–95.

[127] E. M. Gillam, M. Hayes, *Curr. Top. Med. Chem.* **2013**, *13*, 2254–80.

[128] A. J. Warman, O. Roitel, R. Neeli, H. M. Girvan, H. E. Seward, S. A. Murray, K. J. McLean, M. G. Joyce, H. Toogood, R. A. Holt, D. G. Leys, N. S. Scrutton, A. W. Munro, *Biochem. Soc. Trans.* **2005**, *33*, 747–53.

[129] N. Tran, D. N. Nguyen, S. Dwaraknath, S. Mahadevan, G. Chavez, A. Nguyen, T. Dao, S. Mullen, T. Nguyen, L. E. Cheruzel, *J. Am. Chem. Soc.* **2013**, *135*, 14484–7.

[130] M. Kato, D. Nguyen, M. Gonzalez, A. Cortez, S. E. Mullen, L. E. Cheruzel, *Bioorg. Med. Chem.* **2014**, *22*, 5687–91.

[131] M. G. Shapiro, G. G. Westmeyer, P. Romero, J. O. Szablowski, B. Küster, A. Shah, C. R. Otey, R. Langer, F. H. Arnold, A. Jasanoff, *Nat. Biotechnol.* **2010**, *28*, 264–70.

[132] E. M. Brustad, V. S. Lelyveld, C. D. Snow, N. Crook, S. T. Jung, F. M. Martinez, T. J. Scholl, A. Jasanoff, F. H. Arnold, *J. Mol. Biol.* **2012**, *422*, 245–62.

[133] J. R. Halpert, *Metab. Clin. Exp.* **1995**, 14312–22.

[134] D. F. V. Lewis, P. Lee-Robichaud, *J. Steroid Biochem. Mol. Biol.* **1998**, *66*, 217–33.

[135] F. Hannemann, A. Bichet, K. M. Ewen, R. Bernhardt, *Biochim. Biophys. Acta* **2007**, *1770*, 330–44.

[136] D. Appel, S. Lutz-Wahl, P. Fischer, U. Schwaneberg, R. D. Schmid, *J. Biotechnol.* **2001**, *88*, 167–71.

[137] G. E. Tsotsou, A. E. G. Cass, G. Gilardi, *Biosens. Bioelectron.* **2002**, *17*, 119–31.

[138] U. Schwaneberg, C. Schmidt-Dannert, J. Schmitt, R. D. Schmid, *Anal. Biochem.* **1999**, *269*, 359–66.

[139] U. Schwaneberg, C. Otey, P. C. Cirino, E. Farinas, F. H. Arnold, *J. Biomol. Screen.* **2001**, *6*, 111–7.

[140] S. H. Park, D. H. Kim, D. Kim, D. H. Kim, H. C. Jung, J. G. Pan, T. Ahn, D. Kim, C. H. Yun, *Drug Metab. Dispos.* **2010**, *38*, 732–9.

[141] K. Neufeld, S. M. Zu Berstenhorst, J. Pietruszka, *Anal. Biochem.* **2014**, *456*, 70–81.

[142] Q. Cheng, C. D. Sohl, F. P. Guengerich, *Nat. Protoc.* **2009**, *4*, 1258–61.

[143] B. M. A. Lussenburg, L. C. Babel, N. P. E. Vermeulen, J. N. M. Commandeur, *Anal. Biochem.* **2005**, *341*, 148–55.

[144] L. O. Narhi, A. J. Fulco, *J. Biol. Chem.* **1986**, *261*, 7160–9.

[145] L. O. Narhi, A. J. Fulco, *J. Biol. Chem.* **1987**, *262*, 6683–90.

[146] L. P. Wen, A. J. Fulco, *J. Biol. Chem.* **1987**, *262*, 6676–82.

[147] C. J. C. Whitehouse, S. G. Bell, L.-L. Wong, *Chem. Soc. Rev.* **2012**, *41*, 1218–60.

[148] C.-H. Yun, K.-H. Kim, D.-H. Kim, H.-C. Jung, J.-G. Pan, *Trends Biotechnol.* **2007**, *25*, 289–98.

[149] C. J. C. Whitehouse, S. G. Bell, L.-L. Wong, *Chem. Soc. Rev.* **2012**, *41*, 1218–60.

[150] F. P. Guengerich, *J. Biol. Chem.* **2013**, *288*, 17063–4.

[151] H. Renault, J.-E. Bassard, B. Hamberger, D. Werck-Reichhart, *Curr. Opin. Plant Biol.* **2014**, *19C*, 27–34.

[152] J. A. McIntosh, C. C. Farwell, F. H. Arnold, *Curr. Opin. Chem. Biol.* **2014**, *19C*, 126–34.

[153] R. Neeli, H. M. Girvan, A. Lawrence, M. J. Warren, D. G. Leys, N. S. Scrutton, A. W. Munro, *FEBS Lett.* **2005**, *579*, 5582–8.

[154] L. Aigrain, D. Pompon, S. Moréra, G. Truan, *EMBO Rep.* **2009**, *10*, 742–7.

[155] T. L. Sevrioukova, I.F., Li, H., Zhang, H., Peterson, J.A., Poulos, "PDB-ID 1BVY - Complex of the Heme and FMC-binding Domains of the Cytochrome P450(BM-3)," DOI 10.2210/pdb1bvy/pdb, **1998**.

[156] G. Morera, S., Aigrain, L., Truan, "PDB-ID 3FJO - Structure of chimeric YH CPR," DOI 10.2210/pdb3fjo/pdb, **2008**.

[157] G.-D. Roiban, M. T. Reetz, *Chem. Commun.* **2014**, *51*, 2208–24.

[158] R. Agudo, G.-D. Roiban, M. T. Reetz, *ChemBioChem* **2012**, *13*, 1465–73.

[159] G.-D. Roiban, R. Agudo, A. Ilie, R. Lonsdale, M. T. Reetz, *Chem. Commun.* **2014**, *50*, 14310–3.

[160] R. Agudo, G.-D. Roiban, R. Lonsdale, A. Ilie, M. T. Reetz, *J. Org. Chem.* **2015**, *80*, 950–6.

[161] S. Kille, F. E. Zilly, J. P. Acevedo, M. T. Reetz, *Nat. Chem.* **2011**, *3*, 738–43.

[162] S. Hoebenreich, F. E. Zilly, C. G. Acevedo-Rocha, M. Zilly, M. T. Reetz, *ACS Synth. Biol.* **2015**, *4*, 317–31.

[163] K. Zhang, S. El Damaty, R. Fasan, *J. Am. Chem. Soc.* **2011**, *133*, 3242–5.

[164] A. Seifert, S. Vomund, K. Grohmann, S. Kriening, V. B. Urlacher, S. Laschat, J. Pleiss, *Chembiochem* **2009**, *10*, 853–61.

[165] H. M. Girvan, A. J. Dunford, R. Neeli, I. S. Ekanem, T. N. Waltham, M. G. Joyce, D. G. Leys, R. A. Curtis, P. Williams, K. J. Fisher, M. W. Voice, A. W. Munro, *Arch. Biochem. Biophys.* **2011**, *507*, 75–85.

[166] N.-H. Tran, N. Huynh, G. Chavez, A. Nguyen, S. Dwaraknath, T.-A. Nguyen, M. Nguyen, L. E. Cheruzel, *J. Inorg. Biochem.* **2012**, *115*, 50–6.

[167] J. H. Park, S. H. Lee, G. S. Cha, D. S. Choi, D. H. Nam, J. H. Lee, J.-K. Lee, C.-H. Yun, K. J. Jeong, C. B. Park, *Angew. Chemie (Int. Ed.)* **2015**, *54*, 969–73.

[168] A. K. Udit, M. G. Hill, V. G. Bittner, F. H. Arnold, H. B. Gray, *J. Am. Chem. Soc.* **2004**, *126*, 10218–9.

[169] C. van der Felt, K. Hindoyan, K. Choi, N. Javdan, P. Goldman, R. Bustos, A. G. Star, B. M. Hunter, M. G. Hill, A. Nersissian, A. K. Udit, *J. Inorg. Biochem.* **2011**, *105*, 1350–3.

[170] J. Rittle, M. T. Green, *Science* **2010**, *330*, 933–7.

[171] C. M. Krest, E. L. Onderko, T. H. Yosca, J. C. Calixto, R. F. Karp, J. Livada, J. Rittle, M. T. Green, *J. Biol. Chem.* **2013**, *288*, 17074–81.

[172] G. Di Nardo, G. Gilardi, *Int. J. Mol. Sci.* **2012**, *13*, 15901–24.

[173] R. Neeli, O. Roitel, N. S. Scrutton, A. W. Munro, *J. Biol. Chem.* **2005**, *280*, 17634–44.

[174] H. M. Girvan, H. E. Seward, H. S. Toogood, M. R. Cheesman, D. G. Leys, A. W. Munro, *J. Biol. Chem.* **2007**, *282*, 564–72.

[175] C. Jung, *Leakage in Cytochrome P450 Reactions in relation to Protein Structural Properties* in *Ubiquitous Roles Cytochrome P450 Proteins* (Eds.: A. Sigel, H. Sigel, R.K.O. Sigel), John Wiley & Sons, Ltd, Chichester, UK, **2007**, pp. 187–234.

[176] J. B. Lim, K. A. Barker, K. A. Eller, L. Jiang, V. Molina, J. F. Saifee, H. D. Sikes, *Protein*

Sci. **2015**, *24*, 1874–83.

[177] F. Alexis, E. M. Pridgen, R. Langer, O. C. Farokhzad, *Drug Delivery*, Springer Berlin Heidelberg, Berlin, Heidelberg, **2010**.

[178] B. P. Timko, K. Whitehead, W. Gao, D. S. Kohane, O. C. Farokhzad, D. Anderson, R. Langer, *Annu. Rev. Mater. Res.* **2011**, *41*, 1–20.

[179] D. J. A. Crommelin, A. T. Florence, *Int. J. Pharm.* **2013**, *454*, 496–511.

[180] N. Martinho, *J. Biomater. Nanobiotechnol.* **2011**, *02*, 510–26.

[181] C. Kaparissides, S. Alexandridou, K. Kotti, S. Chaitidou, *Open Access Reward. Syst.* **2006**, *2*, 1–11.

[182] S.-D. Clas, R. I. Sanchez, R. Nofsinger, *Drug Discov. Today* **2014**, *19*, 79–87.

[183] N. Nishiyama, Y. Kato, Y. Sugiyama, K. Kataoka, *Pharm. Res.* **2001**, *18*, 1035–41.

[184] S. C. Semple, A. Akinc, J. Chen, A. P. Sandhu, B. L. Mui, C. K. Cho, D. W. Y. Sah, D. Stebbing, E. J. Crosley, E. Yaworski, I. M. Hafez, J. R. Dorkin, J. Qin, K. Lam, K. G. Rajeev, K. F. Wong, L. B. Jeffs, L. Nechev, M. L. Eisenhardt, M. Jayaraman, M. Kazem, M. A. Maier, M. Srinivasulu, M. J. Weinstein, Q. Chen, R. Alvarez, S. A. Barros, S. De, S. K. Klimuk, T. Borland, V. Kosovrasti, W. L. Cantley, Y. K. Tam, M. Manoharan, M. A. Ciufolini, M. A. Tracy, A. de Fougerolles, I. MacLachlan, P. R. Cullis, T. D. Madden, M. J. Hope, *Nat. Biotechnol.* **2010**, *28*, 172–6.

[185] F. Bahadori, A. Dag, H. Durmaz, N. Cakir, H. Onyuksel, U. Tunca, G. Topcu, G. Hizal, *Polymers* **2014**, *6*, 214–42.

[186] S. De Koker, B. G. De Geest, S. K. Singh, R. De Rycke, T. Naessens, Y. Van Kooyk, J. Demeester, S. C. De Smedt, J. Grooten, *Angew. Chemie (Int. Ed.)* **2009**, *48*, 8485–9.

[187] Y. Ma, R. J. M. Nolte, J. J. L. M. Cornelissen, *Adv. Drug Deliv. Rev.* **2012**, *64*, 811–25.

[188] K. M. Huttunen, H. Raunio, J. Rautio, *Pharmacol. Rev.* **2011**, *63*, 750–71.

[189] Y. Ikeda, J. Ban, T. Ishikawa, S. Hashiguchi, S. Urayama, H. Horibe, *Chem. Pharm. Bull. (Tokyo).* **2008**, *56*, 1406–11.

[190] K. R. Lynch, *Biochem. J.* **2012**, *444*, e1–2.

[191] P. Agarwal, *Neuropsychiatr. Dis. Treat.* **2010**, *Volume 6*, 151.

[192] D. M. Aronoff, O. Boutaud, L. J. Marnett, J. A. Oates, *J. Pharmacol. Exp. Ther.* **2003**, *304*, 589–95.

[193] D. L. Cooper, C. M. Conder, S. Harirforoosh, *Expert Opin. Drug Deliv.* **2014**, *11*, 1661–80.

[194] T. Sun, Y. S. Zhang, B. Pang, D. C. Hyun, M. Yang, Y. Xia, *Angew. Chemie (Int. Ed.)* **2014**, *53*, 12320–64.

[195] B. K. Lee, Y. H. Yun, K. Park, *Chem. Eng. Sci.* **2015**, *125*, 158–64.

[196] V. P. Torchilin, *Nat. Rev. Drug Discov.* **2005**, *4*, 145–60.

[197] T. Smart, H. Lomas, M. Massignani, M. V. Flores-Merino, L. R. Perez, G. Battaglia, *Nano Today* **2008**, *3*, 38–46.

[198] P. Rivera-Gil, L. L. del Mercato, P. del Pino, A. Muñoz Javier, W. J. Parak, *Nano Today* **2008**, *3*, 12–21.

[199] X. Cao, C. Chen, H. Yu, P. Wang, *Biotechnol. Lett.* **2015**, *37*, 81–8.

[200] X.-D. Wang, K. S. Rabe, I. Ahmed, C. M. Niemeyer, *Adv. Mater.* **2015**, *27*, 7945–50.

[201] R. Tang, C. C. S. Kim, D. J. Solfiell, S. Rana, R. Mout, E. M. Velázquez-Delgado, A. Chompoosor, Y. Jeong, B. Yan, Z.-J. Zhu, J. A. Hardy, V. M. Rotello, N. Nanocapsules, R. Tang, C. C. S. Kim, D. J. Solfiell, S. Rana, R. Mout, E. M. Vela, A. Chompoosor, Y. Jeong, B. Yan, Z.-J. Zhu, C. C. S. Kim, J. A. Hardy, V. M. Rotello, N. P. Street, U. S. C. S. Kim, D. J. Sol, E. M. Velázquez-Delgado, A. Chompoosor, Y. Jeong, B. Yan, Z.-J. Zhu, C. C. S. Kim, J. A. Hardy, V. M. Rotello, *ACS Nano* **2013**, *7*, 6667–73.

[202] L. Sánchez-Sánchez, R. D. Cadena-Nava, L. A. Palomares, J. Ruiz-Garcia, M. S. T. Koay, J. J. L. M. Cornelissen, R. Vazquez-Duhalt, *Enzyme Microb. Technol.* **2014**, *60*, 24–31.

[203] G. Fuhrmann, M. A. Gauthier, J.-C. Leroux, *Chim. Int. J. Chem.* **2013**, *67*, 685–685.

[204] L. P. Herrera Estrada, J. A. Champion, *Biomater. Sci.* **2015**, *3*, 787–99.

[205] A. Yarnell, "The Top Pharmaceuticals That Changed The World - Salvarsan," accessed 27th October 2015 under https://pubs.acs.org/cen/coverstory/83/8325/8325salvarsan.html, **2005**.

[206] H. D. Summers, P. Rees, M. D. Holton, M. R. Brown, S. C. Chappell, P. J. Smith, R. J. Errington, *Nat. Nanotechnol.* **2011**, *6*, 170–4.

[207] N. Bertrand, J. Wu, X. Xu, N. Kamaly, O. C. Farokhzad, *Adv. Drug Deliv. Rev.* **2014**, *66*, 2–25.

[208] J. L. Arias, *Mini-Reviews Med. Chem.* **2011**, *11*, 1–17.

[209] A. S. Narang, R. I. Mahato, *Targeted Delivery of Small and Macromolecular Drugs*, CRC Press, **2010**.

[210] M. Licciardi, G. Giammona, J. Du, S. P. Armes, Y. Tang, A. L. Lewis, *Polymer* **2006**, *47*, 2946–55.

[211] M. A. Firer, G. Gellerman, *J. Hematol. Oncol.* **2012**, *5*, 70.

[212] D. Łubgan, Z. Jóźwiak, G. G. Grabenbauer, L. V. R. Distel, *Cell. Mol. Biol. Lett.* **2009**, *14*, 113–27.

[213] J. Nix, D. Sussman, C. Wilson, *J. Mol. Biol.* **2000**, *296*, 1235–44.

[214] M. A. D. Neves, O. Reinstein, M. Saad, P. E. Johnson, *Biophys. Chem.* **2010**, *153*, 9–16.

[215] S. B. Long, M. B. Long, R. R. White, B. a Sullenger, *RNA* **2008**, *14*, 2504–12.

[216] P. del Pino, A. Munoz-Javier, D. Vlaskou, P. Rivera-Gil, C. Plank, W. J. Parak, *Nano Lett.* **2010**, *10*, 3914–21.

[217] M. Ochs, S. Carregal-Romero, J. Rejman, K. Braeckmans, S. C. De Smedt, W. J. Parak, *Angew. Chemie (Int. Ed.)* **2013**, *52*, 695–9.

[218] P. M. Drake, D. Rabuka, *Curr. Opin. Chem. Biol.* **2015**, *28*, 174–80.

[219] M. Kimoto, R. Yamashige, K. Matsunaga, S. Yokoyama, I. Hirao, *Nat. Biotechnol.* **2013**, *31*, 453–7.

[220] X. Fang, W. Tan, *Acc. Chem. Res.* **2010**, *43*, 48–57.

[221] G. Mayer, *Angew. Chemie (Int. Ed.)* **2009**, *48*, 2672–89.

[222] M. M. Evers, L. J. A. Toonen, W. M. C. van Roon-Mom, *Adv. Drug Deliv. Rev.* **2015**, *87*, 90–103.

[223] R. S. Geary, D. Norris, R. Yu, C. F. Bennett, *Adv. Drug Deliv. Rev.* **2015**, *87*, 46–51.

[224] G. Ozcan, B. Ozpolat, R. L. Coleman, A. K. Sood, G. Lopez-Berestein, *Adv. Drug Deliv. Rev.* **2015**, *87*, 108–19.

[225] G. McClorey, M. J. Wood, *Curr. Opin. Pharmacol.* **2015**, *24*, 52–8.

[226] M. Jinek, K. Chylinski, I. Fonfara, M. Hauer, J. A. Doudna, E. Charpentier, *Science* **2012**, *337*, 816–21.

[227] F. A. Ran, P. D. Hsu, J. Wright, V. Agarwala, D. A. Scott, F. Zhang, *Nat. Protoc.* **2013**, *8*, 2281–308.

[228] S. Reardon, *Nature* **2015**, DOI 10.1038/nature.2015.18947.

[229] J. A. Doudna, E. Charpentier, *Science* **2014**, *346*, 1258096–1258096.

[230] P. D. Hsu, E. S. Lander, F. Zhang, *Cell* **2014**, *157*, 1262–78.

[231] M. V Kiryukhin, *Curr. Opin. Pharmacol.* **2014**, *18C*, 69–75.

[232] J. R. Weiser, W. M. Saltzman, *J. Control. Release* **2014**, *190*, 664–73.

[233] N. Nischan, H. D. Herce, F. Natale, N. Bohlke, N. Budisa, M. C. Cardoso, C. P. R. Hackenberger, *Angew. Chemie (Int. Ed.)* **2014**, *53*, 1–5.

[234] A. Erazo-Oliveras, K. Najjar, L. Dayani, T.-Y. Wang, G. A. Johnson, J.-P. Pellois, *Nat. Methods* **2014**, *11*, 861–7.

[235] B. J. Bruno, G. D. Miller, C. S. Lim, *Ther. Deliv.* **2013**, *4*, 1443–67.

[236] N. Klonis, W. H. Sawyer, *J. Fluoresc.* **1996**, *6*, 147–57.

[237] X. Chen, Z. Su, J. H. Horner, M. Newcomb, *Org. Biomol. Chem.* **2011**, *9*, 7427–33.

[238] E. T. Farinas, M. Alcalde, F. H. Arnold, *Tetrahedron* **2004**, *60*, 525–8.

[239] N. Shirane, Z. Sui, J. A. Peterson, P. R. Ortiz de Montellano, *Biochemistry* **1993**, *32*, 13732–41.

[240] N. E. Hopkins, M. K. Foroozesh, W. L. Alworth, *Biochem. Pharmacol.* **1992**, *44*, 787–96.

[241] T. N. Waltham, H. M. Girvan, C. F. Butler, S. R. Rigby, A. J. Dunford, R. Holt, A. W. Munro, *Metallomics* **2011**, *3*, 369–78.

[242] A. J. Ruff, A. Dennig, G. Wirtz, M. Blanusa, U. Schwaneberg, *ACS Catal.* **2012**, *2*, 2724–8.

[243] M. Rajasekar, S. M. Khan, S. N. Devaraj, T. M. Das, *Carbohydr. Res.* **2011**, *346*, 1776–85.

[244] H. Schewe, B.-A. Kaup, J. Schrader, *Appl. Microbiol. Biotechnol.* **2008**, *78*, 55–65.

[245] C. Schmidt-Dannert, F. H. Arnold, *Trends Biotechnol.* **1999**, *17*, 135–6.

[246] Schrödinger LLC., "The PyMOL Molecular Graphics System, Version 1.4," **2011**.

[247] J. A. Haines, D.C., Tomchick, D.R., Machius, M., Peterson, "PDB-ID 1JPZ - Crystal structure of a complex of the heme domain of P450BM-3 with N-Palmitoylglycine," DOI 10.2210/pdb1jpz/pdb, **2001**.

[248] S. Kille, *Dissertation*, Flavoproteins in Directed Evolution - Iterative CASTing to Evolve YqjM and P450_BM3, Ruhr-Universität, Bochum, **2010**.

[249] H. Zhang, S. C. Gay, M. Shah, M. K. Foroozesh, J. Liu, Y. Osawa, Q. Zhang, C. D. Stout, J. R. Halpert, P. F. Hollenberg, *Biochemistry* **2013**, *52*, 355–64.

[250] N. Nett, *Master Thesis*, Cytochrom P450_BM3 Katalysierte Oxidative Spaltung von Etherschutzgruppen, Philipps-Universität, Marburg, **2014**.

[251] A. Abate, V. Dimartino, P. Spina, P. L. Costa, C. Lombardo, A. Santini, M. Del Piano, P. Alimonti, *Drugs Exp. Clin. Res.* **2001**, *27*, 223–31.

[252] V. B. Lokeshwar, L. E. Lopez, D. Munoz, A. Chi, S. P. Shirodkar, S. D. Lokeshwar, D. O. Escudero, N. Dhir, N. Altman, *Cancer Res.* **2010**, *70*, 2613–23.

[253] F. Piccioni, M. Malvicini, M. G. Garcia, A. Rodriguez, C. Atorrasagasti, N. Kippes, I. T. Piedra Buena, M. M. Rizzo, J. Bayo, J. Aquino, M. Viola, A. Passi, L. Alaniz, G. Mazzolini, *Glycobiology* **2012**, *22*, 400–10.

[254] H. Urakawa, Y. Nishida, J. Wasa, E. Arai, L. Zhuo, K. Kimata, E. Kozawa, N. Futamura, N. Ishiguro, *Int. J. Cancer* **2012**, *130*, 454–66.

[255] R. Tamura, Y. Yokoyama, H. Yoshida, T. Imaizumi, H. Mizunuma, *J. Ovarian Res.* **2014**, *7*, 94.

[256] A. Benitez, T. J. Yates, N. Shamaldevi, T. Bowen, V. B. Lokeshwar, *J. Urol.* **2013**, *190*, 285–90.

[257] J. G. Deluca, G. R. Dysart, D. Rasnick, M. O. Bradley, *Biochem. Pharmacol.* **1988**, *37*, 1731–9.

[258] D.-H. Kim, K.-H. Kim, D.-H. Kim, K.-H. Liu, H.-C. Jung, J.-G. Pan, C.-H. Yun, *Drug Metab. Dispos.* **2008**, *36*, 2166–70.

[259] I. Kosiova, S. Kovackova, P. Kois, *Tetrahedron* **2007**, *63*, 312–20.

[260] C. Springer, *Bachelor Thesis*, Cytochrom P450_BM3-Katalysierte Oxidative Spaltung Chiraler Schutzgruppen, Philipps-Universität, Marburg, **2015**.

[261] B. Testa, P. Jenner, *Drug Metab. Rev.* **1981**, *12*, 1–117.

[262] F. P. Guengerich, M. V Martin, C. D. Sohl, Q. Cheng, *Nat. Protoc.* **2009**, *4*, 1245–51.

[263] M. R. Karver, R. Weissleder, S. A. Hilderbrand, *Angew. Chemie (Int. Ed.)* **2012**, *51*, 920–2.

[264] T. Kitazume, D. C. Haines, R. W. Estabrook, B. Chen, J. A. Peterson, *Biochemistry* **2007**, *46*, 11892–901.

[265] T. L. Li, H., Poulos, "PDB-ID 1BU7 - Cryogenic Structure of Cytochrome P450BM-3 Heme Domain," DOI 10.2210/pdb1bu7/pdb, **1998**.

[266] C. F. Butler, C. Peet, A. E. Mason, M. W. Voice, D. G. Leys, A. W. Munro, *J. Biol. Chem.* **2013**, *288*, 25387–99.

[267] C. F. Oliver, S. Modi, M. J. Sutcliffe, W. U. Primrose, L. Y. Lian, G. C. K. Roberts, *Biochemistry* **1997**, *36*, 1567–72.

[268] Q.-S. S. Li, U. Schwaneberg, M. Fischer, J. Schmitt, J. Pleiss, S. Lutz-Wahl, R. D. Schmid, *Biochim. Biophys. Acta - Protein Struct. Mol. Enzymol.* **2001**, *1545*, 114–21.

[269] O. Lentz, Q.-S. S. Li, U. Schwaneberg, S. Lutz-Wahl, P. Fischer, R. D. Schmid, *J. Mol. Catal. - B Enzym.* **2001**, *15*, 123–33.

[270] H. Venkataraman, S. B. A. de Beer, D. P. Geerke, N. P. E. Vermeulen, J. N. M. Commandeur, *Adv. Synth. Catal.* **2012**, *354*, 2172–84.

[271] H. Li, T. L. Poulos, *Biochim. Biophys. Acta* **1999**, *1441*, 141–9.

[272] J. Catalano, K. Sadre-Bazzaz, G. A. Amodeo, L. Tong, A. McDermott, *Biochemistry* **2013**, *52*, 6807–15.

[273] P. K. Chowdhary, M. Alemseghed, D. C. Haines, *Arch. Biochem. Biophys.* **2007**, *468*, 32–43.

[274] W. F. Scherer, *J. Exp. Med.* **1953**, *97*, 695–710.

[275] J. J. M. Landry, P. T. Pyl, T. Rausch, T. Zichner, M. M. Tekkedil, A. M. Stütz, A. Jauch, R. S. Aiyar, G. Pau, N. Delhomme, J. Gagneur, J. O. Korbel, W. Huber, L. M. Steinmetz, *Genes Genomes Genet.* **2013**, *3*, 1213–24.

[276] Fermentas Life Sciences, *Manual*, Turbofect Transfection Reagent, **2014**.

[277] Invitrogen Life Technologies, *Manual*, Lipofectamine®, **2000**.

[278] S. Carregal-Romero, M. Ochs, W. J. Parak, *Nanophotonics* **2012**, *1*, 171–80.

[279] A. W. Munro, J. G. Lindsay, J. R. Coggins, S. M. Kelly, N. C. Price, *Biochim. Biophys. Acta - Protein Struct. Mol. Enzymol.* **1996**, *1296*, 127–37.

[280] B. Rowlatt, J. A. Yorke, A. J. Strong, C. J. C. Whitehouse, S. G. Bell, L.-L. Wong, *Protein*

Cell **2011**, *2*, 656–71.

[281] R. S. Matson, R. S. Hare, A. J. Fulco, *Biochim. Biophys. Acta - Lipids Lipid Metab.* **1977**, *487*, 487–94.

[282] A. Paillard, F. Hindré, C. Vignes-Colombeix, J. P. Benoit, E. Garcion, *Biomaterials* **2010**, *31*, 7542–54.

[283] S. Govindaraj, T. L. Poulos, *J. Biol. Chem.* **1997**, *272*, 7915–21.

[284] L. H. Estrada, S. Chu, J. A. Champion, *J. Pharm. Sci.* **2014**, *103*, 1863–71.

[285] J. D. Keasling, A. Mendoza, P. S. Baran, *Nature* **2012**, *492*, 188–9.

[286] S. Wallace, E. P. Balskus, *Curr. Opin. Biotechnol.* **2014**, *30*, 1–8.

[287] M. Fischer, *Nucleic Acids Res.* **2003**, *31*, 319–21.

[288] H. E. Gottlieb, V. Kotlyar, A. Nudelman, *J. Org. Chem.* **1997**, *62*, 7512–5.

[289] G. R. Fulmer, A. J. M. Miller, N. H. Sherden, H. E. Gottlieb, A. Nudelman, B. M. Stoltz, J. E. Bercaw, K. I. Goldberg, *Organometallics* **2010**, *29*, 2176–9.

[290] F. W. Studier, *Protein Expr. Purif.* **2005**, *41*, 207–34.

[291] W. L. F. Armarego, C. Chai, *Purification of Laboratory Chemicals*, Butterworth-Heinemann, Oxford, UK, **2012**.

[292] R. J. Naik, M. V Kulkarni, K. Sreedhara Ranganath Pai, P. G. Nayak, *Chem. Biol. Drug Des.* **2012**, *80*, 516–23.

[293] C. K. Hazra, M. Oestreich, *Org. Lett.* **2012**, *14*, 4010–3.

[294] B. M. A. Van Vugt-Lussenburg, E. Stjernschantz, J. Lastdrager, C. Oostenbrink, N. P. E. Vermeulen, J. N. M. Commandeur, *J. Med. Chem.* **2007**, *50*, 455–61.

[295] C. G. Acevedo-Rocha, M. T. Reetz, **no date**, *in prep.*

[296] T. A. Hall, *Nucl. Acids. Symp. Ser.* **1999**, *41*, 95–8.

[297] C. J. C. Whitehouse, S. G. Bell, H. G. Tufton, R. J. P. Kenny, L. C. I. Ogilvie, L.-L. Wong, *Chem. Commun.* **2008**, *1*, 966–8.

[298] A. Adams, *Dissertation*, DNA-Katalysierte Acyltransferreaktionen: Ein Neuer Ansatz Zur Generierung von Bioaktiven Peptiden, Humboldt-Universität zu Berlin, **2012**.

[299] Ambion, *Manual*, Capped RNA Transcription - mMESSAGE mMACHINE ® Kit, **2012**.

[300] Applied Biosystemd, *Manual*, Poly (A) Tailing Kit, **2009**.

7 Appendices

Appendix 1. List of Abbreviations

^{1}H-NMR	proton nuclear magnetic resonance spectroscopy
^{13}C-NMR	carbon nuclear magnetic resonance spectroscopy
CCE	carboxycoumarin-ethylester
$CDCl_3$	chloroform deuterated
cf.	*confer* (lat.: compare)
conc.	concentrated
CYP	cytochrome P450
d	doublet
δ	chemical shift
DCM	dichloromethane
Dex	dextrane
DexS	dextrane sulfate
DMF	dimethylformamide
DMSO	dimethyl sulfoxide
DNA	deoxyribonucleic acid
E.coli	*Escherichia coli*
EDTA	ethylenediaminetetraacetate
e.g.	*exempli gratia* (lat.: for example)
EPR	enhanced permeability and retention effect
ESI	electrospray ionization
et al.	*et alii* (lat.: and others)
EtOAc	ethyl acetate
FAD	flavin adenine dinucleotide
FMN	flavin mononucleotide
FPLC	fast protein liquid chromatography

GFP	green fluorescence protein
HeLa	human cell-line, derived from a tumor taken from Henrietta Lacks
HEPES	2-[4-(2-hydroxyethyl)piperazin-1-yl]ethanesulfonic acid
HPLC	high performance liquid chromatography
HR	high resolution
Hz	Hertz
IPTG	isopropyl β-D-1-thiogalactopyranoside
IR	infrared spectroscopy
ISM	iterative saturation mutagenesis
J	coupling constant
KPi	potassium phosphate buffer
NAD(P)H	nicotinamide adenine dinucleotide (phosphate)
n	nano (10^{-9})
n.o.	not observed
λ	wavelength
m	unit: meter; prefix: milli (10^{-3}); NMR: multiplet
M	molarity
μ	micro (10^{-6})
MD	molecular dynamics
MeOH	methanol
min	minute
MS	mass spectroscopy
PAH	poly(allylamine) hydrochloride
PBS	phosphate buffered saline
PG	protection group
PolyR	poly-arginine
ppm	parts per million
PSS	sodium polystyrene sulfonate
q	quartet
RNA	ribonucleic acid
R_f	retention factor
rpm	revolutions per minute
RT	room temperature
s	singlet
SDS	sodium dodecyl sulfate
t	triplet
TLC	thin layer chromatography
UV	ultraviolet (light)
wt	wild type

Appendix 2. List of Figures

Appendix 3. List of Schemes

Appendix 4. List of Tables

Appendix 5. Calibration Curves

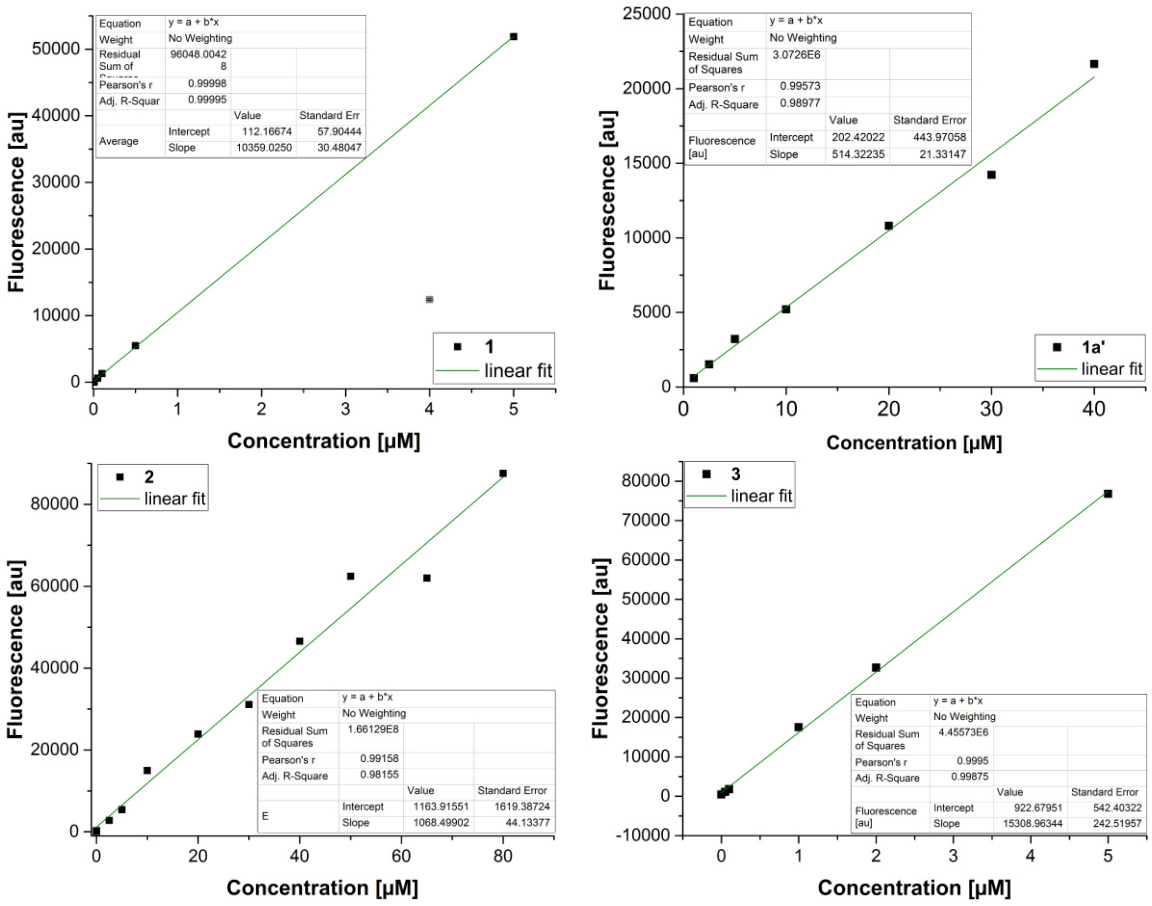

Figure 7-1. Fluorescence calibration – shown are linear ranges of fluorophores **1** (outlier shown in gray, but excluded from fit), **1a'**, **2** and **3**.

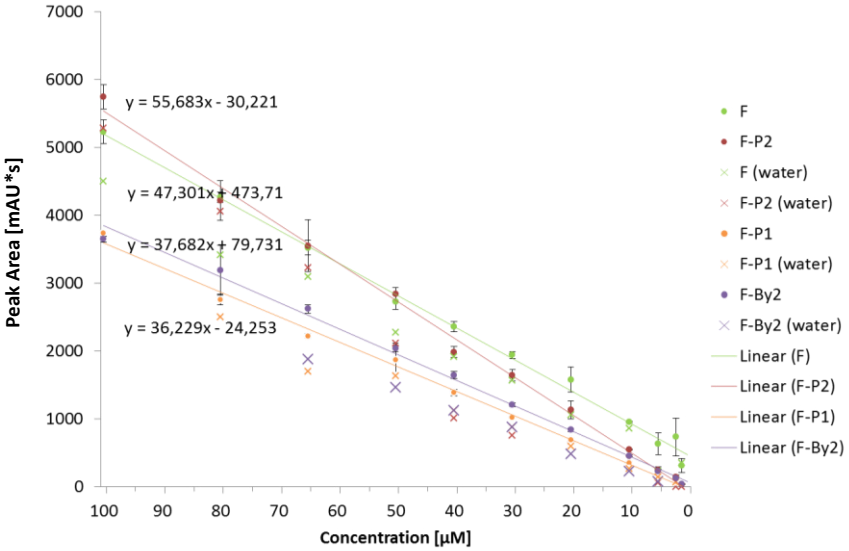

Figure 7-2. HPLC calibration curve for fluorescein derivatives **1**, **1a**, **1a'** and **1d** at set concentrations.

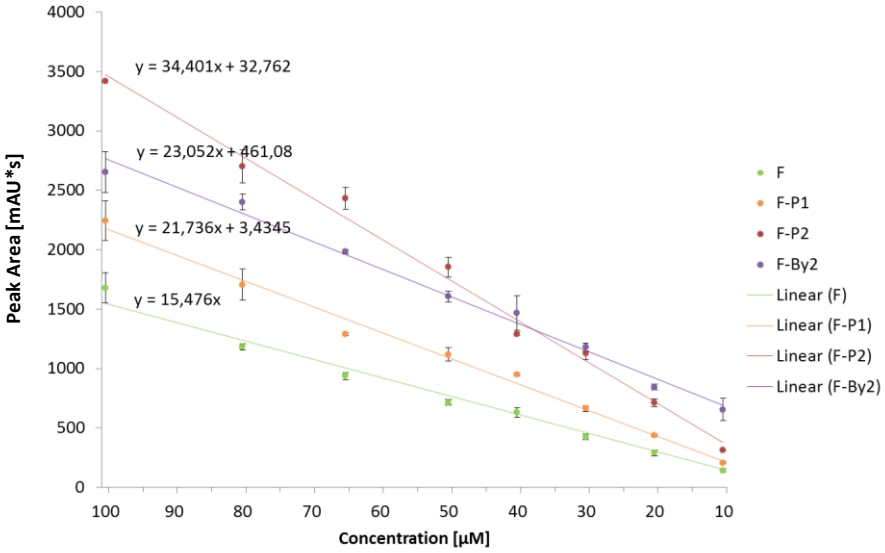

Figure 7-3. HPLC calibration curve for fluorescein derivatives derivatives **1**, **1a**, **1a'** and **1d** after extraction.

Appendix 6. 1st Generation Screen Sequencing Data

Table 7-1. Mutations of the hits found for first generation substrates, as determined from the sequencing results. Entries are ranked by activity towards substrate **1a**. Gray entries are duplicate variants with lower expression levels.

		Activity		Selectivity	Mutations								
Entry	**Short Name**	**1a**	**1b**	**1b/1a**	**R47**	**AS2**	**S72**	**V78**	**A82**	**F87**	**V178**	**V314**	**L437**
1	LSFIS	8848	3715	0.42	L				F	I			S
2	TFFIS	8443	3180	0.38	T		F		F	I			S
3	TFFIS	7509	3536	0.47	T		F		F	I			S
4	LSFIS	7252	3282	0.45	L				F	I			S
5	TFFVS[a]	6577	1661	0.25	T		F		F	V			S
6	TFFIS	6460	2796	0.43	T		F		F	I			S
7	RSFIS	6290	934	0.15					F	I			S
8	TFFIS	5660	2554	0.45	T		F		F	I			S
9	SIFIS[b]	5228	1457	0.28	S		I		F	I			S
10	WFWIS	4968	2129	0.43	W		F		W	I			S
11	RSFIS	4799	2488	0.52					F	I			S
12	WFWIS	4796	2730	0.57	W		F		W	I			S
13	LSWIS	4656	2722	0.58	L				W	I			S
14	TFFVS	4342	2709	0.62	T		F		F	V			S
15	TVFVS[c]	3694	1900	0.51	T		V		F	V			S
16	TSWIA[d]	3668	2843	0.78	T				W	I			A
17	RVFIN	3667	1031	0.28			V		F	I			N
18	TVFFS	3663	359	0.10	T		V		F				S
19	RSFIS	3656	2084	0.57					F	I			S
20	TSFVS	3643	2258	0.62	T				F	V			S
21	RVFFA	3446	469	0.14			V		F				A
22	TVFVS	3352	1867	0.56	T		V		F	V			S
23	TSFFN	3231	838	0.26	T				F				N
24	LSWIS	3209	1989	0.62	L				W	I			S
25	RFFIN	3198	1077	0.34			F		F	I			N
26	WSWIA	3090	3117	1.01	W				W	I			A
27	TIFFN	3050	386	0.13	T		I		F				N
28	LFFFA	3024	732	0.24	L		F		F				A
29	TFFVS	2879	2248	0.78	T		F		F	V			S
30	TVFVS	2794	1458	0.52	T		V		F	V			S
31	TFWIN	2669	926	0.35	T		F		W	I			N
32	*bad seq.*	2612	659	0.25	~~	~~	~~	~~	~~	~~	~~	~~	~~
33	TFFIL	2587	519	0.20	T		F		F	I			
34	LSWIN	2498	1066	0.43	L				W	I			N
35	WFFFS	2477	298	0.12	W		F		F				S
36	TSFFN	2423	296	0.12	T				F				N

Entry	Short Name	Activity 1a	Activity 1b	Selectivity 1b/1a	Mutations R47	AS2	S72	V78	A82	F87	V178	V314	L437
37	TFFIL	2402	586	0.24	T		F		F	I			
38	TFVFL	2290	654	0.29	T		F		V				
39	TSWIA	2246	824	0.37	T				W	I			A
40	LFFAL	2240	957	0.43	L		F		F	A			
41	WSWIA	2047	1078	0.53	W				W	I			A
42	LIFIL	2018	551	0.27	L		I		F	I			
43	RSFAx+AIVV	1075	648	0.60				I	F	A			~~
44	RSFAL+AMVV[e]	720	465	0.65				M	F	A			
45	YSFAL+FWVI	239	60	0.25	Y	F		W	F	A		I	
46	RSFAL+ALEV	161	82	0.51				L	F	A	E		
47	YSFAL+FAVI	144	79	0.55	Y	F		A	F	A		I	
48	RSVAL+AWVV[f]	114	53	0.47				W	V	A			

Additional mutations: a) E293 silent: GAA→GGA; b) T245?: ACG→.CG; c) E293G: GAA→GGA;
d) D222Y: GAT→TAT; e) L57 silent (CTA→TTA), E293 silent: GAA→GGA; f) L57 silent (CTA→TTA).

Appendix 7. Collected Screening Results of all Purified Mutants

Table 7-2. Overview over screening results of purified mutants as determined from original lysate reactions. Hit pairs are highlighted. Substrate derivatives which are not listed were discontinued.

Screen	Substrate → / Mutant Name ↓	1a [au]	1d [au]	2a [au]	2c [au]	2d [au]	3c [au]	3d [au]
	wt	113	1192	4267	4374	4225	16396	12722
	wt+His	148	1160	4269	4258	4282	16435	12533
Gen I	TFFIS	5090	1190	4559	4217	4848	11391	12057
Gen II	YFM-WEI-A	70	2066	4360	4285	3765	21359	20231
	PC-A	46	2430	4000	3906	3899	50556	12984
Gen III	M01	429	1026	9155	6763	4931	32183	41289
	M11	384	1189	10061	7458	5351	30120	29038
	WMV	171	1141	5643	13689	4768	134361	56853
	LV	150	1152	4974	7219	4365	91942	22792
	WWV-MQ'	201	1376	4618	4680	4913	38869	97405

Appendix 8. Screening Data as plotted in Figure 3-9

Table 7-3. Exemplary screening results for fluorescein-based derivatives **1a-f** (plate number **3** of the MegaSite library). The hit mutant TFFIS showing the highest activity is highlighted.

Entry	Substrate → Well	1a	1b	1c	1d	1e	1f
1	1A	70	62	62	358	70	71
2	2A	60	42	31	115	57	39
3	3A	58	42	33	668	34	45
4	4A	51	45	32	457	61	33
5	5A	57	47	34	396	60	42
6	6A	77	60	43	435	49	65
7	7A	67	60	39	485	47	47
8	8A	66	48	30	371	55	42
9	9A	149	168	38	134	107	71
10	10A	70	52	40	909	61	51
11	11A	116	115	47	208	75	64
12	12A	70	66	43	703	75	78
13	1B	3656	2084	61	887	76	72
14	2B	73	64	45	96	79	74
15	3B	860	297	39	1104	63	45
16	4B	64	62	43	96	49	55
17	5B	87	76	60	785	45	51
18	6B	815	229	59	45	102	54
19	7B	91	83	53	900	53	63
20	8B	67	78	56	366	116	48
21	9B	1706	603	63	529	128	86
22	10B	76	60	52	698	115	52
23	11B	67	60	42	115	53	69
24	12B	75	51	28	745	69	48
25	1C	65	55	41	42	58	45
26	2C	96	72	64	910	52	65
27	3C	84	64	56	165	56	41
28	4C	64	61	41	134	38	32
29	5C	71	58	38	870	64	48
30	6C	98	91	53	176	57	49
31	7C	8443	3180	52	1805	54	68
32	8C	288	82	43	972	83	44
33	9C	66	50	32	118	45	35
34	10C	57	53	35	79	46	45
35	11C	1482	475	65	1162	106	72
36	12C	61	80	38	151	74	55
37	1D	62	59	40	89	56	45
38	2D	112	92	61	155	65	52
39	3D	1812	842	45	904	75	56

Entry	Substrate → Well	1a	1b	1c	1d	1e	1f
40	4D	314	111	47	280	66	45
41	5D	97	72	47	117	70	62
42	6D	73	66	52	837	68	48
43	7D	68	65	44	402	54	33
44	8D	68	63	46	163	53	54
45	9D	71	57	40	154	56	45
46	10D	56	47	31	957	42	30
47	11D	63	55	39	146	64	56
48	12D	56	47	29	727	34	36
49	1E	78	64	55	149	129	51
50	2E	72	59	45	747	37	45
51	3E	68	66	36	304	60	41
52	4E	129	66	45	141	48	56
53	5E	81	68	57	717	49	52
54	6E	63	54	41	32	64	36
55	7E	78	73	48	903	46	38
56	8E	62	55	40	134	60	29
57	9E	177	123	47	189	62	65
58	10E	52	47	27	962	43	32
59	11E	61	49	33	326	46	47
60	12E	1415	476	60	52	78	69
61	1F	70	56	46	830	77	55
62	2F	71	61	45	118	41	48
63	3F	70	57	43	740	36	36
64	4F	85	64	41	124	62	48
65	5F	74	71	53	730	62	48
66	6F	68	62	40	112	50	53
67	7F	59	39	29	63	33	33
68	8F	558	177	58	1067	57	58
69	9F	62	46	31	146	55	29
70	10F	1873	166	50	646	63	65
71	11F	49	43	28	1105	44	35
72	12F	69	74	44	156	121	112
73	1G	47	47	25	286	26	21
74	2G	62	48	33	101	44	25
75	3G	65	57	40	715	46	35
76	4G	69	61	44	152	46	63
77	5G	87	66	55	112	66	48
78	6G	69	62	49	1103	53	39
79	7G	152	105	59	180	126	37
80	8G	272	103	46	697	60	59
81	9G	77	59	49	104	56	44
82	10G	90	65	31	713	46	41
83	11G	127	127	43	40	94	46
84	12G	63	58	38	826	58	67

Entry	Substrate → Well	1a	1b	1c	1d	1e	1f
85	1H	59	51	33	159	65	44
86	2H	81	58	47	711	80	72
87	3H	731	256	59	279	70	68
88	4H	69	66	46	712	81	48
89	5H	60	54	34	147	41	40
90	6H	61	55	44	768	69	55
91	7H	75	61	46	137	49	42
92	8H	70	61	53	727	52	51
93	9H	87	70	49	118	88	61
94	10H	1226	682	76	932	54	48
95	11H	422	236	66	259	105	48
96	12H	1080	375	47	891	89	83

Table 7-4. Screening results for coumarin-based derivatives **2a**, **c**, **d** and **3a**, **c**, **d** (mutant collection based on this and other projects). Hit mutants M01 (8A) and WMV (5B) are highlighted.

Entry	Substrate → Well	2a	2c	2d	3a	3c	3d
1	1A	4486	4171	4375	10115	9827	8092
2	2A	4267	4374	4225	7878	16396	12722
3	3A	4694	5186	4856	30327	70824	36663
4	4A	4002	4436	3760	16229	19769	17824
5	5A	4974	7219	4365	16609	91942	22792
6	6A	5023	6062	4458	50627	67375	39858
7	7A	4920	6292	4302	32562	81684	27725
8	8A	9155	6763	4931	23385	32183	41289
9	9A	4759	5300	4506	18304	48006	27099
10	10A	4940	5604	4332	16647	27762	30112
11	11A	4116	4165	4120	13861	14939	15341
12	12A	10061	7458	5351	40634	30120	29038
13	1B	5112	5252	4274	12480	16314	16516
14	2B	5321	4151	5057	11624	17204	19026
15	3B	5869	4439	4792	17283	19423	26383
16	4B	4859	6485	4652	69919	80450	40783
17	5B	5643	13689	4768	16672	134361	56853
18	6B	4701	4348	4324	10426	13099	14001
19	7B	5088	4155	4938	5915	16307	13825
20	8B	4713	4595	4597	13657	20245	18501
21	9B	4580	4466	4444	11463	14681	17125
22	10B	4780	4704	4492	13091	18614	16884
23	11B	4792	4351	4496	12655	13727	14060
24	12B	5019	5451	4219	12440	19235	32366
25	1C	5977	5013	4959	10229	12343	8900
26	2C	4782	5062	4228	13786	15582	15992
27	3C	5541	4720	5329	15890	16263	15059

Entry	Substrate → Well	2a	2c	2d	3a	3c	3d
28	4C	5307	6045	4633	9845	16031	10976
29	5C	4570	4646	4859	12838	16036	13569
30	6C	4701	4898	4596	12870	19479	20343
31	7C	4451	4264	4267	14926	15654	14585
32	8C	4836	4536	4560	8592	22604	17931
33	9C	4987	5420	4968	22800	20287	26313
34	10C	4957	4282	4597	23135	35712	54947
35	11C	4853	6024	4620	12169	63490	22713
36	12C	4269	4258	4282	12679	16435	12533
37	1D	4343	4377	4425	11879	12066	9788
38	2D	4634	4315	4386	19781	28310	29731
39	3D	4699	4263	4592	14934	15994	15199
40	4D	4315	4444	4433	14490	15366	16135
41	5D	4560	4600	4529	13426	16178	14627
42	6D	5342	4670	4507	13597	20483	19235
43	7D	4351	4375	4172	13084	14938	13235
44	8D	4682	4467	4532	10966	16453	15781
45	9D	4485	4590	4465	14263	16647	13839
46	10D	5099	4194	4634	12038	17252	26797
47	11D	4516	4297	4367	11970	14357	12564
48	12D	4790	4353	4491	10606	13070	14609
49	1E	4547	4969	4422	10466	18602	12896
50	2E	4579	4250	4493	11154	10248	15410
51	3E	4545	4176	4308	13776	13610	13037
52	4E	4695	4438	4601	18279	17341	34156
53	5E	4565	4363	4585	19348	36064	47552
54	6E	4969	4152	4336	25007	22942	24889
55	7E	4618	4680	4913	28786	38869	97405
56	8E	4984	4541	4593	18816	47754	43357
57	9E	4632	4292	4536	16419	16008	24293
58	10E	4718	4282	4586	10389	22359	51820
59	11E	4717	4449	4362	15179	23651	23898
60	12E	4827	4286	4997	27873	59342	25015
61	1F	4758	4054	4391	10071	9567	6501
62	2F	4328	4384	4423	15049	27581	22188
63	3F	5503	4207	5728	15096	22804	19518
64	4F	4389	4349	4259	14014	12748	12576
65	5F	4580	4321	4473	11975	15397	12191
66	6F	4396	4363	4427	13523	18566	17445
67	7F	4545	4151	4173	10687	30116	12933
68	8F	5091	4353	4707	9755	17366	21478
69	9F	4626	5159	4370	10677	63223	13924
70	10F	4643	4262	4370	16957	50857	29007
71	11F	4559	4217	4848	8658	11391	12057
72	12F	4493	4432	4285	12183	15969	13417

Entry	Substrate → Well	2a	2c	2d	3a	3c	3d
73	1G	4827	4183	4274	6222	8788	6511
74	2G	4762	5111	4748	8594	31546	13622
75	3G	4654	4020	4287	12259	11282	12099
76	4G	4840	4164	4796	7962	7953	8385
77	5G	4811	4045	4323	13467	18653	12729
78	6G	5290	4345	4502	14664	44351	23882
79	7G	4642	4093	4636	10832	12459	11322
80	8G	4626	4126	4405	10106	13519	14317
81	9G	4215	4089	4354	11886	16442	11893
82	10G	4464	4438	4086	10142	12752	14685
83	11G	4696	4167	4312	12259	13487	14916
84	12G	4418	4154	4172	13741	27094	15441
85	1H	4436	4118	4172	8150	7552	7787
86	2H	4113	4219	4303	7107	18612	30973
87	3H	4484	3980	4272	11512	8398	7747
88	4H	4412	4379	4371	31740	61897	30474
89	5H	4451	4529	4261	15657	50738	59251
90	6H	4380	4145	4170	16270	17804	14251
91	7H	4082	4775	4346	16545	71471	15676
92	8H	4568	4219	4240	9747	23584	45599
93	9H	4461	4234	4248	30625	53907	34310
94	10H	4419	4220	4217	10708	48242	16432
95	11H	4203	3940	4011	11291	35054	16753
96	12H	4417	4399	4205	10924	64997	15900

Appendix 9. Enzymatic Activity Data as plotted in Figure 3-15

Table 7-5. Enzymatic activity as obtained from purified enzymes at a concentration of 0.1 µM.

Substrate →	**TFFIS**		**WMV**		**M01**		**wt**	
Mutant ↓	org. Data	norm.	org. Data	norm.	org. Data	norm.	org. Data	norm.
1a	6991	100%	373	5%	153	2%	135	2%
1d	1478	21%	622	9%	560	8%	474	7%
2a	2496	20%	12281	100%	4581	37%	1132	9%
2c	709	6%	8210	67%	3264	27%	675	5%
3c	2426	1%	142665	55%	13230	5%	8463	3%
3d	5423	2%	260904	100%	16447	6%	4355	2%

Fluorescence activity was measured, buffer signal subtracted (sometimes leading to negative signals) and then normalized to the highest observed signal measured in this experiment for the corresponding parent compound (highlighted).

Appendix 10. Live Cell Activity Data as plotted in Figure 3-31

Table 7-6. Fluorescence signals measured in supernatant and lysates obtained after reactions in living *E. coli*.

Substrate →		**1a**		**2a**		**3d**		**3c**	
Mutant ↓		org. Data	norm.	org. Data	norm.	org. Data	norm.	org. Data	norm.
WT	Sup	18	7%	134	8%	6502	8%	1936	2%
	Lys	-6	-2%	-13	-1%	-864	-1%	-3951	-5%
TFFIS	Sup	51	19%	57	4%	7877	10%	1186	1%
	Lys	262	100%	0	0%	-1164	-1%	-4913	-6%
WMV	Sup	48	18%	762	47%	81943	100%	6327	8%
	Lys	-12	-5%	235	14%	27244	33%	-2445	-3%
M01	Sup	34	13%	1627	100%	12214	15%	2651	3%
	Lys	-6	-2%	347	21%	6696	8%	-270	0%
LV	Sup	17	7%	-115	-7%	23753	29%	5351	7%
	Lys	-6	-2%	53	3%	34716	42%	10121	12%

Fluorescence activity was measured, buffer signal subtracted (sometimes leading to negative signals) and then normalized to the highest observed signal measured in this experiment for the corresponding parent compound (highlighted).

Appendix 11. Details for SABRINA's Collection

Table 7-7. List of $P450_{BM3}$ mutants in SABRINA's collection.[161,162,248] All P450 variants from the synthetized gene libraries (ZFE and KSA-297) contain silent mutations at L57 (CTA → TTA) and A225 (GCA → GCT).

Plate/position	ID number of mutant	mutations
KSA-01-01	BM3 wt	BM3
KSA-01-04	F87A	F87A
KSA-01-07	KSA-KB-102-02-82	F87V
KSA-01-10	KSA-KB-102-02-11	F87T
KSA-01-13	KSA-KD-347-01-45	F87A-S72A
KSA-01-16	KSA-KD-337-01-85	F87A-A330L
KSA-01-19	KSA-KD-337-01-28	F87A-A330V
KSA-01-22	KSA-KD-337-01-73	F87A-A330W
KSA-01-25	KSA-KB-131-11-02	R47V-T49Y-Y51F-F87A
KSA-01-28	KSA-KB-131-12-58	R47F-T49V-F87A
KSA-01-31	KSA-KB-131-20-96	R47C-T49F-Y51C-F87A
KSA-01-34	KSA-KB-131-21-79	R47Y-T49Y-F87A
KSA-01-37	KSA-KB-131-25-05	R47Y-T49N-F87A
KSA-01-40	KSA-KB-131-29-32	R47F-T49F-F87A
KSA-01-43	KSA-KB-131-32-26	R47Y-T49F-F87A-K224E-I314V
KSA-01-46	KSA-KB-131-38-42	R47F-T49I-F87A
KSA-01-49	KSA-KB-131-02-96	R47I-T49I-Y51I-F87A
KSA-01-52	KSA-KB-131-43-60	R47N-T49I-F87A
KSA-01-55	KSA-KB-131-44-47	R47N-T49C-Y51F-F87A
KSA-01-58	KSA-KB-131-44-51	R47F-T49F-Y51F-F87A
KSA-01-61	Mix of mutants	
KSA-01-64	KSA-KB-131-49-67	R47C-T49C-F87A
KSA-01-67	Mix of mutants	
KSA-01-70	KSA-KB-131-50-35	R47Y-T49I-Y51N-F87A
KSA-01-73	KSA-KB-131-52-34	R47F-T49S-F87A
KSA-01-76	KSA-KB-131-53-40	R47F-T49N-Y51F-F87A
KSA-01-79	KSA-KB-131-53-77	R47C-T49F-F87A
KSA-01-82	KSA-KB-131-54-07	R47F-T49Y-F87A
KSA-01-85	KSA-KB-131-54-15	R47Y-T49F-Y51F-F87A
KSA-01-88	KSA-KB-131-54-73	R47I-T49F-F87A
KSA-01-91	ZFE-ZC-020-03-72	R47I-T49T-F87A
KSA-01-94	ZFE-ZC-020-05-55	R47N-T49Y-F87A

Plate/position	ID number of mutant	mutations
KSA-02-01	F87A	F87A
KSA-02-04	ZFE-ZC-020-06-40	R47C-T49D-F87A
KSA-02-07	ZFE-ZC-020-10-95	R47C-T49Y-F87A
KSA-02-10	ZFE-ZC-020-14-96	T49V-F87A
KSA-02-13	ZFE-ZC-020-17-51	R47Y-T49I-F87A
KSA-02-16	ZFE-ZC-020-29-83	R47F-T49H-F87A
KSA-02-19	ZFE-ZC-020-41-90	R47Y-T49L-F87A
KSA-02-22	KSA-KB-131-42-12	R47C-T49L-F87A
KSA-02-25	KSA-KB-131-07-28	R47V-T49F-Y51N-F87A
KSA-02-28	KSA-KB-131-16-53	R47V-T49I-Y51N-F87A
KSA-02-31	KSA-KB-131-43-87	R47C-T49C-Y51G-F87A
KSA-02-34	KSA-KB-131-43-94	R47C-T49I-Y51V-F87A
KSA-02-37	KSA-KB-131-45-91	R47I-T49V-Y51I-F87A
KSA-02-40	KSA-KB-131-46-65	R47I-T49L-Y51N-F87A
KSA-02-43	KSA-KB-131-48-76	R47I-T49I-Y51N-F87A
KSA-02-46	KSA-KB-131-49-87	R47I-T49I-Y51V-F87A
KSA-02-49	KSA-KB-131-50-49	R47I-T49C-Y51V-F87A
KSA-02-52	ZFE-ZC-020-02-55	R47N-T49I-Y51V-F87A
KSA-02-55	ZFE-ZC-020-02-72	R47V-T49L-Y51N-F87A
KSA-02-58	ZFE-ZC-020-04-73	T49V-Y51I-F87A
KSA-02-61	ZFE-ZC-020-05-43	T49I-Y51I-F87A
KSA-02-64	ZFE-ZC-020-06-48	R47N-T49L-Y51L-F87A
KSA-02-67	ZFE-ZC-020-06-59	R47C-T49L-Y51I-F87A
KSA-02-70	ZFE-ZC-020-06-96	R47V-T49C-Y51I-F87A
KSA-02-73	ZFE-ZC-020-10-26	R47S-T49I-Y51I-F87A
KSA-02-76	ZFE-ZC-020-17-60	R47V-T49I-Y51I-F87A
KSA-02-79	ZFE-ZC-020-23-73	T49L-Y51I-F87A
KSA-02-82	ZFE-ZC-020-25-06	R47N-T49L-Y51I-F87A
KSA-02-85	ZFE-ZC-020-29-72	R47N-T49I-Y51I-F87A
KSA-02-88	KSA-KC-297-10-73	V78Y-A82E-F87A
KSA-02-91	KSA-KC-277-09-38	V78I-A82D-F87A
KSA-02-94	KSA-KC-297-01-40	V78L-A82D-F87A

Plate/position	ID number of mutant	mutations
KSA-03-01	F87A	F87A
KSA-03-04	KSA-KC-297-02-48	V78V-A82D-F87A
KSA-03-07	KSA-KC-277-10-25	V78M-A82D-F87A
KSA-03-10	Mix of mutants	
KSA-03-13	KSA-KC-297-09-78	V78M-A82E-F87A
KSA-03-16	KSA-KC-297-07-81	V78V-A82Q-F87A
KSA-03-19	KSA-KC-277-03-94	V78I-A82E-F87A
KSA-03-22	KSA-KC-277-07-82	V78V-A82N-F87A
KSA-03-25	KSA-KC-297-10-53	V78I-A82Q-F87A
KSA-03-28	KSA-KC-297-05-81	V78C-A82N-F87A
KSA-03-31	KSA-KC-297-10-52	V78V-A82S-F87A
KSA-03-34	KSA-KC-277-23-32	V78L-A82E-F87A
KSA-03-37	KSA-KC-297-03-17	V78I-A82S-F87A
KSA-03-40	KSA-KC-277-23-94	V78M-A82N-F87A
KSA-03-43	KSA-KC-277-20-90	V78C-A82G-F87A
KSA-03-46	KSA-KC-277-05-38	V78A-A82A-F87A
KSA-03-49	KSA-KC-297-11-34	V78L-A82C-F87A
KSA-03-52	KSA-KC-297-05-87	V78C-A82L-F87A
KSA-03-55	KSA-KC-277-15-49	V78V-A82L-F87A
KSA-03-58	KSA-KC-277-30-33	V78T-A82L-F87A
KSA-03-61	KSA-KC-297-11-79	V78M-A82L-F87A
KSA-03-64	KSA-KC-297-02-57	V78Y-A82M-F87A
KSA-03-67	KSA-KC-277-30-84	V78V-A82M-F87A
KSA-03-70	KSA-KC-277-03-57	V78M-A82M-F87A
KSA-03-73	KSA-KC-297-05-19	V78L-A82M-F87A
KSA-03-76	KSA-KC-277-31-47	V78T-A82M-F87A
KSA-03-79	KSA-KC-297-11-96	V78S-A82M-F87A
KSA-03-82	KSA-KC-297-10-46	V78L-A82H-F87A
KSA-03-85	KSA-KC-277-02-44	V78L-A82F-F87A[(a)]
KSA-03-88	KSA-KC-277-20-86	V78I-A82F-F87A
KSA-03-91	KSA-KC-297-07-14	V78M-A82F-F87A
KSA-03-94	KSA-KC-277-17-09	V78L-A82F-F87A[(a)]

(a) Mutant 277-17-09 (LF) contains in position 78 a TTG(Leu), in position 82 a TTT (Phe) and in position 87 a GCA (Ala) codon compared to mutant 277-02-44, which contains CTG (Leu), TTC (Phe) and GCG (Ala), respectively. Enzymatic activity in plate screenings is lower in the latter case.

Plate/position	ID number of mutant	mutations
KSA-04-01	F87A	F87A
KSA-04-04	KSA-KC-277-03-80	V78T-A82F-F87A
KSA-04-07	KSA-KC-297-02-56	V78T-A82N-F87A
KSA-04-10	KSA-KC-297-10-24	V78W-A82V-F87A
KSA-04-13	KSA-KC-297-06-87	V78W-A82T-F87A
KSA-04-16	KSA-KC-277-20-52	V78M-A82W-F87A
KSA-04-19	KSA-KC-277-02-90	V78T-A82W-F87A
KSA-04-22	KSA-KC-297-08-62	V78V-A82W-F87A
KSA-04-25	KSA-KC-277-16-79	V78S-A82W-F87A
KSA-04-28	KSA-KC-297-11-11	V78L-A82W-F87A
KSA-04-31	KSA-KC-277-11-40	V78N-A82W-F87A
KSA-04-34	KSA-KC-277-01-08	V78A-A82W-F87A
KSA-04-37	KSA-KC-277-20-71	V78C-A82W-F87A
KSA-04-40	KSA-KB-080-05-84	M185D-L188G-F87A
KSA-04-43	KSA-KC-230-08-83	M185N-L188G-F87A
KSA-04-46	ZFE-ZB-098-22-2-63	M185G-L188G-F87A
KSA-04-49	KSA-KB-080-04-05	M185R-L188G-F87A
KSA-04-52	KSA-KB-080-03-11	M185S-L188G-F87A
KSA-04-55	KSA-KB-080-05-60	M185S-L188A-F87A
KSA-04-58	ZFE-ZB-098-34-45	M185S-L188S-F87A
KSA-04-61	KSA-KB-080-04-33	M185N-L188C-F87A
KSA-04-64	KSA-KB-080-10-94	M185D-L188C-F87A
KSA-04-67	ZFE-ZB-098-24-58	M185R-L188C-F87A
KSA-04-70	KSA-KB-080-03-15	M185M-L188C-F87A
KSA-04-73	ZFE-ZB-098-34-18	M185S-L188C-F87A
KSA-04-76	ZFE-ZB-098-22-2-60	M185G-L188C-F87A
KSA-04-79	KSA-KB-080-03-50	M185S-L188D-F87A
KSA-04-82	KSA-KB-080-11-96	M185G-L188T-F87A
KSA-04-85	KSA-KC-230-04-82	M185G-L188V-F87A
KSA-04-88	KSA-KB-080-04-47	M185D-L188V-F87A
KSA-04-91	ZFE-ZB-098-23-60	M185G-L188L-F87A
KSA-04-94	ZFE-ZB-098-34-15	M185G-L188I-F87A

Plate/position	ID number of mutant	mutations
KSA-05-01	F87A	F87A
KSA-05-04	ZFE-ZB-098-23-77	M185R-L188S-F87A
KSA-05-07	KSA-KB-080-01-03	M185G-L188S-F87A
KSA-05-10	KSA-KB-080-10-03	M185R-L188N-F87A
KSA-05-13	KSA-KB-080-04-46	M185H-L188C-F87A
KSA-05-16	KSA-KB-080-05-11	M185N-L188N-F87A
KSA-05-19	ZFE-ZB-098-34-94	M185S-L188F-F87A
KSA-05-22	ZFE-ZB-098-34-24	M185G-L188T-F87A
KSA-05-25	ZFE-ZB-098-26-26	M185R-L188R-F87A
KSA-05-28	KSA-KC-230-02-53	M185C-L188N-F87A
KSA-05-31	KSA-KC-230-08-59	M185N-L188H-F87A
KSA-05-34	KSA-KB-080-01-55	M185P-L188C-F87A
KSA-05-37	KSA-KC-230-07-20	M185I-L188H-F87A
KSA-05-40	KSA-KC-230-08-21	M185H-L188N-F87A
KSA-05-43	ZFE-ZB-098-34-48	M185P-L188H-F87A
KSA-05-46	KSA-KC-230-08-96	M185I-L188R-F87A
KSA-05-49	KSA-KD-344-01-49	R47Y-T49F-V78I-A82M-F87A-K224E-V314I
KSA-05-52	KSA-KD-344-01-74	R47Y-T49F-V78L-A82M-F87A-K224E-V314I
KSA-05-55	KSA-KD-345-01-43	R47Y-T49F-V78A-A82F-F87A-K224E-V314I
KSA-05-58	KSA-KD-345-01-26	R47Y-T49F-V78T-A82F-F87A-K224E-V314I
KSA-05-61	KSA-KD-345-01-75	R47Y-T49F-V78W-A82F-F87A-K224E-V314I
KSA-05-64	KSA-KD-341-01-82	R47Y-T49F-V78W-A82G-F87A-K224E-V314I
KSA-05-67	KSA-KD-346-01-22	R47Y-T49F-V78S-A82W-F87A-K224E-V314I
KSA-05-70	KSA-KD-346-01-64	R47Y-T49F-V78M-A82W-F87A-K224E-V314I
KSA-05-73	KSA-KD-346-01-84	R47Y-T49F-V78T-A82W-F87A-K224E-V314I
KSA-05-76	KSA-KD-346-01-33	R47Y-T49F-V78V-A82W-F87A-K224E-V314I
KSA-05-79	Mix of mutants	
KSA-05-82	KSA-KD-359-01-90	V78L-A82F-F87A-H266R
KSA-05-85	KSA-KD-357-01-62	V78L-A82F-F87A-V178E
KSA-05-88	KSA-KB-080-04-47	M185D-L188V-F87A
KSA-05-91	empty	empty
KSA-05-94	empty	empty

Appendix 12. Details for 96er Collection

Table 7-8. List of $P450_{BM3}$ variants in the 96er collection. Source projects: a) Rational design mutants, b) 1st round MegaSite project, c) 2nd round MegaSite project, d) Introduction of *N*-terminal His-tag for purification; e) 3rd round MegaSite project, f) 1st Generation uncaging; g) Regio- and stereoselectivity of P450-catalysed hydroxylation.[161]

Entry	BM3 code	Source/ Project	Plas-mid	Mutations																	
				H-Tag	R47	T49	Y51	E64	S72	V78	F81	A82	F87	E143	V178	L181'	L188	E267	V314	A330	G415	L437
1	pRSF	Ruben Agudo	pRSF	-																		
2	WT	Ruben Agudo	pRSF	-																		
3	V	ACE-AB-66-02[a]	pRSF	-									V									
4	I	ACE-AB-66-06[a]	pRSF	-									I									
5	LV	ACE-AB-37-30[a]	pRSF	-	L								V									
6	LVQ	ACE-AB-28[a]	pRSF	-	L								V				Q					
7	LVQS	ACE-AB-34-33[a]	pRSF	-	L								V				Q				S	
8	M01 (LVQVS)	ACE-AB-46-01[a]	pRSF	-	L								V				Q	V			S	
9	M01-W	ACE-AB-46-01[a]	pRSF	-	L							W	V				Q	V			S	
10	M01-IW	ACE-AB-53-01[a]	pRSF	-	L				I			W	V				Q	V			S	
11	M01-VW	ACE-AB-53-02[a]	pRSF	-	L				V			W	V				Q	V			S	
12	M01-GIG (M11)	ACE-AB-54-01[a]	pRSF	-	L			G			I		V	G			Q	V			S	
13	M11-I	ACE-AB-53-03[a]	pRSF	-	L			G	I		I		V	G			Q	V			S	
14	M11-II	ACE-AB-66-10[a]	pRSF	-	L			G	I		I		I	G			Q	V			S	
15	M01-WI	ACE-AB-66-14[a]	pRSF	-	L							W	I				Q	V			S	
16	WWV	ACE-AA-162-02-28[b]	pRSF	-	W							W	V									
17	WMV	ACE-AA-162-02-61[b]	pRSF	-	W							M	V									
18	WMI	ACE-AA-162-02-69[b]	pRSF	-	W							M	I									
19	WV	ACE-AA-162-02-72[b]	pRSF	-	W								V									
20	LIFII	ACE-AA-162-05-26[b]	pRSF	-	L				I			F	I									I

Entry	BM3 code	Source/ Project	Plasmid	Mutations																		
				H-Tag	R47	T49	Y51	E64	S72	V78	F81	A82	F87	E143	V178	L181'	L188	E267	V314	A330	G415	L437
21	TIMI	ACE-AA-162-05-78 [b]	pRSF	-	T				I			M	I									
22	LIFI	ACE-AA-162-06-28 [b]	pRSF	-	L				I			F	I									
23	LWIS	ACE-AA-162-07-19 [b]	pRSF	-	L							W	I									S
24	LIFI-WQ	ACE-AB-52-01-04 [c]	pRSF	-	L		W		I			F	I				Q					
25	LIFI-WQW	ACE-AB-52-01-52 [c]	pRSF	-	L		W		I			F	I				Q			W		
26	LIFI-WQ'Q	ACE-AB-52-01-60 [c]	pRSF	-	L		W		I			F	I			Q	Q					
27	LIFI-CW	ACE-AB-52-01-67 [c]	pRSF	-	L				I			F	I				C			W		
28	LIFI-WQM	ACE-AB-52-03-27 [c]	pRSF	-	L		W		I			F	I				Q			M		
29	LIFI-WQ'M	ACE-AB-52-04-57 [c]	pRSF	-	L		W		I			F	I			Q				M		
30	LIFI-WC'	ACE-AB-52-07-39 [c]	pRSF	-	L		W		I			F	I			C						
31	LIFI-HQ'	ACE-AB-52-07-74 [c]	pRSF	-	L		H		I			F	I			Q						
32	WWV-HH'M	ACE-AB-52-11-19 [c]	pRSF	-	W		H					W	V			H				M		
33	WWV-WQW	ACE-AB-52-11-55 [c]	pRSF	-	W		W					W	V				Q			W		
34	WWV-Q'	ACE-AB-52-12-40 [c]	pRSF	-	W							W	V			Q						
35	WWV-M	ACE-AB-52-15-36 [c]	pRSF	-	W							W	V							M		
36	WT	ACE-AB-81-01 [d]	pRSF	+																		
37	LIFI-WC'	ACE-AB-99-10 [d]	pRSF	+	L		W		I			F	I			C						
38	WWV-Q'	ACE-AB-91-13 [d]	pRSF	+	W							W	V			Q						
39	M11-II	ACE-AB-84-01 [d]	pRSF	+	L			G	I		I		I	G			Q	V			S	
40	M01-WI	ACE-AB-99-01 [d]	pRSF	+	L							W	I				Q	V			S	
41	KIFI-WC'	Outsourced [e]	pRSF	+	K		W		I			F	I			C						
42	WIFI-WC'	Outsourced [e]	pRSF	+	W		W		I			F	I			C						
43	LIFI-HC'	Outsourced [e]	pRSF	+	L		H		I			F	I			C						
44	LIFI-YC'	Outsourced [e]	pRSF	+	L		Y		I			F	I			C						
45	LIFI-WCC'	Outsourced [e]	pRSF	+	L		W		I	C		F	I			C						
46	LIFI-WMC'	Outsourced [e]	pRSF	+	L		W		I	M		F	I			C						
47	LIEI-WC'	Outsourced [e]	pRSF	+	L		W		I			E	I			C						

Entry	BM3 code	Source/ Project	Plasmid	Mutations																	
				H-Tag	R47	T49	Y51	E64	S72	V78	F81	A82	F87	E143	V178	L181'	L188	E267	V314	A330	G415	L437
48	LIWI-WC'	Outsourced [e]	pRSF	+	L		W		I			W	I			C						
49	LIFV-WC'	Outsourced [e]	pRSF	+	L		W		I			F	V			C						
50	LIFI-WG'	Outsourced [e]	pRSF	+	L		W		I			F	I			G						
51	LIFI-WQ'	Outsourced [e]	pRSF	+	L		W		I			F	I			Q						
52	LWV-Q'	Outsourced [e]	pRSF	+	L							W	V			Q						
53	WWV-WQ'	Outsourced [e]	pRSF	+	W		W					W	V			Q						
54	WWV-CQ'	Outsourced [e]	pRSF	+	W					C		W	V			Q						
55	WWV-MQ'	Outsourced [e]	pRSF	+	W					M		W	V			Q						
56	WFV-Q'	Outsourced [e]	pRSF	+	W							F	V			Q						
57	WWI-Q'	Outsourced [e]	pRSF	+	W							W	I			Q						
58	WWV-C'	Outsourced [e]	pRSF	+	W							W	V			C						
59	WWV-G'	Outsourced [e]	pRSF	+	W							W	V			G						
60	LFFA	MS-01-26 [f]	pRSF	-	L				F			F	A									
61	TSWIA	MS-01-03 [f]	pRSF	-	T							W	I									A
62	SIFIS	MS-01-52 [f]	pRSF	-	S				I			F	I									S
63	TFFI	MS-01-41 [f]	pRSF	-	T				F			F	I									
64	TVFFS	MS-01-65 [f]	pRSF	-	T				V			F										S
65	TFWIN	MS-01-90 [f]	pRSF	-	T				F			W	I									N
66	TFFVS	MS-01-31 [f]	pRSF	-	T				F			F	V									S
67	FIS	MS-01-44 [f]	pRSF	-								F	I									S
68	LIFI	MS-01-59 [f]	pRSF	-	L				I			F	I									
69	LFFFA	MS-02- 49 [f]	pRSF	-	L				F			F										A
70	TSFVS	MS-02-85 [f]	pRSF	-	T							F	V									S
71	TFFIS	MS-03-31 [f]	pRSF	-	T				F			F	I									S
72	TSFFN	MS-04-74 [f]	pRSF	-	T							F										N
73	TVFVS	MS-04-28 [f]	pRSF	-	T				V			F	V									S
74	WFFFS	MS-04-79 [f]	pRSF	-	W				F			F										S
75	un-known	MS-04-84 [f]	pRSF	-																		
76	FFIN	MS-05-21 [f]	pRSF	-					F			F	I									N
77	TSWIA	MS-05-57 [f]	pRSF	-	T							W	I									A
78	WFWIS	MS-06-61 [f]	pRSF	-	W				F			W	I									S
79	TFV	MS-06-77 [f]	pRSF	-	T				F			V										
80	LSWIN	MS-07-85 [f]	pRSF	-	L							W	I									N
81	RVFFA	MS-07-62 [f]	pRSF	-					V			F										A
82	TIFFN	MS-07-65 [f]	pRSF	-	T				I			F										N
83	WSWIA	MS-08-32 [f]	pRSF	-	W							W	I									A

Entry	BM3 code	Source/ Project	Plasmid	Mutations																	
				H-Tag	R47	T49	Y51	E64	S72	V78	F81	A82	F87	E143	V178	L181'	L188	E267	V314	A330	G415	L437
84	LSFIS	MS-08-09 [f]	pRSF	-	L							F	I									S
85	LSWIS	MS-08-84 [f]	pRSF	-	L							W	I									S
86	TVFVS	MS-09-64 [f]	pRSF	-	T				V			F	V									S
87	VFIN	MS-10-04 [f]	pRSF	-					V			F	I									N
88	IFA	SC-03-88 [f]	pET-M11	+						I		F	A									
89	MFA	SC-03-91 [f]	pET-M11	+						M		F	A									
90	WVA	SC-04-10 [f]	pET-M11	+						W		V	A									
91	FWVII	SC-05-61 [f]	pET-M11	+	Y	F				W		F	A						I			
92	LFAE	SC-05-85 [f]	pET-M11	+						L		F	A		E							
93	YFAFAI	SC-05-55 [f]	pET-M11	+	Y	F				A		F	A						I			
94	A	Sabrina Kille [g]	pET-M11	+									A									
95	IIIA	Sabrina Kille [g]	pET-M11	+	I	I	I						A									
96	YFLMA	Sabrina Kille [g]	pET-M11	+	Y	F				L		M	A									

Erklärung

gemäß § 10, Abs. 1 der Promotionsordnung der mathematisch-naturwissenschaftlichen Fachbereiche und des Medizinischen Fachbereichs für seine mathematisch-naturwissenschaftlichen Fächer der Philipps-Universität Marburg vom 15.07.2009:

Ich erkläre, dass eine Promotion noch an keiner anderen Hochschule als der PHILIPPS-UNIVERSITÄT MARBURG, Fachbereich Chemie, versucht wurde und versichere, dass ich meine vorgelegte Dissertation

Towards Bioorthogonal Enzymatic Uncaging Reactions

selbst und ohne fremde Hilfe verfasst, nicht andere als die in ihr angegebenen Quellen oder Hilfsmittel benutzt, alle vollständig oder sinngemäß übernommenen Zitate als solche gekennzeichnet sowie die Dissertation in der vorliegenden oder ähnlichen Form noch bei keiner anderen in- oder ausländischen Hochschule anlässlich eines Promotionsgesuchs oder zu anderen Prüfungszwecken eingereicht habe.

Cornelia Ritter
Marburg, den 21.12.2015

Curriculum Vitae

Personal Information

Name	Cornelia Ritter	Nationality	German
Date of Birth	November 13th 1986	Place of Birth	Munich

Education

10/2012 – 10/2015 Philipps-University Marburg
PhD studies in Chemistry / Chemical Biology
Supervisor: Prof. Eric Meggers
Bioorthogonal Enzymatic Activation of Caged Compounds

11/2009 – 7/2012 Ludwig-Maximilians-University Munich
Master of Science in Chemistry (grade 1.4)
Supervisor of the Master Thesis: Prof. Peter Klüfers
Iron Triflate as a Precursor for Complexes containing Weakly Coordinating Ligands

10/2006 – 11/2009 Ludwig-Maximilians-University Munich
Bachelor of Science in Chemistry and Biochemistry (grade 2.1)
Supervisor of the Bachelor Thesis: Prof. Andreas Kornath
Protonation of Acetamide and Thioacetamide in Superacidic Systems

9/1997 – 6/2006 Franz-Marc-Gymnasium Markt Schwaben (Secondary School)
awarded qualification: Abitur – university entrance diploma (grade 1.7)
Major Subjects: Chemistry, English

Experience Abroad

10/2010 – 12/2010 University of Auckland, New Zealand
Research Internship (grade 1.0)
Supervisor: Prof. Penny Brothers
Synthesis and Characterization of Co(III)-Hydroxamates

03/2004– 04/2004 John F. Kennedy High School, Seattle, WA, USA
Student Exchange Program